Exploring the Fundamentals of Platelet Granular Storage and Secretion at the Single Cell Level

A DISSERTATIONSUBMITTED TO THE FACULTY OF THE GRADUATE SCHOOL OF THE UNIVERSITY OF MINNESOTA

BY

Secil Koseoglu

IN PARTIAL FULFILLMENT OF THE REQUIREMENTS

FOR THE DEGREE OF

DOCTOR OF PHILOSOPHY

Christy L. Haynes, Advisor

Phil Buhlmann, Advisor

January, 2013

Acknowledgements

I would like to express my deep appreciation and gratitude to my advisor Christy Haynes for her guidance and support. I feel really fortunate to work with Christy Haynes; her passion for science, endless energy, dedication to her family and her students always inspired me. One simply could not wish for a better or friendlier advisor. This Ph. D. would not be completed without her.

I would also like to thank my co-advisor Phil Buhlmann for his encouragement and support. I have learned a lot from our scientific conversations; especially thinking at molecular level.

I cannot find words to express my gratitude to the members of the Haynes and Buhlmann group. Besides being great co-workers they have become my family in the US. I would like to thank Dr. Sara Love and Dr. Shencheng Ge for helping me learn single cell measurements. The phospholipid work described in Chapter 4 would not be possible without Audrey Meyer's and Donghyuk Kim's expertise in mass spectrometry and microfluidic devices. I would like to thank Sarah Gruba for her help in Chapter 2.

I have been fortunate to collaborate with great platelet biologists, Prof. Robert Flaumenhaft, Dr. James Dilks, and Dr. Christian Peters from Harvard Medical School who helped me with Drp1 project covered in Chapter 3. I would also like to thank Prof. S. Wally Whiteheart and Dr. Deepa Jonnalagadda from University of Kentucky who gave me the chance to work with amazing mouse models with distinct platelet types.

I would like to thank my family for their unconditional love and support. It was their encouragements and dedications enabled me to step out of Turkey and study in the U.S.

For my mom, Semiha Koseoglu

Abstract

Platelets are critical cells in hemostasis and thrombosis, but they are also involved in many important physiological events including inflammation, host defense, wound healing and malignancy. Platelets pursue their physiological functions mainly as secretory cells. The three distinct platelets granules, α- and δ- granules and lysosomes, serve as storage units for critical biological mediators. Upon action of a stimulus, platelets release their granules through a conserved mechanism called exocytosis. Because blood platelets are quite small (2-3 μm in diameter) and activate easily, until the recent work in the Haynes group, measurements were limited largely to morphological studies (electron/light/fluorescence microscopy) and ensemble aggregation and release assays, missing fundamental dynamics about chemical messenger delivery. The measurements of platelet δ-granule secretion by using carbon fiber microelectrode amperometry (CFMA) enabled real-time monitoring secretion of serotonin from platelet δ-granules with sub-ms time resolution. The aim of this thesis is to exploit these single cell measurements to study the fundamentals of platelet secretion behavior and advance our current understanding of platelet exocytosis.

A brief introduction to the platelet biology and single cell platelet measurements are given in Chapter 1. Since the major step involved in platelet granular secretion is fusion of the granules to either the membrane tubular system known as the open canalicular system (OCS) or the plasma membrane, Chapter 2 investigates the difference in the secretory behavior of the platelets of different species that has OCS or does not have an OCS. CFMA measurements performed on mouse, rabbit and cow platelets indicate that OCS is necessary for an efficient secretory function.

Fusion of the granular membrane with the plasma membrane is mediated by both membrane protein and lipid components. While membrane proteins anchor granular membrane with plasma membrane and facilitate fusion, membrane lipids not only regulate the membrane fluidity and curvature they also mediate localization of the fusion proteins on the site of the fusion. Although dynamin-related protein1 (Drp1) is best known as a mediator of membrane fission, recent work showed that it also contributes to granule exocytosis by mediating fusion pore expansion in chromaffin cells. However, there was not any information on the role of Drp1 on platelet granule secretion. To assess whether Drp1 functions in platelet exocytosis, we tested the effect of mdivi-1, a Drp1 inhibitor, on the release of dense granules by using single-cell amperometry (Chapter 3). The results demonstrate the role of Drp-1 in fusion pore dynamics, and indicate that regulation of platelet fusion pore expansion can be used to control thrombus formation *in vivo*.

Phospholipids are the major components of the plasma and granule membrane, and in addition to their structural importance as a cellular barrier that separates the intracellular and extracellular environment, they are also dynamically involved in and regulate many cellular processes. However, there is not much known about how the different phospholipids regulate platelet behavior. Chapter 4 examines the effect of membrane phospholipids on the major platelet functions of aggregation and exocytosis and demonstrates that different phospholipids can act on different aspects of platelet function.

Besides their physiological importance, platelets can serve as an ideal model system for studying exocytosis. In the last part of the thesis, we compare the effect of cholesterol on chromaffin cells, a well-studied model cell for neural secretion, and platelets. Chromaffin cell exocytosis at altered cellular cholesterol levels was measured at single cell level and results were compared to the previously published work by Ge et al on cholesterol effects on platelet secretion. This work demonstrated that the effect of cholesterol on each cell type was different which is likely due to the fact that, unlike platelets, chromaffin cells have a nucleus and a significant synthesis capacity that enables them to tightly regulate various cell functions.

Overall, the experiments performed herein expand our current understanding of the mechanism of platelet secretion and demonstrate that studying platelet

secretion at the molecular level is essential to control platelet function for therapeutic purposes.

Table of Contents

Chapter 2

Comparison of Platelet δ- Granule Secretion from Different Species using Single Cell Measurements

Chapter 3

Dynamin-Related Protein-1 Controls Fusion Pore Dynamics During Platelet Granule Exocytosis

Chapter 4

Exploring the Role of Phospholipids in Platelet Aggregation and Secretion

Chapter 5

Cholesterol Effects on Granule Pools in Chromaffin Cells Revealed by Carbon-Fiber Microelectrode Amperometry

List of Tables

List of Figures

Chapter 1

Chapter 2

Chapter 3

Chapter 4

Chapter 5

List of Abbreviations and Symbols

ACD: acid citrate dextrose

ATP: adenosine triphosphate

CFM: carbon-fiber miroelectrode

CFMA: carbon-fiber microelectrode amperometry

Drp1: dynamin related protein 1

FSCV: fast-scan cyclic voltammetry

HPLC: high performance liquid chromatography

mdivi-1: mitochondrial division inhibitor 1

MBCD: methyl-β-cyclodextrin

MS: mass spectrometry

OCS: open canalicular system

PF4: platelet factor 4

PRP: platelet rich plasma

SEM: standard error of mean

SNAP 23: synaptosome associated protein of 23 kDa

SNARE: soluble N-ethylmaleimide-sensitive factor attachment protein receptors

TEM: transmission electron microscopy

VAMP: vesicle associated membrane protein

vWF: von Willebrand factor

Chapter 1

Introduction to Platelet Granules and Their Secretion

In part from:

Kim D, Koseoglu S, Manning BM, Meyer AF, Haynes CL. Electroanalytical eavesdropping on single cell communication. *Anal Chem*. 2011;83:7242-7249

1.1. General Overview

Platelets were first described by Osler in the 1870s as “organisms” found in the blood that cause blood to coagulate, and it was not until the early 1900s that they were identified as anuclear cells derived from megakaryocytes in bone marrow.[1] Since then, there has been a massive amount of research performed to understand and demonstrate the function of platelets in many important physiological events. Even though platelets are best known for their role in hemostasis and thrombosis, researchers are now well aware of platelet involvement in inflammation, atherosclerosis, angiogenesis, wound healing, and host defense. Platelets are quite small, with a diameter of 2-5 μm. The average lifespan of a platelet in the blood stream is 7-10 days unless they get activated due to a vascular injury.[1] After circulating for 7-10 days, they are taken up by the reticuloendothelial system. Although they lack nuclei, platelets are highly specialized cells with three different granule types and a special membrane tubular unit known as the open canalicular system (OCS) in addition to the all other organelles that are common in other cell types.[2] There are more than 80 granules present in a single human platelet. α- granules are the most abundant platelet granule type, serving as a storage unit for biologically important proteins, including growth factors, adhesion proteins, and various chemokines. δ-granules contain relatively lower molecular weight ionic and molecular species including Ca^{2+}, Mg^{2+}, ATP, polyphosphate, and the important neurochemical serotonin. The last class of granules found in platelets is lysosomes for endosomal

digestion.[1, 3-5] Platelets are dynamic secretory cells, and they communicate with other cells during important biological processes by secreting granule-stored chemical messengers through a conserved mechanism called exocytosis.[4, 5] Platelet secretion is a crucial step in all the important physiological processes involving platelets. Unfortunately, the actual mechanism of platelet granular storage and secretion is not well understood. Although bulk secretion assays are useful to monitor platelet secretion for diagnostic purposes or to evaluate average platelet behavior in certain physiological conditions, they cannot give any mechanistic information about the secretion event. The small size of platelets and the unique membrane features make them difficult to study with electrophysiological techniques. Recently, the Haynes group pioneered measurement of platelet δ-granule secretion at the single cell level by using carbon-fiber microelectrodes and enabled the detailed analysis of platelet secretion from each individual granule with sub-ms time resolution.[6-8] This opened the possibility of studying the effect of membrane proteins and lipids that are involved in platelet exocytosis and filling important gaps in our current understanding of platelet secretion.

1.2. Platelet Granules

TEM images of platelets show the presence of three different granular structures in a single platelet. α-granules constitute the largest granule population in platelets and can be identified in transmission electron micrograph (TEM) images

based on their round shape and uniform dark color (Figure 1.1). [9] Immunofluorescence can also be used to monitor α-granules by labeling certain resident proteins. However, recent evidence showed that heterogeneity of the constituents of the α-granules may not allow visualization of all the α-granules present in platelets by immunofluorescence. [10, 11]

α- granule formation initiates in megakaryocytes whereas development and maturation continues both in megakaryocytes and formed platelets. Formation of the α-granules within megakaryocytes occurs via two different mechanisms: endogenous synthesis and endocytosis. In the synthetic pathway, the proteins synthesized in the endoplasmic reticulum (ER) are transferred through trans-Golgi where the multivesicular bodies are formed and bud off. Alternatively, α-granules can be formed via endocytosis of plasma-bound proteins and targeted as α-granules by the clathrin-coated vesicle pathway. [9, 12] Although most of the α-granule proteins are synthesized in megakaryocytes, including platelet factor 4 (PF4), some of the proteins are taken up by receptor-mediated endocytosis, including fibrinogen and albumin.[13] α-granules store more than 300 biologically active proteins including adhesion molecules, chemokines, procoagulant molecules, growth factors, angiogenic modulators, and fibrinolytic regulators (Table 1.1).[1] Storage of high protein content requires intragranular maintenance of the osmolarity at a level similar to that of the cytosol; this may be achieved via aggregation of the proteins during protein sorting.[9, 12] Normal human platelets contain about 5-7 dense granules (δ-granules) per platelet although the number

of delta granules can be as high as 20 in other species such as rabbit platelets. δ-granules can be identified in TEM images by their bulls eye-like shape, with a dense core and halo region.[1, 14] Initial studies regarding delta granule formation suggested that δ- granules did not propagate from the Golgi network; in fact, they originate from endosomal compartments. Furthermore, recent confocal imaging studies have demonstrated the formation and maturation of the δ- granules from both early and late endosomes, regulated by AP-3, Rab32, and Rab38 proteins. [4, 15]

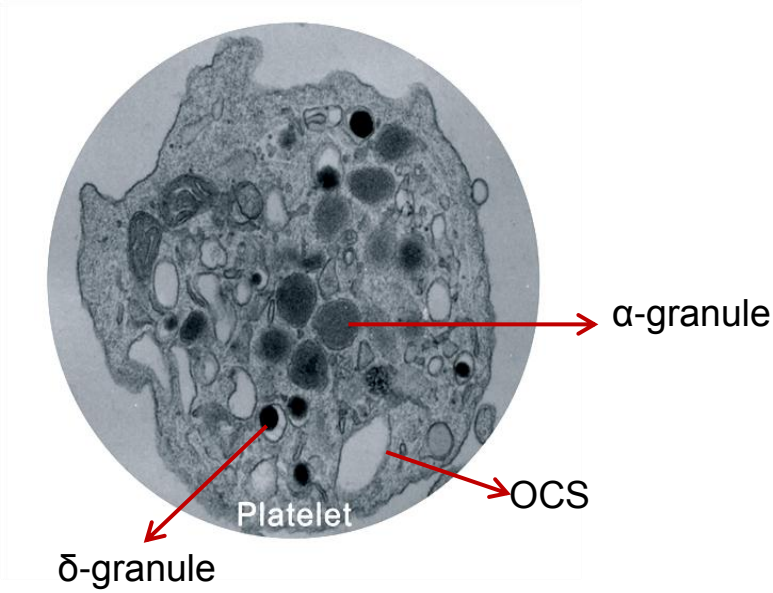

Figure 1.1 TEM image of a platelet. Apparent structural features; δ- and α-granules and OCS are shown with arrows.

The content of δ-granules include ATP, Ca^{2+}, Mg^{2+}, polyphosphate and serotonin, among others, which are up taken by receptor-mediated endocytosis (See table 1.1 for the full list). [1, 6] The pH of the δ- granules is kept around 5.4 by proton pumps that reside on the granular membrane. High concentrations of Ca^{2+} and polyphosphate can be stored in these granules through ionic interactions without disturbing the osmolarity of the granule.

Lysosomes are ubiquitous granules in all cell types. In platelets, lysosomes contain a variety of enzymes, including β-*N*-acetyl-$_D$-hexosaminidase, proline carboxypeptidase, and cathepsins. Although there have not been many studies performed on lysosomal function in platelets, they may act as endosomal digestion unit as they do in nucleated cells. [1, 16]

1.3. Platelet Granular Release

Platelets are dynamic secretory cells and, similar to neurons and chromaffin cells, platelets secrete their granular content via exocytosis.[4, 5, 17] Upon activation, intracellular Ca^{2+} concentration increases which leads to docking of the granules and fusion of granular and plasma membrane facilitated by a class of anchoring proteins called SNARE (soluble N-ethylmaleimide-sensitive factor attachment protein receptor) proteins (Figure 1.2). Some of the soluble granular contents start to diffuse from granules into the extracellular matrix. As the fusion pore loses its stability and starts to expand, the exchange between granular

content and extracellular matrix acts as a driving force to further extrude granular content.

Table 1.1 A partial list of platelet granule content [1]

α-Granule	Adhesion molecules	P-Selectin, von Willebrand factor, fibrinogen, fibronectin, integrin αIIbβ3,
	Chemokines	Platelet factor 4, β-thromboglobulin, CCL3, CCL5 (RANTES), CXCL5, CXCL8
	Coagulation pathway	Factor V, multimerin, factor VII
	Fibrinolytic pathway	α2-Macroglobulin, plasminogen, plasminogen activator inhibitor 1
	Growth and angiogenesis	Basic fibroblast growth factor, epidermal growth factor, hepatocyte growth factor, vascular endothelial growth factor C, platelet growth factor
	Immunologic molecules	β1H Globulin, factor D, c1 inhibitor, IgG
	Other proteins	Albumin, α_1- antitrypsin, Gas6, histidine rich glycoprotein, high molecular weight kininogen, osteonectin protease nexin-II
δ- Granule	Ions	Ca, Mg, P, pyrophosphate
	Nucleotides	ATP, GTP, ADP, GDP
	Membrane proteins	CD63 (granulophysin), LAMP2
	Transmitters	Serotonin
Lysosomes		Cathepsin D and E, β-*N*-acetyl-$_D$-hexosaminidase, proline carboxypeptidase

However, as has been recently shown by Ewing and coworkers, even at the stage commonly known as “full fusion” in which the complete fusion of granular and plasma membrane takes place, not all the content of the granules is secreted. [18] In fact, PC12 cells, a model primary cell line for neural secretion, only release 40% of their content. Although such analysis has not been done for platelet granular release, comparison of the released serotonin to total serotonin content with bulk HPLC measurements suggests that platelets also release only a portion of their granular content. Moreover, initially formed fusion pores may pinch closed, allowing only limited chemical messenger release known as kiss-and- run exocytosis. [7, 19] Unlike other secretory cells, platelets can also secrete their content by fusion of the granules to the OCS.[20] This brings up the question of if the platelets are “smart” secretory cells and how their granular secretion is regulated. Although the mechanism of platelet granular secretion is not well understood, it is clear that there are multiple levels that control the extent of secretion.[21] One of the key steps involved in exocytosis is the fusion of the granular membrane with the plasma membrane. Recent evidence in the literature shows that fusion pore stability regulates not only the mechanism but also the quantity of molecules secreted.[22-25] Moreover, fusion pore diameter can act as a physical barrier, allowing only the molecules below a certain size to move into the extracellular space. Although the actual structure of the fusion pore is under debate, it is clear that both protein and lipid membrane components play an active role in the formation and regulation of the membrane fusion site.

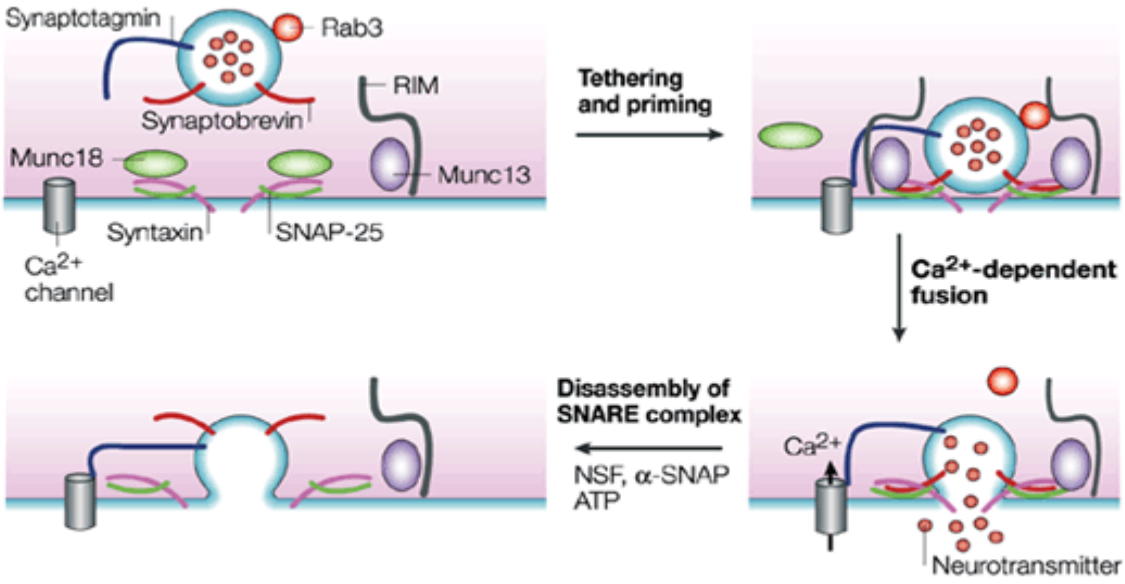

Figure 1.2 Steps of exocytosis. [21]

1.3.1 Membrane Proteins

Although the granular and plasma membranes in platelets, both critically important in secretion, are mostly composed of lipids, membrane proteins play a central role in facilitating the membrane mixing process. Similar to many secretory cells, platelets use SNARE machinery for membrane fusion. The SNARE proteins that reside on the granular membrane are called vesicle associated membrane proteins (VAMPs) or synaptobrevins.VAMP2, 3, 7 and 8 constitute the VAMP proteins of platelet secretory machinery.[26-28] The relative importance of the various VAMP proteins during platelet exocytosis has been studied using a variety of genetic knockout mice. Deletion of the VAMP2 and VAMP3 gene did not cause any secretion defect in platelets. However, defects in secretion and aggregation were observed with VAMP8-/- (VAMP 8 double knockout) platelets with low concentration thrombin stimulation. [27, 29, 30] The platelet secretion defect in the VAMP8 knockout platelets was rescued when higher concentration thrombin stimulation was applied, implying that other VAMP proteins compensate for the lack of VAMP8 at high agonist concentrations. Moreover, impaired VAMP8-/- platelet secretion resulted in compromised thrombus formation in mice with laser-induced injury. [26, 27] VAMP7 is unique as it is the only VAMP with a N-terminal profilin-like domain. Recent work from Flaumenhaft group demonstrated that VAMP7 is mainly found on α-granule surfaces and it plays a central role in granule relocalization during platelet spreading. Granules expressing normal VAMP3 and VAMP8 move toward the

center of the platelet following activation; however, VAMP7-expressing granules reside at the platelet periphery.[28]

The cell membrane-associated SNARE proteins (also known as t-SNAREs) found in platelets are syntaxin-2, -4, -7, -11 and SNAP23, 25 and 29.[4, 31-33] Currently, there is no known effect of syntaxin-7 on platelet granule release; however, antibody-based work focused on syntaxin-2 and syntaxin-4 showed that syntaxin-2 was required for release of all granule types in platelets and syntaxin-4 was crucial for release of α-granules and lysosomes. Due to the inconsistencies in the results from different groups, the Whiteheart group (Haynes group collaborator who prepares SNARE knockout mice) recently revisited the role of syntaxin-2 and -4. They saw normal release behavior from syntaxin-2-/-, syntaxin-4-/- and syntaxin-2,-4 double knockout mouse platelets, arguing that, in fact, none of these syntaxin isoforms are required for normal platelet exocytosis.[32, 34, 35]

In addition to SNAREs, platelets also have Ca^{2+}-binding proteins that are shown to regulate exocytosis. In neurons and chromaffin cells, Ca^{2+}-binding proteins have been identified that regulate SNARE assembly and fusion pore formation. Synaptotagmins are major regulators of the fusion pore feature both based on interaction with t-SNAREs and also with phosphatidylserine (PS), which is known to regulate membrane curvature.[36, 37] Synaptotagmin-like proteins (Slp) 1 and 4 are found in platelets. Neumueller et. al. showed that Slp1 binds to Rap1GAP2 in platelets although Slp1 appears to have the opposite effect on platelet δ-granule

release as that seen in chromaffin cells.[38] Addition of Slp1 to permeabilized platelets inhibits δ-granule release in a dose-dependent manner whereas Rap1GAP2 addition facilitates δ-granule release. Addition of Slp1 and Rap1GAP1 together does not change the inhibitory effect of Slp1 on platelet δ-granule release, implying that although Slp1 binds to RapGAP1 in platelets, this interaction does not play a role inhibiting Slp1. Munc 18 is another SNARE regulatory protein, and it was shown that the inhibition of Munc 18 action attenuates secretion as well.[39]

Although the studies on platelet protein secretory machinery has provided the basis of the regulation of platelet secretion knowledge, a more detailed analysis is required even for the proteins that has not shown any effect on platelet secretion. It is possible that those proteins may control the kinetics of the release but not the quantity, a characteristic that cannot be detected with traditional bulk assays.

1.3.2 Membrane Lipids

Phospholipids constitute the major lipids of the cell membrane, and they are asymmetrically distributed. In resting conditions, phosphatidylethanolamine (PE) and phosphatidylserine (PS) reside largely on the inner leaflet of the plasma membrane whereas the outer leaflet is dominated by cholinephospholipids, including phosphatidylcholine (PC) and sphingomyelin (SM).[40, 41] Exocytosis, a process that relies on asymmetric distribution of phospholipids, causes

redistribution of these phospholipids between the inner and outer leaflets; the arrangement of phospholipid species in the inner and outer leaflet has been shown to regulate both quantity and kinetics of release from PC12 cells (a model exocytotic system).[41] Phospholipids in the membrane regulate fusion pore formation both by changing the curvature of the membrane and by accommodating the proteins that are essential for fusion pore formation. For example, the PS - synaptotagmin interaction is known to regulate fusion pore stability in PC12 cells in a calcium-dependent manner.[40] In platelets, the maintenance of this asymmetric phospholipid distribution has critical physiological implications for hemostasis.[42, 43] For example, circulating platelets maintain the majority of the aminophospholipids (PS and PE) on the inner membrane leaflet, whereas activated platelets rapidly lose their asymmetric phospholipid distribution and elevate otherwise low levels of PS. This change makes the platelet membrane surface negatively charged and presents more catalytically active lipid membrane surface for hemostatic purposes.[43, 44] The dynamic platelet activation-induced phospholipid redistribution occurs during platelet secretion but secretion has not been monitored with controlled or characterized phospholipid composition.

In addition to phospholipids, cholesterol is a ubiquitous sterol molecule, highly enriched in all mammalian cell membranes and abundant in the platelet membrane.[23, 45-47] Structurally, cholesterol is a short and rigid molecule known to modulate membrane physical properties, including fluidity and elasticity, by

intercalating into the long and flexible phospholipid bilayer. In addition to its structural role in the lipid membrane, cholesterol is widely known to play versatile roles in various membrane-based cellular processes. For platelets, cholesterol is clearly a molecule of physiologic importance and known to regulate various aspects of platelet functions in the blood stream, including the tendency for aggregation.[45] In fact, previous studies have clearly shown that the abundance of platelet cholesterol is closely tied to the reactivity of circulating platelets in the blood stream. Hypercholesterolemia is often considered a high risk factor for various diseases, including stroke and heart attack. It is widely recognized that platelet cholesterol plays critical roles in various normal and dysfunctional platelets. Several recent studies on non-platelet secretory cells have clearly indicated that membrane cholesterol plays a vital role in the delivery of various chemical messengers, such as insulin from β-cells and neurotransmitters from neurons.[48, 49] Mechanistic investigations have shown that cholesterol not only spatially organizes the exocytotic SNARE complex in the lipid membrane, likely by forming cholesterol-enriched microdomains or lipid rafts, but also actively regulates the membrane fusion process during granule secretion on the basis of its physical character.

1.4. Importance of Platelet Granular Secretion in Physiological Events

Undoubtedly, platelet secretory function is critical for not only hemostasis but it is involved in many physiological events including thrombosis, inflammation and

malignancy. Herein, the contribution of platelet secretion to each of these events is summarized.

One major function of platelets is to stop bleeding upon vascular injury. The pathology of the hemostatic function of platelets is called thrombosis, wherein overactive platelets cause inappropriate clot formation that can lead to stroke and heart attack. Bleeding disorders encountered with α- and δ- granule release deficiencies (α-granule deficiency is called gray platelet syndrome; Hermansky-Pudlak syndrome and Chediak Higashi syndrome are associated with the absence of δ-granules) prove that the secretory function of platelets is crucial for hemostasis.[50] Upon a vascular injury, subendothelial extracellular matrix, which contains VWF, laminin, thrombospondin, and fibronectin, is exposed and binds platelet receptors to promote platelet adhesion and secretion.[50] Although the role of platelet α-granules in hemostasis is not clear, the stored VWF and fibrinogen not only enhance the adherence of the platelets with each other but also enables the recruitment of more platelets to the site of the injury. α- granules also store coagulation factors that are essential for formation of a stable clot.[50] Platelet δ granules are the main players in hemostasis. Both serotonin and ADP are platelet agonists which enable the activation and recruitment of additional circulating platelets.[3, 14, 51] Moreover, recent evidence shows that polyphosphate found in platelet δ-granules also acts as a procoagulant.[52]

Platelets participate in both immune and inflammatory reactions by secreting important mediators from α- and δ- granules that target the cells of the innate and

adaptive immune systems.[53] TNF-α produced during early stages of inflammation promotes fibrin and thrombin formation and activates platelets. Activated platelets contribute to inflammatory action by secreting proinflammatory cytokines and chemokines, including P-selectin, CD40L, interleukin-Iβ, RANTES, PF4, and β-thromboglobulin.[12, 53] During atherosclerosis, a typical example of chronic inflammation, platelets secrete P-selectin and VWF that are involved in atherosclerotic lesion development.[3, 53] As immune cells, platelets help monocyte recruitment and neutrophil adhesion and degranulation by releasing PF4 and β-thromboglobulin. Platelet δ- granule polyphosphate has been shown to induce vascular leakage and edema formation in vivo.[52]

Rapid tumor destabilization in the case of thrombocytopenia (low platelet count) evidenced that platelets are required for tumor stability. P-selectin mediates direct interaction of platelets with tumors and initiates platelet-tumor aggregation. Tumor cells use platelets like a Trojan horse and hide from immune cells this way. In fact, platelet growth factor (PGF) secreted from platelet α-granules promotes tumor growth. Moreover, the angiogenesis factors secreted from α-granules mediate tumor angiogenesis, growth and metastasis.[12, 54] The mitogenic effect of serotonin secreted from platelet δ-granules has also been shown in variety of cancer types.[55]

Involvement of platelet granule secretion in variety of physiological events makes the studies on platelet secretory dynamics important to reveal the fundamental underpinnings of disease.

1.5. Common Methods Used to Assess Platelet Granular Storage and Secretion.

In addition to basic research interest, platelet granular secretion is routinely analyzed for diagnosis and for monitoring the prognosis of a disease in clinics. Either P-selection expression or ELISA assays are used to analyze α- granule release. Platelet delta granule release is commonly monitored by measurement of released ATP/ADP or radiolabelled serotonin.

P-selectin secreted from platelet α-granules is expressed on the surface of the platelets and thus, can be labeled by using a fluorophore-conjugated P-selectin antibody for flow cytometry analysis.[56] Although this method is useful for quantitative analysis, it does not provide any information about the kinetics of the release event. ELISA is an alternative to flow cytomety for α-granule analysis; for instance, there is a commercially available PF4 ELISA assay that is commonly used. Although both of these methods are precise and accurate, they require long sample preparation and incubation times and a lot of pipetting.

Secretion of serotonin from platelet δ-granules is often monitored following incubation with radiolabelled serotonin, [^{3}H]-serotonin or [^{14}C]-serotonin, for about 1 hour.[56] Secretion of the platelets upon activation with an agonist is measured via scintillation measurements. The results are recorded as percent release where unstimulated samples are used as basal controls.

[(Sample-mean basal)/ (mean total-mean basal)]X100=% 5-HT release.

One of the drawbacks of this method is that it only measures the release of the radiolabelled serotonin that was taken up by platelets (rather than an endogenous species), and thus it does not provide information about granular storage. A luciferin-luciferase assay can also be used to measure ADP/ATP release to monitor δ- granule secretion.[56, 57] Conversion of the luciferin to oxyluciferin is a common example of chemoluminescence and catalyzed by ATP; thus, this reaction is used for the detection of the ATP from platelet δ-granules. For the detection of ADP, pyruvate kinase/ phosphoenolpyruvate (PK/PEP) is added to the system which converts ADP to ATP. Any increase in the luminescence output upon addition of (PK/PEP) is used for the analysis of ADP. This assay is very sensitive and allows the measurement of ADP at picomolar levels.

β-hexosaminadase is a lysosomal enzyme that catalyzes the hydrolysis of N-acetylglucoseamines and N-acetylgalactoseamines. To detect the lysosomal release from platelets, nitro-phenyl derivatives of N-acetylglucoseamines and N-acetylgalactoseamines are used as a substrate for the β-hexosaminadase-catalyzed formation of nitrophenol.[58]

1.6 Single Cell Study of Platelet δ- Granule Secretion

Ensemble measurements of platelet secretion provide useful insights about platelet secretion behavior under certain conditions. The main weakness of bulk measurements is that they average the parameters, making it impossible to

characterize heterogeneity in cellular function. Moreover, the molecular dynamics of cell function is often not accessible with these techniques.[59, 60] Ensemble measurements of cellular function are often performed with the cell densities ranging from 10^3-10^7cells/mL and may require large sample volumes. Assessment of the cellular function at the single cell level is gaining popularity due to the advantages it provides over ensemble cellular assays. The main advantage of single cell analysis is that it enables the identification of the distribution of cell behaviors and identification of outliers that reflect the diversity of cellular function.[59, 61] Since measurement from a single cell type in a mixture of cells is possible, tedious sample preparation and purification procedures are not required. Single cell analysis often enables real time analysis of the cellular function and provides mechanistic insights. Due to their small size, single platelet measurements are challenging. However, recent advances in single cell microelectrochemical analysis of platelet serotonin release from δ- granules made measurement of platelet secretion at the single granule level, with sub-ms time resolution, possible.

1.7 Carbon Fiber Microelectrochemistry

The use of carbon as an electrode material was first popularized by Ralph Adams in the 1950s. [62] Since its inception, carbon has been a popular choice for electrochemical applications, as carbon electrodes demonstrate a wide working potential window, stable background currents, low noise, and high sensitivity.

The development of carbon electrodes with active surfaces on the scale of several micrometers introduces several additional advantages. For voltammetry experiments, microelectrodes offer the ability to observe diffusion-limited currents at high scan rates and thus provide very fast time resolution. The small surface area of microelectrodes enables the use of high scan rates with relatively low background currents. Because of the small number of molecules that must be detected at the single cell level, however, most electrochemical measurements made with carbon microelectrodes produce currents in the nanoampere or picoampere range, depending on the method used. These current levels require electrodes that are both sensitive and exhibit low levels of noise, and carbon microelectrodes meet both of these criteria. Conveniently, using microelectrodes requires only a two electrode system, as such low currents render the use of an auxiliary electrode unnecessary. Perhaps most importantly, microelectrodes provide much greater spatial resolution, and thus permit electrochemical measurements to be made from single cells.[63] Although other forms of carbon can also be used to fabricate microelectrodes, carbon fiber microelectrodes (CFM) are often favored because they can be fabricated in large quantities and are relatively inexpensive. R. Mark Wightman and co-workers first demonstrated the utility of carbon fiber microelectrodes for the detection of exocytosis from single cells in 1990.[64] Carbon-fiber microelectrodes of different geometries are used depending on the intended application; for single cell electrochemical techniques, beveled and polished disk microelectrodes are most widely used.

While Wightman's initial demonstration explored exocytosis from chromaffin cells, the cells responsible for the release of electroactive adrenaline, exocytosis is highly conserved across several cell types including neurons, chromaffin cells, platelets, and a variety of immune cells such as mast cells and macrophages. Accordingly, the technique has the capacity to reveal critical mechanistic details about exocytosis in these cell types, providing new insight into the fundamental behavior of normal and dysfunctional secretory cells.

Electrochemical methods using carbon-fiber microelectrodes (CFMs) are the gold-standard for studying single cell exocytosis. Carbon-fiber microelectrode amperometry (CFMA) and fast scan cyclic voltammetry (FSCV) are the most widely used methods, as they allow the direct measurement of secreted molecules without damaging cells or interfering with endocytosis, which is a common issue in capacitance-based measurement methods such as patch-clamp techniques.[65] In FSCV, individual voltammograms are obtained by repeated application of triangular waveform scans through a range of potentials at regular intervals.[18, 66-72] Any electroactive species that can be oxidized/reduced in the potential window are monitored "simultaneously". Each scan starts with the electrode placed on a single cell and held at a resting potential to relax the diffusive layer at the electrode tip. Potential sweep in a positive direction results in an oxidative peak in the trace. The potential then comes back in the negative direction, and if the species has a reversible redox process, it results in a reduction peak in the voltammogram. The amplitude of the current signal

depends on the number of analyte molecules diffusing to the electrode surface.[66] As the scan rate is hundreds of volts per second, a large background current occurs during the measurement.[69, 72] This background current is relatively stable for CFMs and can be subtracted from later scans.[69] In single cell exocytosis studies, time-resolved chemical changes in the local environment of the electrode tip are obtained for each scan as the cell of interest is stimulated. Voltammograms obtained before stimulation of the cell are subtracted from voltammograms containing information related to the local chemical change after stimulation. This method provides chemical identification of oxidized/reduced species and also can be used to monitor multiple electroactive species simultaneously based on their oxidation potentials.[70, 71] Accordingly, FSCV is most commonly used to identify molecules secreted from a cell. The temporal resolution of single cell FSCV measurements can reach the 100 ms level,[72, 73] limiting insight into the real-time kinetics of exocytosis; as a result, CFMA is commonly employed as a complementary technique for in-depth exocytosis kinetics studies. In CFMA experiments, a constant potential sufficient to oxidize/reduce the chemical messenger of interest is supplied at the tip of CFM.[63, 65, 74, 75] Current at the electrode tip is monitored as a function of time. Oxidative current from the analyte at a positive potential is monitored while detection of reductive current at a negative potential can be troublesome due to the interference from oxygen. Upon stimulation of a single cell, exocytotic behavior of the cell is revealed as current spikes that represent vesicles/granules

of chemical messenger molecules stored in a quantal fashion, meaning that the concentration in each granule is approximately the same.[76, 77] Each spike may represent one granule but it is also possible, though statistically improbable, to simultaneously detect multiple granules. As electron transfer is faster than diffusion of chemical messengers to the electrode surface, redox reactions occurring at the electrode are limited by diffusion of chemical messengers.[63, 76] This allows the CFMA method to achieve sub-millisecond temporal resolution and enables real-time monitoring of exocytotic events. In an amperometric trace, each spike has a fast rising and slower decaying phase due to the convolution effects of diffusion and dissociation of chemical messenger molecules.[74] Analysis of various spike characteristics reveals several aspects of exocytosis such as granule release kinetics and membrane properties.[63, 74]

1.7.1 Instrumentation (Experimental Setup)

The experimental setups for amperometry and voltammetry techniques share many common features. CFMs are typically fabricated in-house, and the fabrication methods may vary slightly by laboratory. Generally, a single carbon fiber with 5-10 μm diameter is aspirated into a glass capillary, which is then pulled using a capillary puller that applies thermal and magnetic fields. With the use of a microscope, the extruded carbon fiber is cut back as desired depending on application. The carbon-fiber is next sealed in the capillary using epoxy resin for insulation and cured at high temperatures (100-150 ºC). Prior to

electrochemistry experiments, cured electrodes are polished at 45º (angle can vary depending on applications) using a micropipet polisher and stored tip-down in isopropyl alcohol to remove any surface contaminants. A typical instrument for CFMA and FSCV techniques includes a working electrode (the CFM) and a reference electrode (often a purchased Ag/AgCl electrode). Both the CFM and the reference electrode are connected to the potentiostat that controls the voltage between electrodes. Because currents due to the contents of single granules are quite small (nanoamp to picoamp level), a low-noise measuring device or patch-clamp amplifier is often employed between the CFM and the potentiostat. Usually, the cells of interest are cultured in a Petri dish and are placed in a culture dish warmer to maintain physiological temperature. An inverted microscope is used to visualize cells and the position of the CFM. For cell stimulation, a pulled capillary containing stimulant is connected to a pressure-driven flow controller and positioned near the cell of interest. Positioning of the carbon fiber microelectrode (adjacent to the single cell) and stimulating pipet is accomplished using piezoelectric micromanipulators (Figure 1.3).

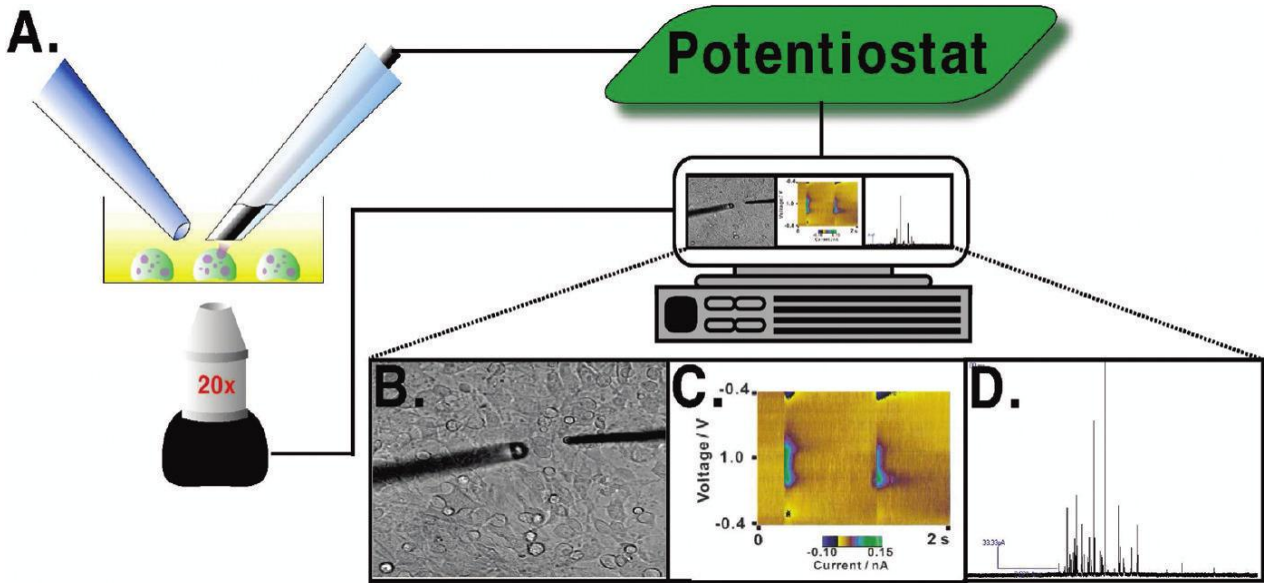

Figure 1.3 Instrumental setup for a CFM electrochemistry experiment. (A) CFM (right) is p laced on a single cell with the stimulating pipet (left) near the cell. (B) Bright field image of the experimental setup showing the CFM and stimulating pipet positioned on a single mast cell. (C) Representative color plot obtained by FSCV. (D) Representative amperometric trace obtained using CFMA on a mast cell.[19]

1.7.2 Sensitivity, Selectivity, and Resolution

With regard to sensitivity and selectivity, the chemical messengers that are most commonly analyzed using CFM have an adsorption affinity for the carbon surface. As more adsorption of analyte onto the electrode surface occurs, measured current increases at the cost of temporal resolution.[67, 68, 78] Adjusting the potential range, especially the resting potential in FSCV measurements, can control adsorption.[67, 68, 79] Carbon electrode surface coatings have been used to increase selectivity and sensitivity of the measurement for specific chemical messengers, but these methods add another physical layer for analyte to diffuse through, sacrificing temporal resolution. The dimensions of the CFM can also significantly influence the measurement; small diameter CFMs significantly reduce the number of superimposed spikes in a trace but it also reduces the total number of events detected.[80] In summary, there are the expected trade-offs between sensitivity, selectivity, and resolution when performing CFM measurements but adjusting the parameters mentioned above will facilitate optimal outcomes.

1.7.3 FSCV Data Analysis

In FSCV, properties of detected molecules, such as electron transfer rate, stability, and carbon adsorption affinity, contribute to the CV shape, peak position, and the ratio of forward and reverse peak intensities; therefore, confirmation of the identity of chemical messengers from single cells by FSCV is normally done by comparing obtained voltammograms to those of control

solutions.[74, 76, 81] FSCV data is often represented in the format of a color plot where voltammograms (current versus potential) obtained as a function of time are stacked together with time on the x-axis, potential on the y-axis, and current coded in false color (Figure 1.4B). In this color plot format, identification of a specific chemical messenger is done by extracting individual CVs and comparing them to standards. Identity of a chemical messenger is then confirmed using a calculated correlation coefficient, and once identified, quantification is done by measuring the peak current and comparing the value with the values in a calibration curve previously prepared. As shown in Figure 1.4B, this color-plot representation facilitates visualization of the redox reactions occurring over the entire measurement period in one 2-D plot and has been widely used to interpret FSCV data, though not those measured from complex mixtures. Addressing the difficulty of complex mixture detection, the Wightman group has recently employed chemometric methods such as principal component analysis and principal component regression to identify feature variation within voltammograms and has successfully resolved and quantified nine components in a mixture.[72, 82]

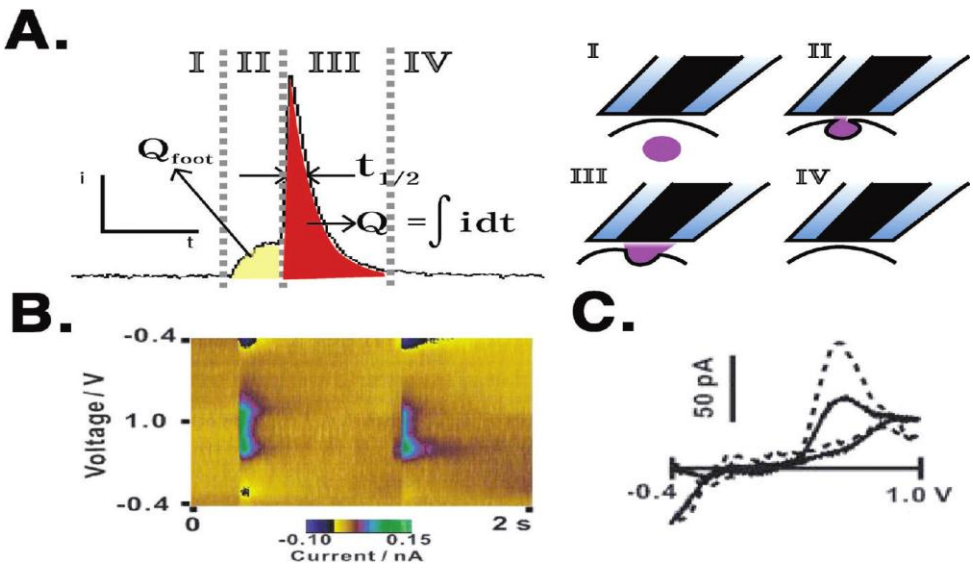

Figure 1.4 (A) Correlation of spike parameters and phases of exocytosis. (B) Example false color plot of serotonin release from a platelet. (C) Voltammogram obtained from serotonin release of a single platelet (solid line) and serotonin standard solution (dotted line).[19]

1.7.4 Spike Determination and Analysis in CFMA

After amperometric traces are obtained, the data analysis first requires identifying spikes and the corresponding baseline current. Usually, the root-mean-square current noise is measured before cell stimulation, and the spike detection threshold is set using a multiple of the measured noise.[83] In the case of overlapping spikes or spikes with abnormal shape, spikes are visually selected. Upon baseline determination and spike selection, each trace is analyzed for basic spike parameters to characterize single cell exocytosis. The area underneath individual spikes (Q), full-width at half-maximum ($T_{1/2}$), and frequency of spikes in a trace (f) are commonly used as basic spike parameters to describe each cell's exocytotic behavior (Figure 1.4).

Applying Faraday's law, the number of moles of detected redox-active species (N) can be quantified. $T_{1/2}$ yields kinetic information about the time required to release a granule's chemical messenger content.[74] f is a measure of the granule release pattern of a single cell upon stimulation, and it provides information about how granules are recruited to the plasma membrane during exocytosis. These parameters are reliably used to quantify the exocytotic processes of single cells under various circumstances.[74, 83, 84] As maximum exocytosis of a granule generates a fast rising slope and slower decaying slope in a spike,[74] several additional kinetic parameters can be extracted from each spike, including T_{rise}, time spent from 10% to 90% of maximum intensity in the rising phase, and T_{decay},

time spent from 90%to 10% of the maximum intensity in the decaying phase.[63] T_{rise} is especially interesting as it provides important information about the kinetics of the release event, such as the rate of dilation of the fusion pore to the full exocytosis state immediately following granule-cell membrane fusion and dynamics of molecules escaping the matrix that they are stored in.[85, 86] The flux of redox-active chemical messengers before full exocytosis results in a characteristic prespike feature known as a prespike foot.[74, 83] Prespike foot features, which were first investigated by Chow and co-workers, are diverse in magnitude, duration, and shape, yielding information about the dynamic nature of the fusion site.

Analysis of prespike foot features often includes consideration of the number of spikes preceded by a foot event, charge within the foot portion of the feature (Q_{foot}), and duration of the foot before full exocytosis occurs (T_{foot}) relative to the corresponding value for the full exocytosis spike since, for a given condition, the portion of the messengers released through the fusion pore should be similar.[23, 73] While much insight is accessible through detailed foot analysis, the analysis methods are not nearly as well established as those for full exocytosis amperometric spikes. Standard statistical procedures are used to compare the mean amperometric trace characteristics for different populations of single cells.[63, 79]

Class of Cell	Cell Type	Chemical Messenger (Detected by CFM)	Molecules per Granule (zeptomoles)†	Reference
Neuroendocrine/Endocrine Cells	Adrenal Chromaffin	Epinephrine,	5,000-10,000	63, 64
	Pancreatic β-Cell	norepinephrine	600	87
		Insulin		
	Melanotrophs	α-melanocyte stimulating	320	88
		hormone		
Neurons	Retinal Amacrine	Dopamine	8-170	89
	Somatic Leech	Serotonin	7.8	90
			13.3	90
	Superior Cervical Ganglion	Dopamine	58	91
	Cultured Midbrain	Dopamine	5^{92}	92
Hematopoetic	Mast Cells	Serotonin, Histamine*	1.24×10^{6} **	93
	Platelets	Serotonin	1000	94
	Dendritic Cells	Serotonin	49.8 – 215.9	95
Immortal Cell Lines	PC-12	Dopamine	190	96
	MN9D	Dopamine	82	97

*Histamine is co-stored and co-secreted with 5-HT, but has yet to be quantified per granule, due to the concomitant oxidation of serotonin at potentials sufficient to oxidize histamine.
**Zmol serotonin in table refers to mast cells cultured alone. When co-cultured with fibroblasts, mast cell secretion of serotonin per granule increases to 1×10^{7} zmol.[93]
†The oxidations of epinephrine, norepinephrine, dopamine and serotonin are two electron processes. The oxidation reaction of histamine has yet to be conclusively deciphered. For insulin and α-melanocyte stimulating hormone, although several oxidizable moieties are present, the oxidation reactions for the two proteins in Table 1 are two electron processes.

1.7.5 Chemical Messengers and Cell Types

As many cell types release electroactive chemical messengers stored within granules through exocytosis, FSCV and CFMA have been used to monitor these important biological processes. Table 1.2 provides an overview of the cell types and secreted chemical messenger species that have been examined with CFMA and FSCV on the single cell level, and more detail regarding electroactive chemical messengers and the cells from which they are secreted is provided here.

Adrenal chromaffin cells are neuroendocrine cells located in the central layer of the adrenal gland and are of interest because of their role in the fight-or-flight response.[63, 64, 98] Additionally, the similarities between chromaffin cells and neurons make chromaffin cells a good model for studying exocytosis.[64] The first effort in monitoring single cell exocytosis was performed using stimulated single bovine chromaffin cells, confirming that epinephrine and norepinephrine are co-stored and released during chromaffin cell exocytosis, with an oxidation to an *o*-quinone at approximately +460 mV and reduction at approximately 150 mV vs Ag/ AgCl. However, because of the structural similarities of norepinephrine and epinephrine (Figure 1.5A,B), discrimination of these two compounds was only achieved at a very high potential (+1400 mV vs Ag/AgCl) where the oxidation of the secondary amine of epinephrine was observed.[71] This approach revealed that some chromaffin cells store either epinephrine or norepinephrine while

others store both. Norepinephrine and epinephrine have been similarly detected from murine and rat adrenal medullary cells. Melanotrophs are neuroendocrine cells located in the pituitary gland that secrete α-melanocyte stimulating hormone (α-MSH).[88] Kennedy and colleagues detected peptide exocytosis from rat melanotrophs, and used both CFMA and FSCV to probe the exocytosis of these cells. Their results indicated that the oxidation of α-MSH was the primary source of the amperometric spikes.

As communication between neurons is achieved through exocytosis, the chemical signaling among neurons with a variety of origins and functions are of broad interest. Both dopaminergic and serotonergic neurons have been isolated and examined with CFMA. Zhou and Misler isolated cervical ganglia from rats, cultured individual dopaminergic and serotinergic neurons, and used CFMA to record amperometric spikes, the amplitudes of which were approximately 1% of the amperometric spike amplitudes of chromaffin cells.[91] Sulzer and co-workers detected dopamine exocytosis from cultured midbrain neurons of rat pups.[92, 99] Dopamine has also been detected from retinal amacrine cells, which are dopaminergic neurons located in the retina, by Wightman and colleagues. Serotonergic leech neurons, called Retzius cells, have also been isolated and examined with CFM techniques.[90, 100] Retzius cells are large (80 μm diameter) and can be cocultured with a receptor cell to form a serotonergic connection. Bruns and Jahn used CFMA to examine the exocytosis of both large dense core granules and small clear granules from isolated Retzius cells.[90]

Mast cells are a tissue-bound granulated cell found in organs as diverse as skin, brain, lungs, and connective tissue. These cells have a complex function in the immune system, providing a line of defense against parasitic organisms but also playing a primary role releasing mediators of allergic response. Millar and co-workers used FSCV to detect exocytosis from single mast cells and to identify the substance exocytosed as serotonin.[101] De Toledo et al. used amperometry as well as FSCV to probe mast cell exocytosis and determined the amount of serotonin secreted was 1.24×10^{6} zmol/granule.[102] Wightman and co-workers later employed FSCV and CFMA to determine that histamine and serotonin are co-stored in mast cell granules.[103] The CVs of histamine and serotonin each have unique features that were used to discriminate between the two compounds. Histamine release has yet to be detected amperometically due to the concomitant oxidation of serotonin at potentials sufficient to oxidize histamine, but the concentration of secreted histamine has been quantified voltammetrically using its oxidation peak at +1250 mV vs Ag/AgCl.[103]

In addition to primary culture cells, single cell detection of exocytotic events has been achieved from immortal cell lines as well; this is advantageous in that the cells are homogeneous, proliferate in culture indefinitely, and require no animal sacrifice. The most frequency examined cell line is the rat pheochromocytoma (PC12) cell line, which is derived from an adrenal medullary tumor and widely used as a model nerve cell for examining neurochemical processes. Unlike chromaffin cells, PC12 cells have dopamine levels 2-300 times higher than that

of norepinephrine levels.[75, 104] Ewing and colleagues used electrochemical methods to probe the exocytosis of PC12 cells for the first time and established the identity of the exocytosed mediator as dopamine using FSCV.[75, 104]

1.7.6 Fundamentals of Exocytosis Revealed

Beyond the utility of quantitative detection of chemical messengers released from the granules of single cells for fundamental characterization, CFMs have been used to probe more general exocytotic phenomena such as chemical messenger storage and release mechanisms, fusion pore formation, and intragranular matrix swelling. Correlated single cell electron microscopy and CFMA studies have revealed that the concentration of chemical messengers within granules, across cell types, is 0.5- 1.0M, which is much higher than previously thought possible.[105] Most cell granules have two phases: a dense core and liquid halo.

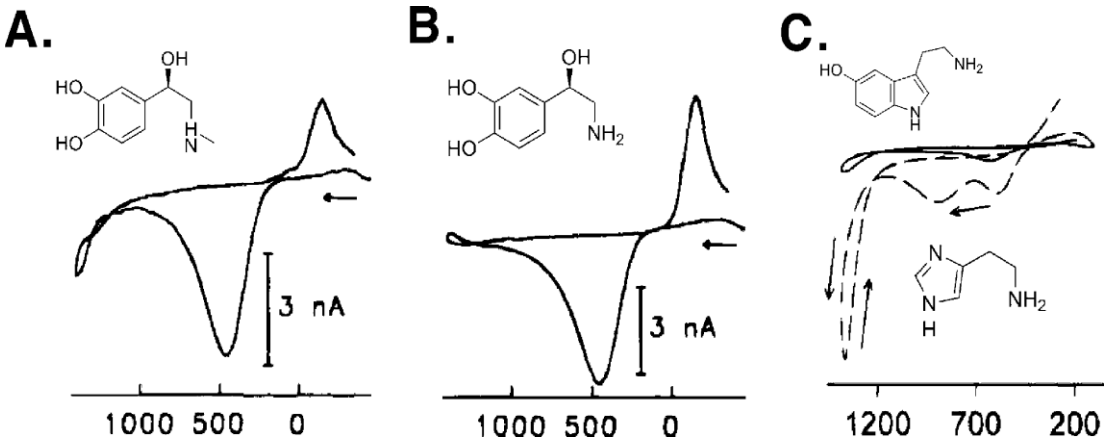

Figure1.5. Molecular structure and cyclic voltammograms of (A) epinephrine, (B) norepinephrine, and (C) serotonin (upper, solid line in the voltammogram) and histamine (lower, dotted line in the voltammogram).[19]

Highly sulfonated biopolymers, such as negatively charged chromogranins in chromaffin cells and heparin and chondroitin sulfate in mast cells, constitute the dense core matrix. Ionic interactions between the matrix and chemical messengers and hydrogen bonding between the two at the acidic granular pH are suggested as the possible driving forces that allow the interior of the granule to be isosmotic with the cell cytoplasm by allowing only a minute amount of chemical messenger solubilized in the halo region. It has been shown that the rate of the release is strongly influenced by the dissociation of the chemical messengers from the matrix in chromaffin and mast cells.[106-108]

As previously discussed, the formation of a fusion pore does not always lead to full exocytosis; in some cases, the fusion pore recloses in a process known as “kiss-and-run” exocytosis. This “kiss-and-run” process may be a method for cells to send a less than quantal signal, and it also represents a more efficient granule recycling process. CFMA experiments show that midbrain neurons release dopamine multiple times from the same granule through this mechanism. Moreover, “kiss-and-run” exocytosis has also been observed in chromaffin, mast, and PC12 cells. While it is likely that swelling and dissociation of the intragranular matrix play a role in determining the fate of the fusion pore,[107, 108] the species or processes that regulate whether a fusion pore reseals or dilates is currently unresolved.

Moreover, CFMA has been used to study the fusion pore stability and regulation. CFMA results show that both membrane proteins and lipids influence the exocytotic process. The previously mentioned SNARE proteins and their subgroups are often implicated in fusion pore formation models. Chapman and co-workers studied the exocytotic release from PC12 cells with genetically altered synaptotagmin using CFMA and concluded that a synaptotagmin-SNARE complex during exocytosis triggers formation of the fusion pore, and subgroups of synaptotagmin (I and IV) regulate the fate of that fusion pore.[25] Amperomety studies accompanied by capacitance measurements on chromaffin cells[109, 110] demonstrated that both synaptotagmin I and VII may act as a Ca^{2+} sensor which regulates the fusion machinery and especially the latter one increases the release through kiss-and-run exocytosis.[25] Moreover, syntaxin (another SNARE protein) has been shown as a necessary component of fusion pore formation and exocytosis. Synaptobrevin and SNAP-25 are the other two SNARE proteins whose function in fusion pore formation and stability is studied.[111, 112]

As some groups explore the role of protein components, others focus on the role of the lipids themselves. The effect of membrane phospholipid components and distribution on exocytosis has been studied using CFMA in both PC12 and chromaffin cells by adding exogeneous lipid species to the membrane.[41, 113] Results showed that phosphotidylserine, phosphatidylethanolamine, sphingomyelin, and phosphatidylcholine influence the exocytotic process either by changing the frequency, quantity, and/or kinetics of release. In addition to

membrane phospholipids, cholesterol is another major species found in the membrane and has both structural and functional importance in exocytosis. It has been shown that SNARE proteins are localized in cholesterol-rich lipid rafts, and removal of cholesterol disrupts these rafts, reducing exocytosis in PC12 cells, chromaffin cells, and platelets.[23, 40] Since cholesterol stabilizes the negative curvature of the fusion pore, removal of cholesterol decreases fusion pore stability, and decreases the percentage of spikes with fusion pore (foot) events.

Although CFMA measurements are a relatively new technique for single cell analysis, platelet CFM measurements have only been performed in the last few years. In 2008,[6] FSCV was used to detect exocytosis of electroactive species from individual rabbit platelets and identify it as serotonin. By maintaining the potential of the electrode at the oxidation potential of serotonin, CFMA was used to explore the biophysical properties of platelet exocytosis with the well-understood serotonin redox reaction both in rabbit and human platelets. In the light of this work and follow-on studies, it is clear that, like other secretory cells, platelets also store granular content in a quantal fashion.[6, 7] CFMA measurements performed at varying pH and osmolarity provided a better understanding of how serotonin is stored and how its secretion is regulated.[7] Moreover, in-depth analysis of varied cholesterol levels in platelet secretion showed that, besides being a ubiquitous lipid for membrane support, cholesterol regulates fusion pore stability during exocytosis via a biophysical, rather than biochemical, mechanism.[23] Although invaluable knowledge has been acquired

since the first CFMA analysis of platelets, there are still a lot of questions to answer.

1.8 Goals and Scope of Thesis

Platelets are specialized secretory cells with three distinct types of granules loaded with important mediators for platelet function. Understanding the mechanism of platelet granular secretion is big interest not only for diagnostic but also for therapeutic purposes. Although ensemble assays that elucidate platelet secretory behavior provide insightful knowledge of platelet function at certain physiological conditions, since their output is the average response of more than millions of platelets, the heterogeneous platelet function is lost in the data. Moreover, the molecular dynamics of cell function is often not accessible with these techniques. Amperometric recording of δ-granule secretion from single platelet brought a new perspective to studying platelet function and enabled analysis of δ-granule exocytosis with sub-ms time resolution. Since then, we learned how serotonin is stored in those granules and how extracellular environment modulate the secretory function. However, there is still a lot to learn. The main motivation of the work detailed in this thesis is to provide in depth understanding of platelet granular secretion by using CFMA.

In chapter 2, I explore the similarities and differences of platelet secretion behavior among the platelets isolated from different species that have structural differences aiming to clarify the role of each component of platelet secretion.

Chapter 3 demonstrates the unrecognized function of (Dynamin related protein 1) Drp1 in platelet physiology. Although Drp 1 is a well-known protein involved in endocytosis, this work showed that Drp 1 also regulates platelet δ-granule secretion and thrombotic function.

Chapter 4 elucidates the function of membrane phospholipids by taking advantage of variety of analytical techniques and study platelet aggregation and secretion at altered phospholipid concentrations.

Chapter 5 compares a very well-studied secretory cell model, chromaffin cells with platelets in terms of the effect of cholesterol in their secretory behavior.

Chapter 2

Comparison of Platelet δ- Granule Secretion from Different Species using Single Cell Measurements

2.1 Introduction

Platelets are an important component of the hemostatic response, and their secretory behavior dictates much of their physiological function. α- granules, δ- granules and lysosomes are the chemical messenger storage units in platelets. While α- granules store important protein species, including adhesion molecules, growth factors, and chemokines, δ- granules supply critical ions and small molecules, including Ca^{2+}, Mg^{2+}, ADP, and serotonin from a polyphosphate matrix. Small numbers of lysosomes are also found in platelets to facilitate endosomal digestion.[1] Similar to neurons, platelets release their granule content via exocytosis.

Although platelets isolated from different species share some common features, there are also both structural and functional differences. [2-4] One of the major differences between platelets from different species is the presence or absence of a membrane-bound tubular system known as the open canalicular system (OCS).[4, 5] Many species, including human, mouse, and rabbit platelets have an OCS whereas horse, cow and camel platelets are known to be devoid of this membrane structure. The OCS is likely an important determinant of granular secretion characteristics, serving as an anchor between the granular and plasma membrane. During exocytosis, granules can either fuse first to the OCS or to the plasma membrane to release their content.[1, 5-7] These two distinct release behaviors may influence both secretion kinetics and the amount of the released chemical messengers. In platelets that have an OCS, different identity or amount

of stimulant may influence the order of membrane interaction, and thus, the secretion pattern. While these variations in chemical messenger delivery behavior will have significant implications in platelet biology, traditional platelet measurement methods, examining thousand to millions of platelets at a time, obscure these subtleties. Herein, we employ a single cell analysis tool, carbon-fiber microelectrode amperometry (CFMA), to reveal serotonin secretion behavior across species and with various stimulants. [8-10]

δ- granule secretion is critical in hemostasis;[11] the procoagulant functions of δ-granule contents, including both serotonin and polyphosphate, have been shown while ADP is known to induce platelet aggregation.[12-14] Recently, CFMA has enabled detailed analysis of platelet δ-granular secretion with sub-ms time resolution, revealing the true kinetics of the secretory process and allowing distinction among heterogenous sets of platelets. [8-10] This study exploits CFMA to evaluate δ-granule release among different species, following exposure to various stimulants, to explore the role of the OCS and facilitate appropriate animal model choice. We considered rabbit and mouse as a model for the platelets with OCS, while cow platelets were examined as a model for non-OCS secretion behavior. In brief, the results show that, compared to mouse and rabbit, cow platelets secrete higher amounts of serotonin in spite of releasing fewer granules per stimulation event. This may indicate a role for the OCS in granular trafficking and docking. Stimulation with ionomycin (which bypasses several steps relevant in physiological platelet stimulation) revealed more uniform

behavior between the OCS and non-OCS species compared to thrombin stimulation. Finally, membrane characteristics, including fusion pore formation and stability, varied among species and stimulants, revealing that the stability of the fusion event is stimulant dependent but that there is no correlation between the fusion pore stability and the presence of the OCS. Identifying the similarities and differences among platelets isolated from different species will facilitate understanding of the biophysical roles of the structural components of platelet secretion.

2.2 Materials and Methods

2.2.1 Isolation of platelets

Blood was collected according to protocols approved by the University of Minnesota IACUC. Mid ear artery was used for rabbit blood draw to EDTA-containing tubes. Mouse blood was collected via cardiac stick with syringes containing ACD. Cow blood was drawn from the tail to EDTA-containing tubes. In all cases, blood was diluted with addition of Tyrode's buffer (NaCl, 137 mM; KCl, 2.6 mM; $MgCl_2$, 1.0 mM; D-glucose, 5.6 mM; N-2-hydroxyethylpiperazine-N'-2-ethanesulfonic acid (HEPES) 5.0 mM; and $NaHCO_3$, 12.1 mM with pH adjusted to 7.3) and centrifuged for 10 min at 500xg for rabbit and cow or 130xg for mouse platelets. The (platelet rich plasma) PRP layer was separated, and washed platelets were obtained following a second 10 min centrifugation step (750xg for rabbit and cow, 500xg for mouse platelets). Pelleted platelets were resuspended in Tyrode's buffer.

2.2.2 CFMA measurements

Carbon-fiber microelectrodes were fabricated as was previously described. [8-10] Amperometry experiments were performed with an Axopatch 200B potentiostat (Molecular Devices, Inc., Sunnyvale, CA) using low-pass Bessel filtering (5 kHz), a sampling rate 20 kHz, and gain amplification of 20 mV/pA, all controlled by locally written LabVIEW software and National Instruments data acquisition boards. Platelets were visually monitored during experiments with an inverted microscope equipped with phase contrast optics (40X magnification) (Nikon Instruments, Melville, NY). A drop of platelet suspension was added to the poly-L-lysine-coated glass coverslips containing Tyrode's buffer. As the platelets sedimented onto the coverslip, a CFM was placed on an individual platelet for measurement (Figure 2.1A). A stimulant-filled fire-polished capillary with an average tapered diameter of 10 µm was also placed close to the platelet of interest. Upon delivery of a 3 s bolus of either 10 U/mL thrombin solution in Tyrode's buffer or 10 µM ionomycin in Tyrode's buffer supplemented with 2 mM Ca^{2+}, the platelet under the microelectrode was activated. Serotonin secreted from platelet δ-granules was oxidized at a potential of 700 mV vs Ag/ AgCl reference electrode, and data were recorded for 90s. Each amperometric trace obtained from single platelet secretion was filtered at 500 Hz, and spike by spike analysis was performed using Mini Analysis program. Temporal resolution of the CFMA technique enables analysis of serotonin secretion from individual platelet granules, each appearing as an individual current spike in the amperometric

trace (Figure 2.1C). The amount of serotonin released from a single granule is determined based on the area under the peak (Q= mFn; where Q is the charge, m is number of moles of serotonin, F is the Faraday constant, and n is the number of electrons (2) transferred during serotonin oxidation). The kinetics of release are revealed based on the T_{rise} and T_{half} values for each current spike, indicating the kinetics of transition from fusion pore to full fusion and kinetics of the total release event, respectively. The number of platelets that were monitored per condition was 23 and 32 for mouse, 35 and 34 for rabbit, and 39 and 22 for cow for ionomycin and thrombin stimulation, respectively.

2.2.3 Bulk HPLC analysis:

Platelets in the PRP were counted and the diluted to $5x10^7$ cells/mL in Tyrode's buffer. 125 µL of the diluted PRP was put into a Millipore 96 well Multi Screen HTS filter plate with a 0.45 µm pore. Then, 125 µL of stimulant was added at twice the desired concentration to account for dilution. After a five minute stimulation, the supernatant was spun down at 3000xg for five minutes, and 180 µL of the supernatant was pipetted into a vial with 20 µL of 5 µM dopamine internal standard in 0.5 M perchloric acid. HPLC analysis was performed on an Agilent 1200 HPLC with an auto sampler containing a 5µm, 4.6 x 150mm C18 column (Eclipse XDB-C18) attached to a Waters 2465 electrochemical detector with a glassy carbon-based electrode. The working potential was set at 700 mV vs. an in situ Ag/AgCl reference electrode with a current range of 50 nA. The samples were sent through the HPLC with a flow rate of 2 mL/min in an aqueous

mobile phase mixture consisting of 11.6 mg/L of the surfactant sodium octyl sulfate, 170µL/L dibutylamine, 55.8 mg/L Na_2EDTA, 10% methanol, 203 mg/L sodium acetate anhydrous, 0.1 M citric acid, and 120 mg/L sodium chloride. The ratio of serotonin to dopamine internal standard concentrations were then measured against a 5 point calibration curve made in advance using standard solutions of serotonin diluted in 0.5 M perchloric acid (ranging from 28 to 1000 nM). The standard solutions were supplemented with 0.5 µM dopamine internal standard.

2.2.4 TEM Measurements

TEM samples of cow and mouse platelets were prepared by two step fixation of the platelets first with 0.1% gluteraldehyde (15 min) followed by centrifugation to pellet and then with 3% gluteraldehyde (30 min) in White's saline as it is previously described. [15] After fixation, the cell pellet was exposed to 1% osmic acid at 4ºC for 1h. The platelet pellets were dehydrated slowly in a graded series of alcohol and embedded in the Epon resin. Thin sections were obtained with a diamond knife. Uranyl acetate was used for contrast enhancement. TEM images were analyzed by using ImageJ.

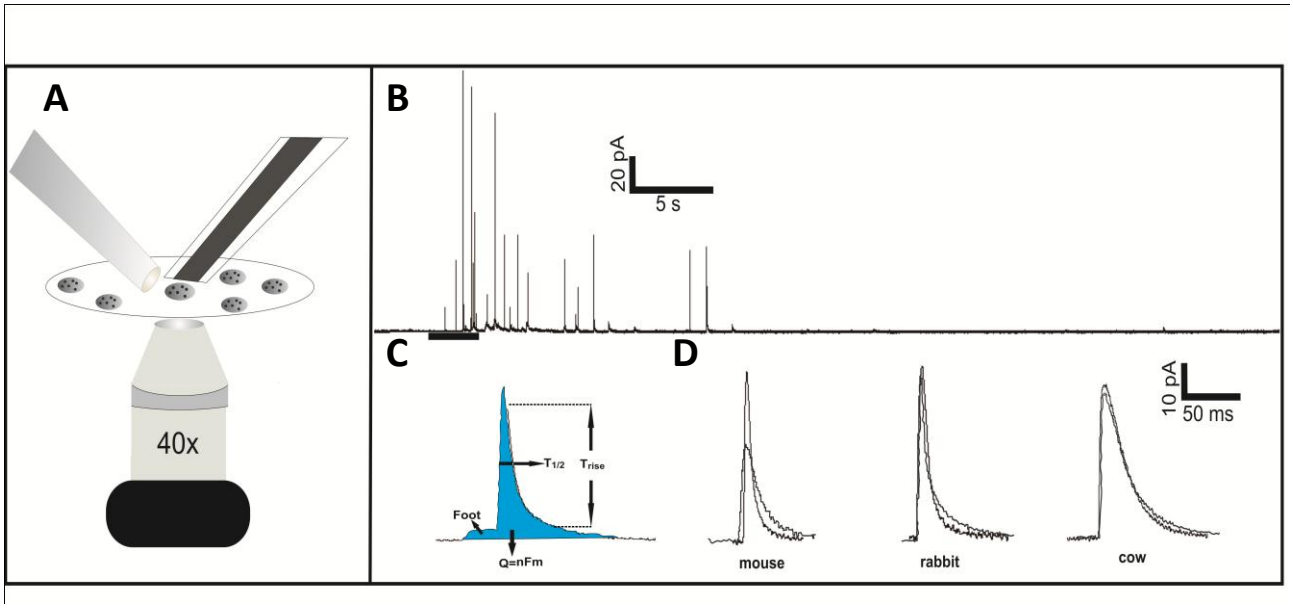

Figure 2.1 CFMA experimental setup and representative spikes. (A) Representative setup for CFMA measurements. CFM is (on the right) placed on a single platelet. Stimulation pipette (on the left) is placed close to the platelet. (B) Typical amperometric trace obtained from single platelet secretion. Each spike corresponds to single δ-granule release event. The bar under the trace shows time and the duration of the stimulation. (C) The parameters that are analyzed for single secretion events. (D) Representative spikes from mouse, rabbit and cow platelet exocytosis upon ionomycin (black) and thrombin (gray) stimulations.

2.3 Results

2.3.1 Platelet Response to Different Stimuli

δ-granule secretion upon exposure to two different agonists was evaluated. Figure 2.1D shows representative spikes corresponding to single release events upon thrombin (10U/mL) and ionomycin (10 μM) stimulations from different species. Although a numerical analysis is always needed, sometimes the shape of the representative trace can tell a lot about the amount and the kinetics of the secretion events. Except the mouse platelet, the spikes resulting from ionomycin and thrombin stimulation looked almost identical within the same species. Compared to the ionomycin stimulation spike, the representative spike for the thrombin-induced mouse platelet secretion is wider and shorter, indicating different secretion behavior that will be discussed later in detail. The representative spikes for cow platelets were both wider and larger than that of mouse and rabbit spikes. This indicates a slower but larger amount of serotonin release that will also be discussed below in detail.

2.3.2. Comparison of the Quantal Secretion Between Different Species

Regardless of the stimulation type, cow platelets released significantly more serotonin per release event (Figure 2.2A and Figure 2.2D) than either mouse or rabbit (Q= 331.2±26.0; Q= 275.7±25.1; Q=498±40.9 fC for mouse, rabbit and cow platelet secretion respectively upon ionomycin stimulation; Q=313.9±29.5; Q=271.5±21.7; Q=654.9±116.4 fC for mouse, rabbit and cow platelets secretion upon thrombin stimulation, respectively). Compared to cow platelets, both rabbit

and mouse platelets released a significantly higher number of discrete δ-granules per exocytotic event (N= 8.09±1.07; 9.61±1.31; 4.18±0.32 granules for mouse, rabbit and cow platelets, respectively, for ionomycin stimulation) that, when considered cumulatively, translates to more serotonin release per platelet (# of moles of serotonin calculated from N*Q values by using Faraday's Law are 13.8×10^{-18}, 17.5×10^{-18}, 9.6×10^{-18} moles of serotonin for mouse, rabbit, and cow platelets, respectively, for ionomycin stimulation). This may indicate that the OCS doesn't regulate the amount of release, but the number of vesicles trafficked and docked. Moreover, previous studies showed that α-granules in cow platelets fuse with each other during exocytosis, prior to fusion with the plasma membrane.[16] A similar explanation for δ-granules would explain the higher Q and lower N values for cow platelet secretion. We analyzed the frequency of the distribution of the Q values (data not shown) expecting a bimodal distribution to show that where δ-granules fuse with each other ahead of plasma membrane fusion.

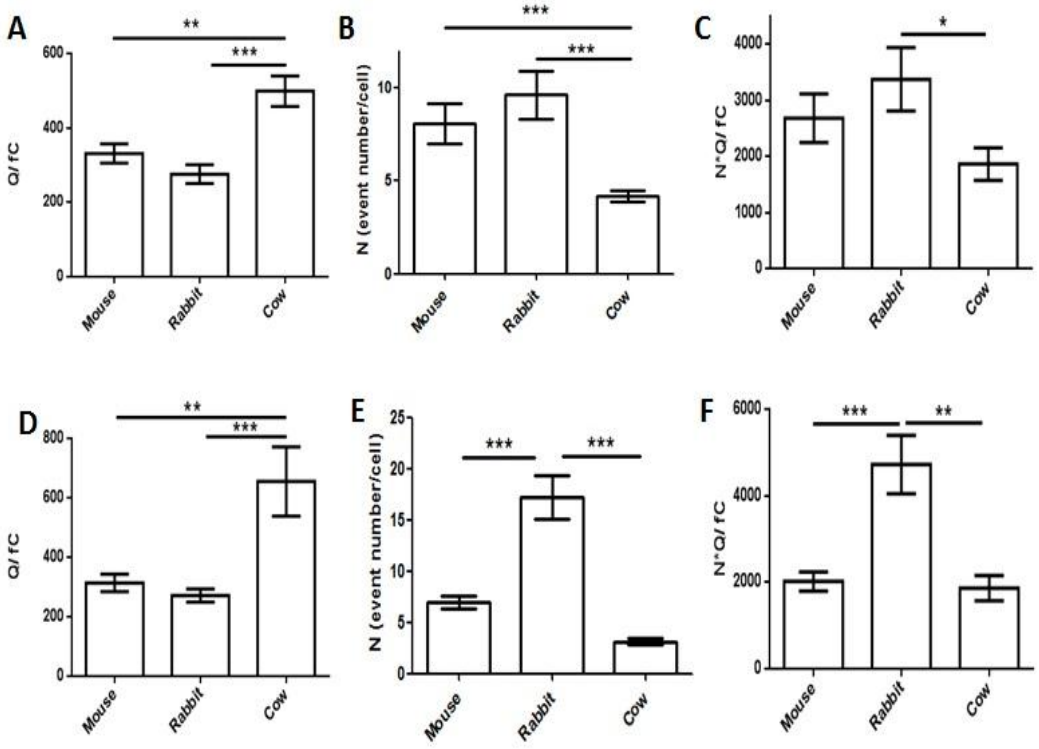

Figure 2.2 Comparison of the quantal release between the species upon ionomycin (A-C) and thrombin (D-F) stimulations. (A, D) Cow platelets release significantly higher number of serotonin molecules per release event. (B, E) Number of granules released per single platelet exocytosis. (C, F) N*Q represents the total amount of serotonin secreted from single platelet. (* for $p<0.05$, ** for $p<0.01$, *** for $p< 0.001$)

However, frequency analysis did not show such a distribution; a single non-Gaussian distribution similar to the previously reported distribution for rabbit granular release was observed instead[9] this makes the possibility of fusion of two δ-granules unlikely. TEM images were used to analyze the size of δ-granules of cow and mouse platelets (Figure 2.3). Results showed that cow platelets not only have larger δ- granules but the dense core of the δ-granules where the most of the serotonin is stored is significantly bigger in cow platelets (average granule diameter is 229.3±6.1 nm for mouse platelet δ-granule, 341.0±11.1 for cow platelet granule. This increases the possibility that more serotonin is stored in cow platelet granules.

As it is evidenced by Ewing and colleagues, it is not necessarily true that the entire content of a granule is released upon stimulation; in fact, PC12 cells, a model exocytotic cell, only release 45% of their vesicular content. [17] Herein, we evaluated the percentage of total δ-granule content release using bulk HPLC measurements by either lysing the cells with $HClO_4$ and analyzing the total serotonin content, or by exposing the cells to 10 U/ml thrombin or ionomycin and measuring the released content. Figure 2.4 data shows the percent lysis data for each species and stimulant.

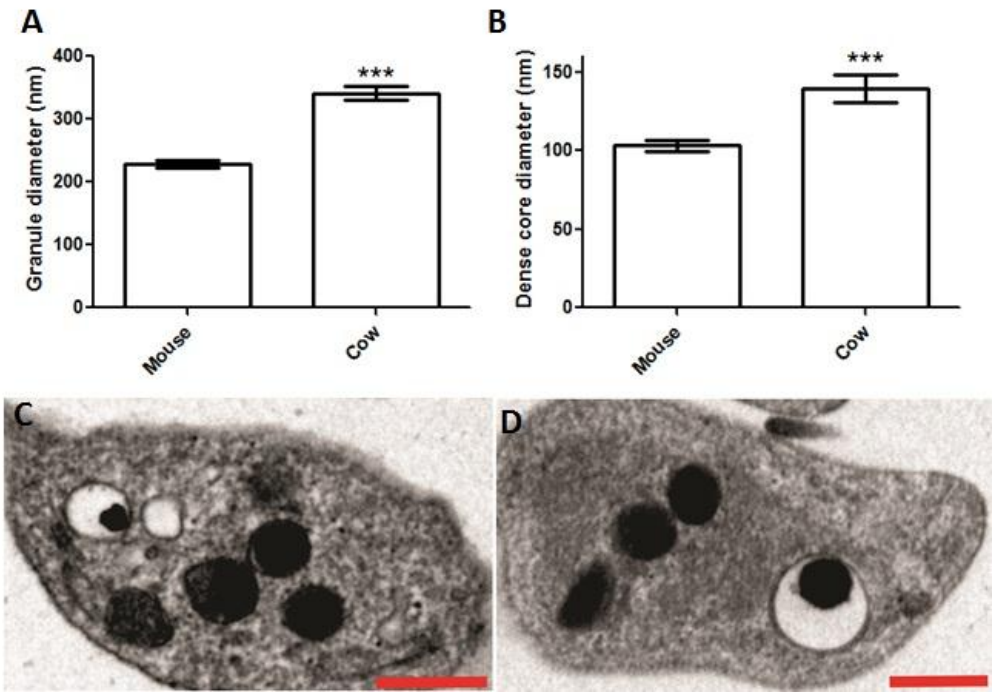

Figure 2.3 TEM analysis of cow and mouse platelets. Cow platelets have significantly larger δ-granules with higher granule diameter (A) and dense core diameter (B). TEM images of a single mouse platelet (C) and cow platelet (D). Red bars represent 1000nm. (***p<0.001).

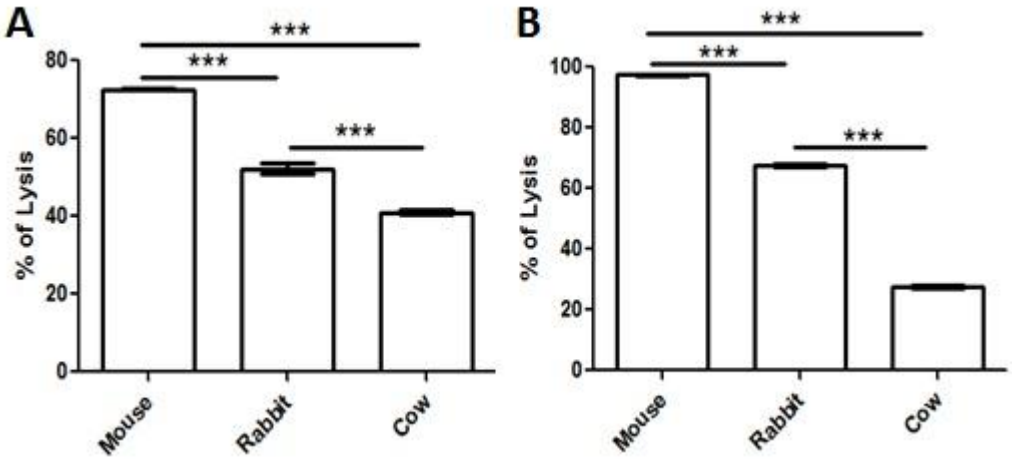

Figure 2.4 Bulk serotonin analysis using HPLC. % of the total serotonin secreted with (A) ionomycin stimulation or (B) thrombin stimulation.

It is clear that more serotonin is released in all species upon thrombin activation as compared to ionomycin activation. In both rabbit and mouse platelets, the granules released more than 50% of the total serotonin content; however, only 27.53 and 41.06% of the serotonin was released from cow platelets with ionomycin and thrombin stimulation, respectively ($p<0.001$) .Use of human thrombin cannot be the reason for this behavior since it has been shown previously that human thrombin was 89% homologous to cow thrombin, and cow platelets are known to respond similarly to human and cow thrombin.[4] This may indicate that the reduced cow platelet secretion, compared to that by rabbit and mouse platelets, may not be due to the effectiveness of the stimulant but efficiency of the response to the stimulant, perhaps related to the use of the OCS. Comparison of secretion kinetics may yield insight on this matter.

2.3.3 Comparison of the Kinetics of Release Between Different Species

T_{rise} values measure the time required for transition from 10% to 90% of the peak maximum, representing the time required for transition from the initial pore opening to full fusion. During this time, the soluble (non-polyphosphate-associated) serotonin present in the granules is released.[18] $T_{1/2}$ is a measure of the total time of a serotonin secretion event which can be influenced by the opening of the fusion pore, the size of the expanded pore, dissolution of the matrix-bound serotonin, and diffusion of that serotonin into the extracellular space. When stimulated with ionomycin, cow platelets showed slower release

kinetics than either rabbit or mouse platelets (higher T_{rise} and $T_{1/2}$ values) (Figure 2.5). This could be attributed to the larger number of serotonin molecules secreted or to less efficient extrusion of the molecules. Mouse and rabbit platelets showed comparable release kinetics upon ionomycin stimulation ($T_{1/2}$= 13.95±1.08 and 14.70±1.6 ms for mouse and rabbit, respectively). Thrombin, however, induced distinct secretion behavior for each species. Although mouse and rabbit platelets release similar amounts of serotonin from δ-granules, mouse platelet secretion was much slower than that from rabbit platelets ($T_{1/2}$= 20.34±1.20; and 15.42±1.21 ms for mouse and rabbit, respectively p=0.0041). This may be due to a difference in sensitivity to the thrombin stimulation which influenced the secretory kinetics. Cow platelet secretion kinetics were slower in thrombin-induced stimulation with a $T_{1/2}$ value of 26.82± 2.09 ms.

2.3.4 Comparison of Fusion Events Between Species

During platelet granular secretion, fusion of the granular membrane with plasma membrane gives rise to formation of a fusion pore of limited stability. Fusion pore formation and stability affects both the quantal release and kinetics of the release.[19, 20] In amperometric traces, the fusion pore can be identified as a subtle increase in the current due to the diffusion of soluble serotonin as the fusion pore opens (Figure 2.1.C); this current feature is commonly known as a “foot.”[18]

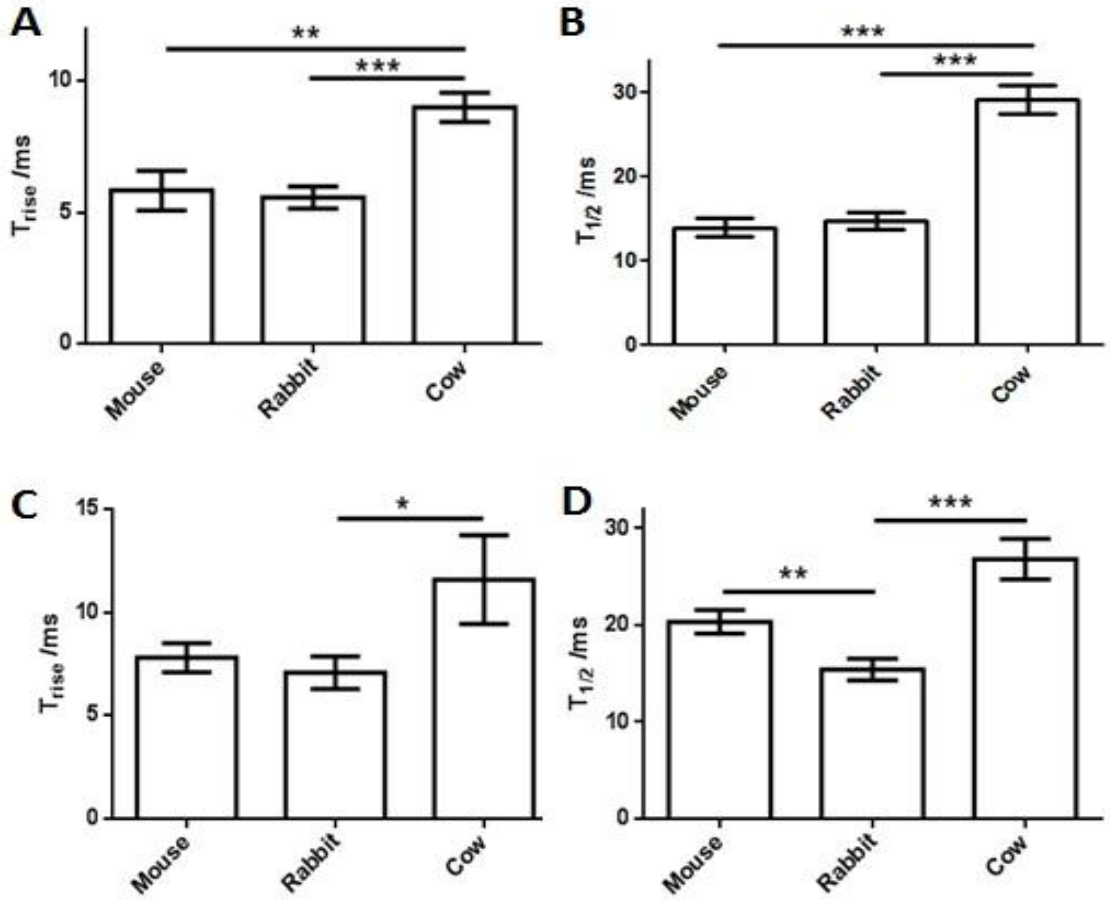

Figure 2.5 Comparison of the secretion kinetics with either (A, B) ionomycin or (C, D) thrombin stimulation. (A, C) Larger T_{rise} values from cow platelet secretion indicate slower transition to maximal release. (B, D) Duration of the total secretion was longest in cow platelets regardless of the stimulant. Although the $T_{1/2}$ values from rabbit and mouse platelets were similar in the ionomycin condition, thrombin stimulation resulted in higher $T_{1/2}$ values, and thus, slower release from mouse platelets compared to rabbit platelets. (*for $p<0.05$, ** for $p<0.01$, *** for $p< 0.001$)

The analysis of the foot events among amperometric spikes shows that the stability of the fusion pore is highly dependent on the mechanism of the activation (Figure 2.6). Mouse platelets showed the highest percentage of fusion pore events when they were activated with ionomycin (18.09±3.60 % of the mouse secretion events showed foot feature as opposed to 9.45±2.00 and 13.50±2.54 % fusion pore events in rabbit and cow exocytosis, respectively). Stimulation with thrombin caused a drastic decrease in secretion events initiated through a stable fusion pore (9.29±2.28 % events with foot). On the other hand, thrombin stimulation caused a significant increase in the stability of the fusion pore of rabbit and cow platelet dense granule secretion (%Foot= 15.01±2.12 and 23.72±5.08 for rabbit and cow platelets, respectively). This indicates that fusion pore stability is both species and stimulant dependent, and there is no correlation between the presence of OCS and fusion pore occurrence.

2.4 Discussion

Addressing the differences among platelets of different species will help clarify the role of each component of platelet secretion and will promote better targeting strategies to control platelet function in many physiological processes. One of the major structural differences between platelets from different species is the presence of a system of tunneling invaginations from the plasma membrane known as the OCS.[2, 4, 7]

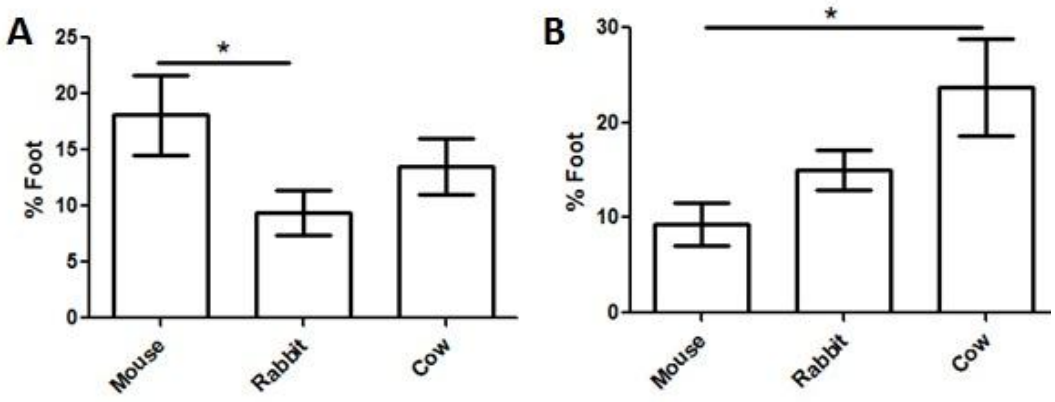

Figure 2.6 Fusion pore analysis. (A) With ionomycin stimulation, mouse platelets have higher % events with foot (B) Thrombin stimulation resulted in the most stable fusion pores in cow platelets compared to mouse and rabbit platelet. (*$p<0.05$)

Work done by various groups has demonstrated that the OCS influences platelet morphology during activation and that the presence of the OCS helps platelets interact with surfaces better by providing platelet spreading and pseudopodia formation.[16, 21] In contrast, platelets without an OCS kept their discoid shape even after 1 h interaction with surfaces.[21] Moreover, it was shown that the OCS membrane contains SNARE proteins, including syntaxin 2, SNAP 23 and VAMP 3 and is involved in platelet granular secretion by serving as intermediate fusion sites for the granules before plasma membrane fusion.[7] Very active hemostatic function of camel platelets (lacking an OCS) raises the question of the actual need and use of these tubular structures in platelets.[2] Whiteheart group showed the proteins that regulate the actin cytoskeleton are expressed at higher levels in OCS-containing platelets.[4] This brought up the possibility of OCS involvement in granule trafficking and docking. Clearly, more insight is needed into the actual influence of OCS in platelet function. Furthermore, diversity in the response to a certain agonist within the OCS containing species[3, 4, 22] necessitates a more careful look at the platelet behavior in different species. Although previous studies with TEM images and bulk assays provided useful insights about the structural and functional differences among platelets of different species, a more detailed analysis of kinetics of the release was not possible until CFMA measurements of platelet δ-granule secretion was available.[8] This work aims to address this need in platelet biology by studying secretion from both OCS-

containing (mouse and rabbit platelets) and OCS- deprived (cow platelets) platelets by CFMA.

Thrombin is a strong stimulant of PAR -mediated platelet activation.[23] Ionomycin is a calcium carrier that not only shuttles extracellular calcium into the cells, but also immobilizes the calcium in δ- granules of platelets, resulting in elevated intracellular calcium levels and thus, triggering exocytosis.[8, 9] Upon exposure to ionomycin or thrombin, cow platelets released more serotonin per secretion event than mouse or rabbit platelets; in fact, the Q values that reveal the amount of serotonin secreted from individual granules were almost double those from rabbit and mouse platelet exocytosis (Figure 2.2). Previous work showed that platelet serotonin storage is quantal [9] which means same concentration of serotonin is stored in each δ-granule. Thus, cow platelet granules should be twice as large as of mouse and rabbit platelets to provide concentrations of serotonin similar to rabbit and mouse platelet granules. Moreover, It is known that cow platelet α-granules fuse with each other and then the plasma membrane during exocytosis.[16] Our results show that a similar mechanism is possible for δ-granule secretion. The histogram showing the frequency of the distribution of the Q values did not show bimodal distribution which makes the fusion of the δ-granules with each other less likely. The large granule size of cow platelets compared to platelets from other species was reported by White et. al. and more likely is the reason for the high Q values obtained.[16] Analysis of the size of the

cow and mouse δ-granules supported the previous report showing that cow δ-granules is much larger than mouse platelets.

Measurement of total vs. secreted serotonin with HPLC allowed the analysis of the efficacy of the secretion. % release from cow platelets was drastically lower than mouse and rabbit platelets. Furthermore, the parameters that were used to determine the kinetics of the secretion event ($T_{1/2}$ and T_{rise} values) were significantly higher for cow platelet. Although the higher $T_{1/2}$ and T_{rise} values may be due to the higher amount of serotonin secreted, it is possible that the absence of the tubular structure retarded secretion kinetics. All these observations indicate that OCS may not be necessary for the secretion but it indeed influences the efficacy of the release.

Time resolution of the CFMA technique enables observation of the fusion pore events in the case of a stable fusion pore formation.[10] The stability of fusion pore is strongly dependent on membrane properties and dissolution of the releasates from the granular matrix.[24] Upon activation, the membrane reorganizes itself to accommodate proteins at the site of fusion. This includes redistribution of phospholipids in the inner and outer leaflet of the membrane and migration of the SNARE proteins as well.[25, 26] Ionomycin and thrombin stimulations showed different trends in the foot parameters. This may be due to the different signaling pathway involved in the activation through ionomycin and thrombin affecting the membrane organization and hence, the stability of the fusion pore differently in different species.

In conclusion, by using CFMA and HPLC, and TEM we have demonstrated the similarities and differences in platelet δ-granule secretion behavior of platelets from different species. Although OCS is an important factor needed for efficient secretion, the differences between rabbit and mouse secretory behavior shows that the absence or presence of the OCS is not the major determinant of chemical messenger secretion behavior.

Chapter 3

Dynamin-Related Protein-1 Controls Fusion Pore Dynamics During Platelet Granule Exocytosis

Adapted from:

Koseoglu S, Dilks J, Peters C, Fitch J, Fadel N, Jasuja R, Italiano JE, Haynes CL, Flaumenhaft R. Dynamin-related protein-1 controls fusion pore dynamics during platelet granule exocytosis. Submitted.

3.1 Introduction

Platelet granules are required for normal hemostasis and contribute to pathological thrombus formation. Platelet granule exocytosis has also been implicated in numerous other physiological functions, including inflammation, microbial host defense, angiogenesis, and wound healing. Platelet granule types include α-granules (50-80 granules/platelet), δ-granules (3-6 granules/platelet), and lysosomes (0-3 granules/platelet). These granules release their contents following stimulation of receptors on the platelet surface. Although much has been learnt about the proximal signal transduction mechanisms that mediate the release of granule contents following stimulation of surface receptors, considerably less is known about the distal mechanisms that facilitate granule exocytosis.[1]

Exocytosis of platelet granule contents requires the fusion of granule membranes with plasma membranes or membranes of the open canalicular system.[2] The release of contents is thought to occur through a fusion pore. Electrophysiological techniques have been used to study the formation, expansion, and collapse of the fusion pore in neurons and neuroendocrine cells. Yet the mechanisms regulating the platelet fusion pore are poorly understood, and the proteins that control platelet fusion pore dynamics have not been identified. Platelet fusion pore dynamics have been difficult to study by standard electrophysiological methods because of platelets' small size and atypical membrane system. Single-cell amperometry, however, has sufficient temporal

and spatial resolution to evaluate fusion pore dynamics in live platelets and has recently been used to study quantal release of serotonin from individual δ-granules.[3-6] Amperometric tracings of platelet δ-granule release demonstrate features previously observed only in nucleated cells, indicating that stable fusion pore formation, fusion pore expansion, and 'kiss-and-run' exocytosis occur in platelets. We have previously used amperometry of individual platelets to evaluate mechanisms of platelet membrane pore dynamics .[3, 5-7]

We now use single-cell amperometry to study the role of dynamin-related protein 1 (Drp1) in platelet granule release. Drp1 belongs to the dynamin superfamily, a group of large GTPases that act as mechanoenzymes and demonstrate oligomerization-dependent GTPase as well as membrane modeling activities.[8] Drp1 is most widely known for its role in mediating mitochondrial fission and fusion. We demonstrate that platelets contain Drp1 and that Drp1 is phosphorylated upon platelet activation. Blocking Drp1 inhibits platelet granule exocytosis and impairs fusion pore stability. Inhibition of Drp1 also interferes with platelet accumulation during thrombus formation *in vivo*. These studies demonstrate a heretofore unrecognized function of Drp1 in platelet physiology.

3.2 Materials and Methods

3.2.1 Platelet Preparation

For human platelets, blood was obtained from healthy donors who had not ingested aspirin or NSAIDs in the 2 weeks prior to donation. Platelets were isolated by centrifugation followed by isolation of washed platelets from platelet-rich plasma. For single cell amperometry experiments, blood was drawn from the midear artery of New Zealand rabbits (Bakkom Rabbitry) according to approved University of Minnesota IACUC protocol #0802A27063. Isolation of washed rabbit platelets in Tyrode's buffer (NaCl, 137 mM; KCl, 2.6 mM; $MgCl_2$, 1.0 mM; D-glucose, 5.6 mM; N-2-hydroxyethylpiperazine- N'-2-ethanesulfonic acid (HEPES) 5.0 mM; and $NaHCO_3$, 12.1 mM with pH adjusted to 7.3) was previously described[9]

3.2.2 Single-cell Amperometry

Amperometry experiments were performed with an Axopatch 200B potentiostat (Molecular Devices, Inc.) controlled by locally written LABVIEW software. Fabrication of carbon-fiber microelectrodes and the experimental instrumentation have been previously described.[3, 5, 10] Rabbit platelets were used for these experiments because they have a substantially higher number of δ-granules per platelet than human platelets. To begin a measurement, a drop of rabbit platelet suspension was added to the experimental chamber that contained either 10 μM mdivi-1 (Tocris), or 10 μM compound E (generous gift of Dr. Jodi Nunnari and Dr. Ann Cassidy-Stone) in Tyrode's buffer (prepared from stock solutions in DMSO)

or the same volume of DMSO in Tyrode's buffer for experimental and control conditions, respectively. Platelets were allowed to sediment on poly L-lysine-coated coverslips for 15 minutes before amperometry measurements. One platelet at a time was stimulated with a 3 s bolus of thrombin solution in Tyrode's buffer (10 U/mL), and the amperometric response was recorded for 60 s. Data were analyzed as has been previously described[5] and reported as mean±SEM; t-tests were used to identify statistically significant differences compared to the control condition. Amperometric measurements were recorded from 107 platelets for control condition, 39 platelets for mdivi-1 condition, and 31 platelets for the compound E condition.

3.2.3 Thrombus Formation Model

Intravital video microscopy of the cremaster muscle microcirculation was performed as previously described.[11] Mouse anti-human fibrin II β-chain monoclonal antibody was purified over protein G-Sepharose (Invitrogen) from a 59D8 hybridoma cell line[12] and labeled with Alexa Fluor 488 (Invitrogen). Digital images were captured with a Cooke Sensicam CCD camera (The Cooke Corporation) connected to a VS4-1845 Image Intensifier GEN III (Video Scope International). Injury to a cremaster arteriolar (30-50 μm diameter) vessel wall was induced with a Micropoint Laser System (Photonics Instruments) focused through the microscope objective, parfocal with the focal plane and tuned to 440 nm through the dye cell containing 5 mM coumarin in methanol. Data were captured digitally from two fluorescence channels, 488/520 nm and 647/670 nm.

Data acquisition was initiated both prior to and following a single laser pulse for each injury. The microscope system was controlled and images were analyzed using Slidebook (Intelligent Imaging Innovations).

3.2.4 Image Analysis

For each thrombus generated, a rectangular mask was defined that included a portion of the vessel upstream of the site of injury. The maximum fluorescence intensity of the pixels contained in this mask was extracted for all frames (pre- and post-injury) for each thrombus. The mean value calculated from the maximal intensity values in the mask for each frame was determined and used as the background value. Finally, for each frame the integrated fluorescence intensity was calculated as per following equation:

Integrated fluorescence intensity = sum intensity of signal – (mean of the maximal background intensity X area of the signal).

This calculation was performed for all frames in each thrombus and plotted versus time to provide the kinetics of thrombus formation. For multiple fluorescence channels, calculations of background were made independently for each channel. The data from 25-30 thrombi were used to determine the median value of the integrated fluorescence intensity to account for the variability of thrombus formation at any given set of experimental conditions.

3.2.5 Statistical Analysis

A value representing area under the curve was calculated for each curve generated by measurement of fluorescence following laser injury of an arteriole.

A Mann-Whitney test was used for statistical comparison of data sets comprised of the indicated number of thrombi formed under each indicated condition. *P* values of 0.05 or less were considered statistically significant and are indicated. Statistical analyses were performed using Prism software package (version 4; GraphPad).

3.2.6 Immunoblot Analysis

Platelet lysates were prepared by lysis of human platelets (2 x 10^8/ml) in sample buffer. To prepare cytosol and membranes, platelets were incubated with 15 U/mL streptolysin-O (Sigma, MO) overnight and subsequently pelleted at 1000*g* for 15 minutes. The cytosol fraction was collected and the pellet was washed in PIPES/EGTA/KCl buffer (25 mM PIPES, 2 mM EGTA, 137 mM KCl, 4 mM NaCl, 0.1% glucose, pH 6.4). Proteins in cytosol and membranes were then solubilized in sample buffer and separated by SDS-PAGE. Immunoblotting was performed using antibodies directed against dynamin 1, dynamin 2, Drp1 (Abcam), phospho-Drp1 serine 616 (Cell Signaling Technology), and phospho-Drp1 serine 637 (Cell Signaling Technology) and FITC-labeled or HRP-labeled secondary antibodies (Jackson Immunorearch Laboratories). FITC-labeled or HRP-labeled secondary antibodies were visualized using fluorescence detection on a Typhoon 9400 Molecular Imager (GE Healthcare) or chemiluminescence using an X-OMAT 2000A Processor (Kodak), respectively.

3.2.7 Immunogold Electron Microscopy

For preparation of cryosections, isolated human platelets were fixed with 4% paraformaldehyde in 0.1 M Na phosphate buffer, pH 7.4. After 2 hours of fixation at room temperature, the cell pellets were washed with PBS containing 0.2 M glycine. Before freezing in liquid nitrogen, cell pellets were infiltrated with 2.3 M sucrose in PBS for 15 minutes. Frozen samples were sectioned at 120°C, and the sections were transferred to formvar-carbon coated copper grids and floated on PBS until the immunogold labeling was carried out. The gold labeling was carried out at room temperature on a piece of parafilm. Anti-Drp1 antibody (Abcam) and Protein A gold were diluted with 1% BSA. The anti-Drp1 antibody recognized a single band of the appropriate molecular weight in immunoblot staining of platelet lysates (Fig. 1A,B). Grids were floated on drops of 1% BSA for 10 minutes to block for nonspecific labeling, transferred to primary antibody, and incubated for 30 minutes. The grids were then washed, transferred to Protein A gold for 20 minutes, and washed in PBS followed by double distilled water. Contrasting/embedding of the labeled grids was carried out on ice in 0.3% uranyl acetate in 2% methyl cellulose for 10 minutes. The grids were examined in a Tecnai G2 Spirit BioTWIN transmission electron microscope (Hillsboro, OR) at 18 500 magnification at an accelerating voltage of 80 kV. Images were recorded with anAMT 2k CCD camera.[13] Control samples using a non-immune antibody demonstrated no staining.

3.2.8 Confocal Microscopy

For colocalization measurements, human platelet mitochondria were labeled by incubation of the PRP with 100 nM Mitotracker Red (Life Technologies) for 45 min at 37 $^{\circ}$C. To label δ- granules, platelets were incubated with (10μM) Oregon Green 488 BAPTA-1 Dextran (Invitrogen) at room temperature for 30 min. PRP with a platelet count of 10^7platelets/mL was then added to poly-L-lysine containing coverslips. Adhered platelets were fixed and permeabilized with 4% formaldehyde (in Tyrode's buffer) and 0.2% Triton X-100, respectively. After incubating with IF blocking buffer (10% FCS, 1% BSA and 0.05% sodium azide in PBS) overnight, platelets were labeled with mouse anti-human Drp-1 antibody (Abcam). FITC-conjugated goat anti-mouse IgG antibody (Abcam) used as a secondary antibody for imaging the Drp-1.[14] An Olympus FluoView F1000 upright confocal microscope was used for capturing images. Sequential scanning with 488 and 543 nm lasers enabled selective imaging of the two fluorescent labels (mitotracker red and FITC) without spectral crosstalk. ImageJ, with the Mander's coefficients plugin, was used for colocalization analysis.

3.2.9 Flow Cytometry

Gel-filtered platelets (10 μL; [0.5-1 x 10^8/mL]) were incubated with the indicated concentrations of inhibitor for 20 minutes. Samples were then exposed to 5 μM SFLLRN (thrombin receptor activating peptide) and analyzed by flow cytometry using a Becton Dickinson FACSCalibur flow cytometer as previously described.[15]

PE-conjugated antihuman P-selectin (BD Biosciences) was used to detect P-selectin exposure. For evaluation of mitochondrial membrane potential, platelets were incubated with 1µM JC-1 (Invitrogen) for 10 minutes and either buffer alone, mdivi-1, or actimycin A (Sigma) for 20 minutes. Platelets were then exposed to either buffer or SFLLRN for 20 minutes and evaluated by flow cytometry. Fluorescent channels were set at logarithmic gain and 1 x 10^4 particles were acquired for each sample. A 530/30 band pass filter was used to measure FL1 fluorescence and a 585/42 band pass filter was used to measure FL-2 fluorescence. Data were analyzed using CellQuest software (BD Biosciences) on a MacIntosh PowerPC (Apple). Data using JC-1 are represented using the ratio of FL2/FL1 as previously reported.[16]

3.2.10 Detection of Adenine Nucleotide Release

A luciferin-luciferase detection system was used to quantify ADP/ATP release to monitor bulk δ- granule secretion.[17] For these experiments, 9 µL human platelets (0.5-1 x 10^8/mL) were incubated in the presence or absence of mdivi-1 and then stimulated with SFLLRN. Samples were then incubated with 1 µL luciferin-luciferase (final concentration of 3 mg/mL) at the indicated time following addition of agonists. Chemoluminescence was quantified using a luminometer (TD 20/20; Turner Design).

3.3 Results

3.3.1 Dynamins in Platelets

Dynamins are a superfamily of large GTPases that serve a wide range of membrane shaping functions.[8] Their expression and function in platelets is not well-understood. Megakaryocytes have previously been shown to express dynamin 3.[18, 19] However, whether other dynamins and dynamin-related proteins are present in platelets has not been assessed. We therefore evaluated platelet lysates for dynamin 1, dynamin 2, and Drp1. Dynamin 1 was not identified under the conditions of our assay. In contrast, dynamin 2 and Drp1 were recognized as single bands with apparent molecular weights of 100 kD and 80 kD, respectively (Figure 3.1A). No additional bands were detected in immunoblots of platelet lysates. To evaluate for the presence of Drp1 in platelet cytosol, platelets were permeabilized with streptolysin-O and subsequently pelleted. Evaluation of platelet cytosol and membranes demonstrated Drp1 in both fractions (Figure 4.1B), indicating that a portion of platelet Drp1 is cytosolic. Evaluation of activation-dependent phosphorylation of platelet Drp1 using phosphorylation site specific antibodies demonstrated that Drp1 is phosphorylated at serine 616 following incubation with SFLLRN to activate PAR1 and at serine 637 following incubation with forskolin to activate adenylyl cyclase (Figure 4.1C). Immunogold electron microscopy was performed to further define the localization of Drp1 in platelets. Studies using a non-immune antibody demonstrated no staining. These results show that Drp1 is found in platelets, is phosphorylated in an activation-

dependent manner, and localizes to both membranes and cytosol. Moreover, confocal analysis showed that Drp1 colocalizes both in mitochondria and platelet δ-granules.

3.3.2 Drp1 Functions in Platelet Granule Exocytosis

Dynamins have a well-established role in endocytosis,[8, 20, 21] associating with the stalk of the maturing endocytotic vesicle and catalyzing vesicle scission. More recently, dynamins have been shown to function in granule exocytosis of nucleated cells.[22-26] To evaluate whether dynamins function in platelet granule exocytosis, we tested the effect of the dynamin inhibitors, dynasore and MiTMAB, on exocytosis using surface expression of P-selectin as a marker of α-granule release (Fig.3.3). Dynasore blocked agonist-induced P-selectin surface expression with an IC_{50} of approximately 20 μM (Fig.3.3), close to its IC_{50} for recombinant dynamin in a GTPase assay.[27] MiTMAB also inhibited P-selectin surface expression with an IC_{50} of approximately 20 μM (Fig. 3.3). These results indicate a role for dynamins in platelet granule exocytosis.

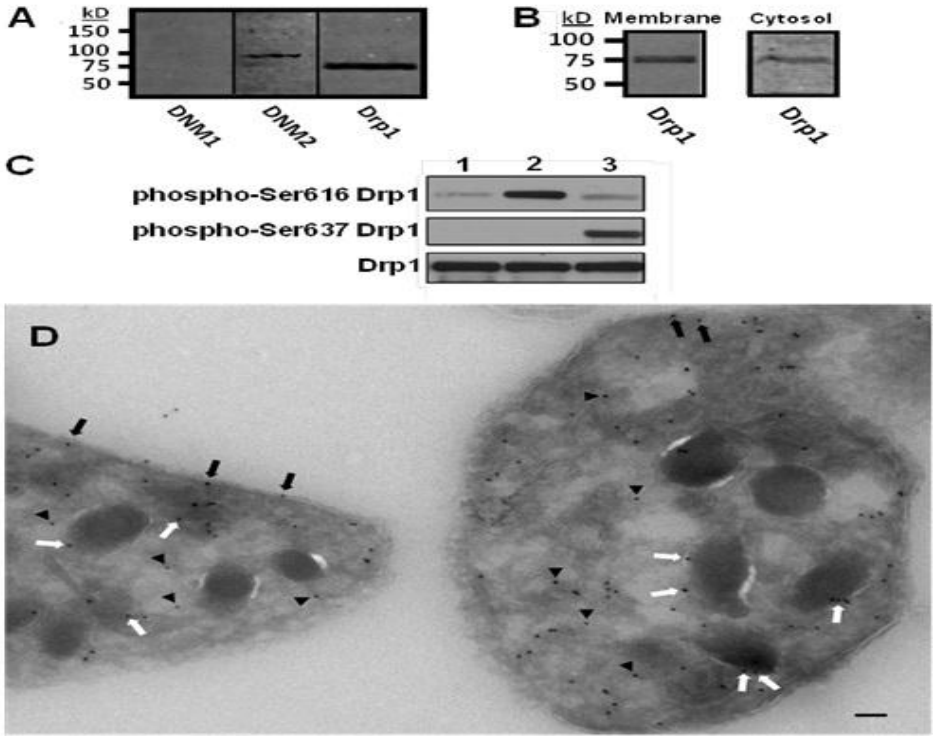

Figure 3.1 Detection and localization of Drp1 in platelets.

(A) Human platelet lysates were evaluated for dynamin 1 (*DNM1*), dynamin 2 (*DNM2*), and dynamin-related protein-1 (*Drp1*) as indicated. (B) Platelet cytosol and membranes were evaluated for Drp1. (C) Platelet were incubated with either 1) buffer alone, 2) 5 µM SFLLRN, or 3) 10 µM forskolin. Lysates were then evaluated using either an anti-Ser616 Drp1 phosphorylation site specific antibody (*phosphor-Ser616 Drp1*), an anti-Ser637 Drp1 phosphorylation site specific antibody (*phosphor-Ser637 Drp1)*, or an antibody to detect total Drp1 (*Drp1*). (D) Immunogold staining of resting platelets demonstrates Drp1 associated with plasma membrane (*black arrow*s), granule membranes (*white arrows*), and cytosol (*black arrowheads*). Scale bar, 100 nm.

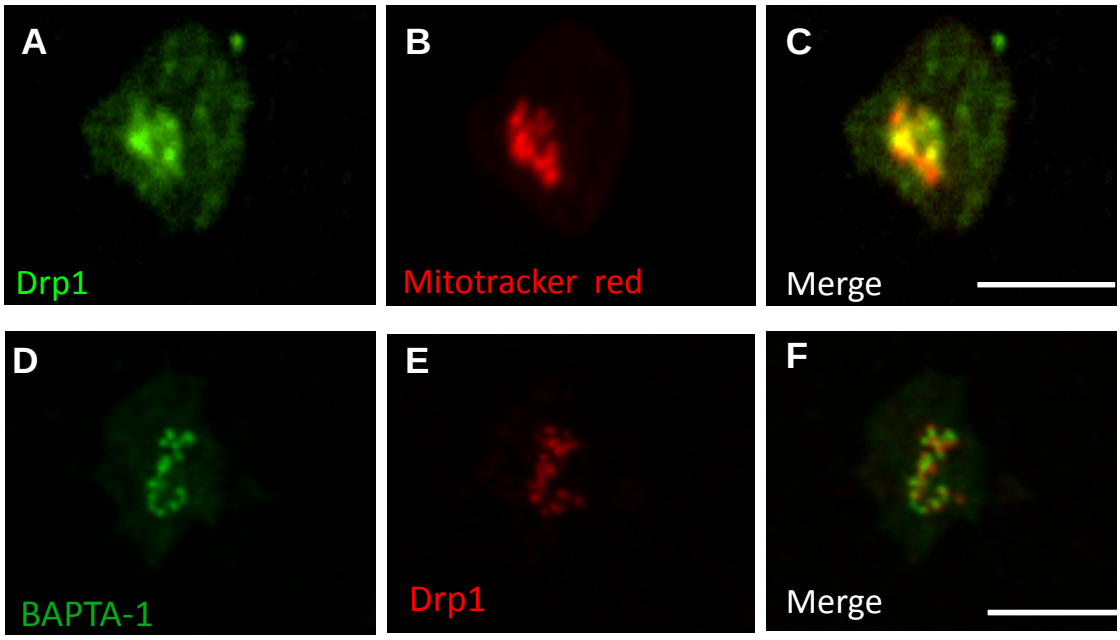

Figure 3.2 Colocalization of Drp1 with platelet mitochondria and δ-granule.

Double staining confocal immunofluorescence microscopy of resting human platelets demonstrates colocalization of anti-Drp1 antibody with the mitochondrial stain, Mitotracker Red and δ-granule stain BAPTA-1. This representative image shows staining of (A) Drp1, (B) mitochondria, and (C) the merged images. Scale bar 5 μm. Analysis of colocalization demonstrate a Pearson's coefficient of 0.675±0.025, an M_1 value (Drp1 associated with mitochondria) of 0.428±0.038), and an M_2 value (mitochondria associated with Drp1) of 0.731±0.067. (D) δ-granule, (E) Drp1, (F) the merged images. Analysis of colocalization demonstrate a Pearson's coefficient of 0.721±0.037, an M_1 value (δ-granule associated with Drp1) of 0.579±0.047), and an M_2 value (Drp1 associated with δ-granule) of 0.707±0.033. Staining with non-immune antibody showed no fluorescence, and no crossover was observed between fluorescence channels.

Dynasore and MiTMAB have been used widely to assess the role of dynamin family proteins in cell function.[27, 28] However, they are general inhibitors of dynamins and cannot be used to assess the role of specific dynamin subtypes in exocytosis.

Drp1 is widely known for its role in mitochondrial fission[29-32] and fusion.[33] However, a role in degranulation has also been described.[34] To determine whether Drp1 functions in granule exocytosis, we used the well-characterized Drp1 inhibitor, mitochondrial division inhibitor-1 (mdivi-1). Mdivi-1 selectively blocks Drp1, but not other dynamin isoforms and acts outside of the GTP binding site.[35] This inhibitor blocked PAR1-mediated α-granule release with an IC_{50} of approximately 10 μM (Fig. 3.4A), similar to its IC_{50} for inhibition of recombinant Drp1 in a GTPase assay.[35]

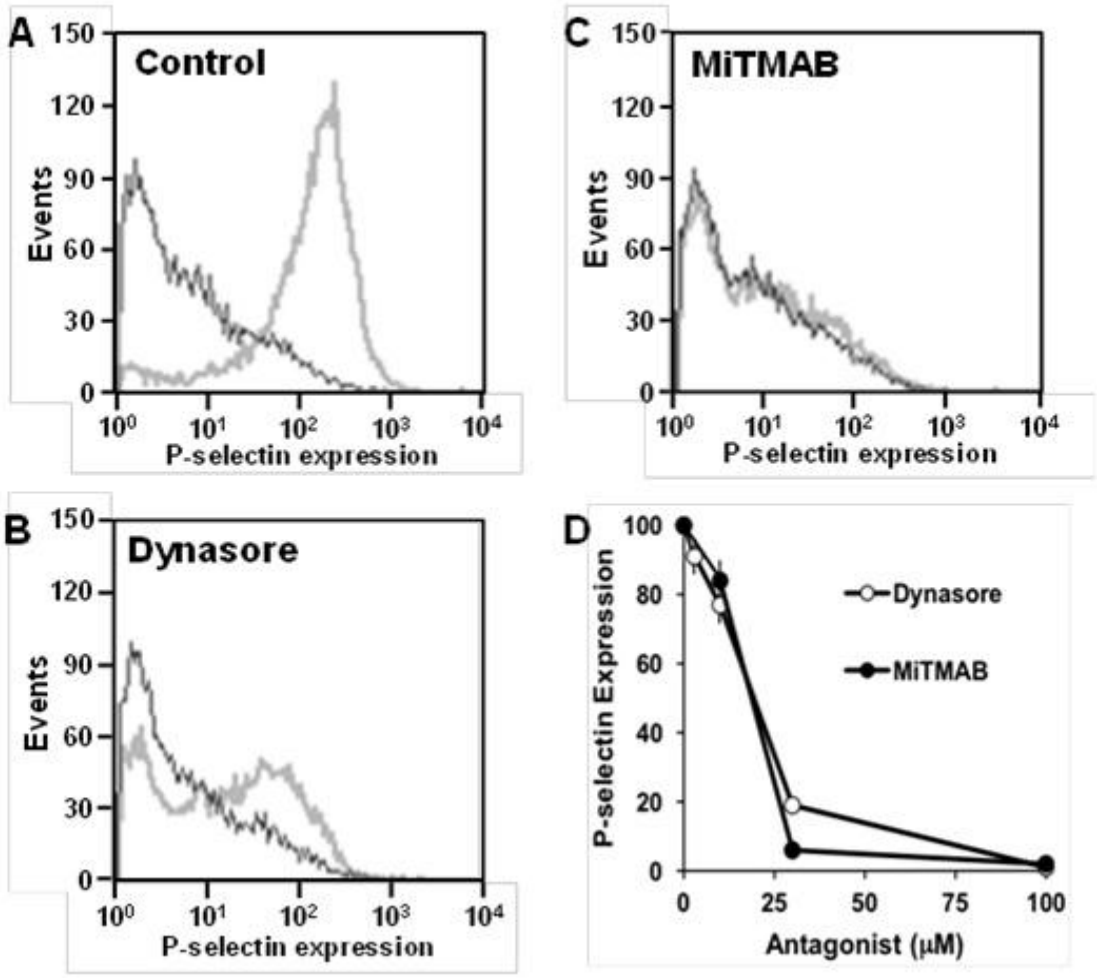

Figure 3.3. Inhibition of dynamins blocks α-granule secretion secretion. Human platelets were incubated in the presence of either (A) vehicle alone, (B) dynasore, or (C) MiTMAB and subsequently exposed to buffer (*black*) or 5 μM SFLLRN (*gray*). P-selectin surface expression was subsequently evaluated by flow cytometry. (D) Both dynasore and MiTMAB inhibited PAR1-mediated P-selectin expression in a dose-dependent manner (n = 3 ± S.D.).

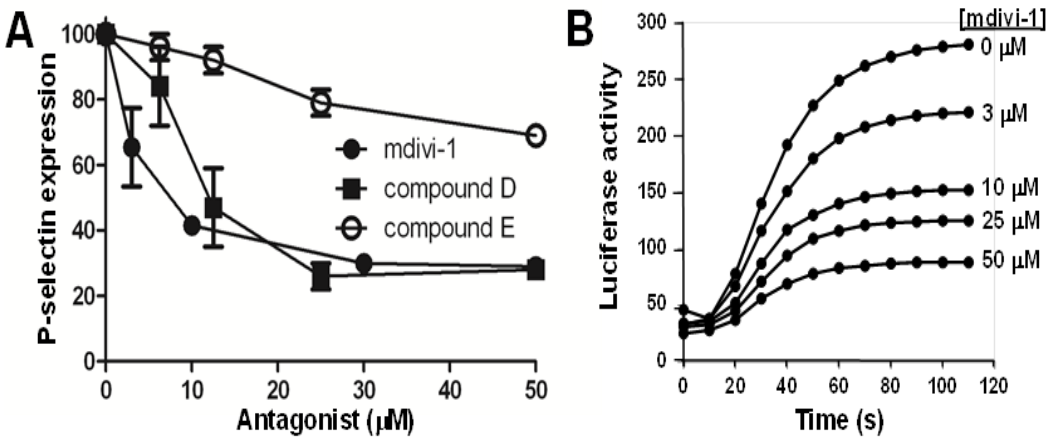

Figure 3.4 Role of Drp1 in α-granule and δ-granule exocytosis.

(A) Platelet P-selectin surface expression in response to 5 μM SFLLRN was assayed in the presence of the indicated concentrations of either mdivi-1 (*black circle*), compound D (*black square*) or compound E (*open circle)*. Data are representative of 3 experiments ± S.D. (B) Platelets were incubated with the indicated concentrations of mdivi-1 for 20 minutes prior to addition of 5 μM SFLLRN. Release of adenine nucleosides was subsequently monitored using a luciferin-luciferase assay. Data are representative of 3 similar experiments.

One method to assess the selectivity of a small molecule for a particular protein target is to use compound analogs that vary in their ability to inhibit the target and determine whether or not their activity is replicated in the cellular system of interest. Analogs of mdivi-1 were used to assess whether Drp1 is the relevant target of mdivi-1 in platelet granule exocytosis. Compound D, an analog with potency equal to that of mdivi-1 against recombinant Drp1 in a GTPase assay;[35] demonstrated similar potency to mdivi-1 in an assay of α-granule release (Fig. 3.4A). Compound E was substantially less potent than mdivi-1 against recombinant Drp1 in a GTPase assay, demonstrating only approximately 45% inhibition at 50 μM.[35] Therefore, if Drp-1 is the relevant target for mdivi-1 in the exocytosis system, then compound E would demonstrate significantly less activity than mdivi-1. Compound E was significantly less active in inhibiting platelet □-granule release (Fig. 3.4A). To determine whether Drp1 functions in δ-granule release as well as α-granule release, we evaluated the role of mdivi-1 on adenine nucleoside release using a lucerifase-based assay. δ- granule release was inhibited by mdivi-1 with an IC_{50} of approximately 10 μM (Fig. 3.4B). These results indicate a role for Drp1 in platelet granule exocytosis.

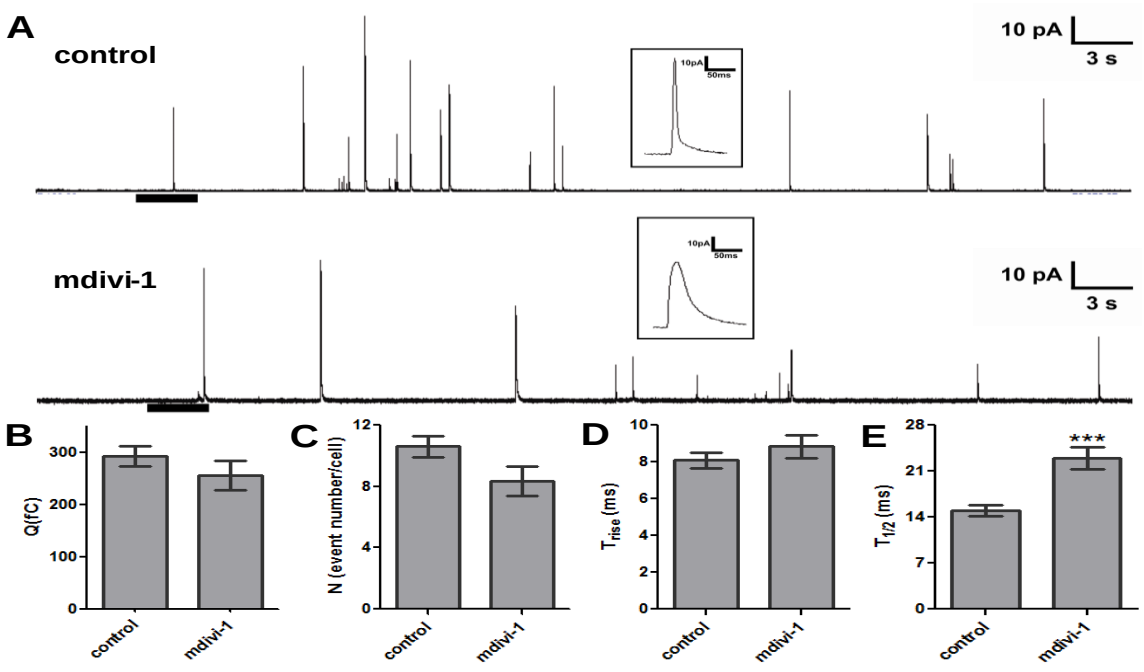

Figure 3.5 Role of Drp1 in kinetics of the platelet granule release.

(A) Representative amperometric traces of rabbit platelet δ-granule release in the presence and absence of mdivi-1. The heavy bar beneath the tracings indicates the time and the duration of the thrombin stimulation. *Insets*: The distinct spike shapes for control (*upper*) and mdivi-1 (*lower*) conditions depicted in the millisecond time scale demonstrate different serotonin release kinetics. Mdivi-1 (10μM) did not influence quantal release (B), the number of granules released per cell (C), or the time required for transition from fusion pore to full fusion (T_{rise}) (D). However, the total time required for the release event ($T_{1/2}$) was longer for platelets exposed to mdivi-1 ($p<0.001$) (E). Data represent the average + S.E.M. of 107 control tracings and 39 tracings from platelets exposed to mdivi-1.

3.3.3 Drp1 Controls Platelet Fusion Pore Dynamics

Drp1 functions in mitochondrial dynamics that contribute to granule secretion in mast cell exocytosis, synapses, and insulin-secreting cells.[34, 36, 37] We used single-cell amperometry to evaluate, with sub-millisecond resolution, the effect of mdivi-1 on the release of serotonin from rabbit platelets (Fig. 3.5A). Statistical analyses of multiple tracings showed that 10 μM mdivi-1 had no effect on the quantal concentration of released serotonin (Fig. 3.5B) or the number of fusion events per platelet (Fig. 3.5C), which enabled unambiguous evaluation of the change in fusion pore behavior and kinetics of release. Results showed that although 10 μM mdivi-1 did not affect the time required for transition from fusion pore to maximal release (T_{rise}) (Fig. 3.5D), it changed the kinetics of the total release event (Fig. 3.5E). The prolonged spike width in amperometric tracings in samples exposed to mdivi-1 indicated that mdivi-1 reduced the efficiency of serotonin release through the fusion pore. Time of half maximal release ($T_{1/2}$) was 14.97±0.81 ms for control and 23.00±1.70 ms for mdivi-1 conditions (Fig. 3.5E). This effect can be observed in figure 3.5A (see inset), where the representative spikes for each condition are shown above the tracings; mdivi-1 treated cells produced wider (larger $T_{1/2}$) and smaller amplitude spikes (since the Q values are similar) upon release of serotonin. Amplitude analysis demonstrated a mean amplitude of 16.58+1.35 pA in control samples compared with 8.96+0.93 pA in samples incubated with mdivi-1 ($p=0.0004$). In contrast,

compound E had no effect on $T_{1/2}$ (Figure 3.6) This result demonstrates that mdivi-1 impairs efficient extrusion of serotonin from platelet δ-granules.

Additional characteristics of amperometric tracings were evaluated to assess the role of Drp1 on the rate of δ- granule release and on fusion pore stability (Fig. 5). Cumulative frequency analyses indicate how efficiently granules are trafficked, docked, and fuse upon stimulation.[7] Since the percent of granules released over time does not change upon mdivi-1 treatment (Fig.3.7B), it is unlikely that mdivi-1 influences delivery of granules to surface connected membranes by cytoskeletal transport or docking at the release site. Following membrane fusion and initial pore formation, pore expansion can ensue, leading to full granule collapse and concomitant extrusion of granule contents. This process can be identified in amperometric spikes as a subtle increase in the current which is called a ‘foot’. Alternatively, the fusion pore can close after partial secretion in an event termed kiss-and-run exocytosis (Fig.3.7A).

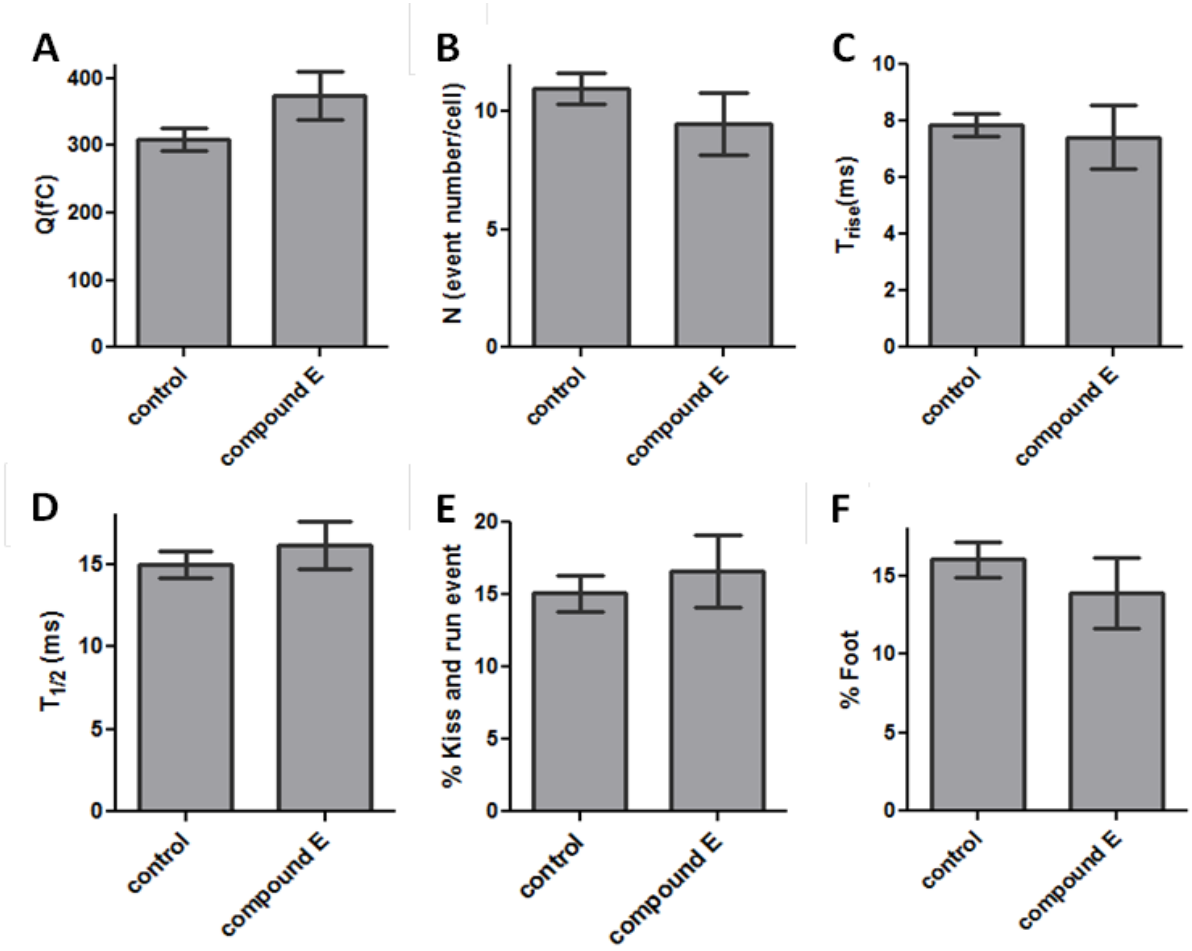

Figure 3.6 Effect of compound E on rabbit platelet pore formation as measured by single cell amperometry. Compound E (10 µM), an mdivi-1 analog that lacks activity against Drp1, did not significantly affect quantal release (A), number of granule released per cell (B), time required for transition from fusion pore to full fusion (C), total time for release (D), % kiss and run events (E), or % foot processes (F). Data represent the average ± S.E.M of 107 control tracings and 31 tracings from platelets exposed to compound E.

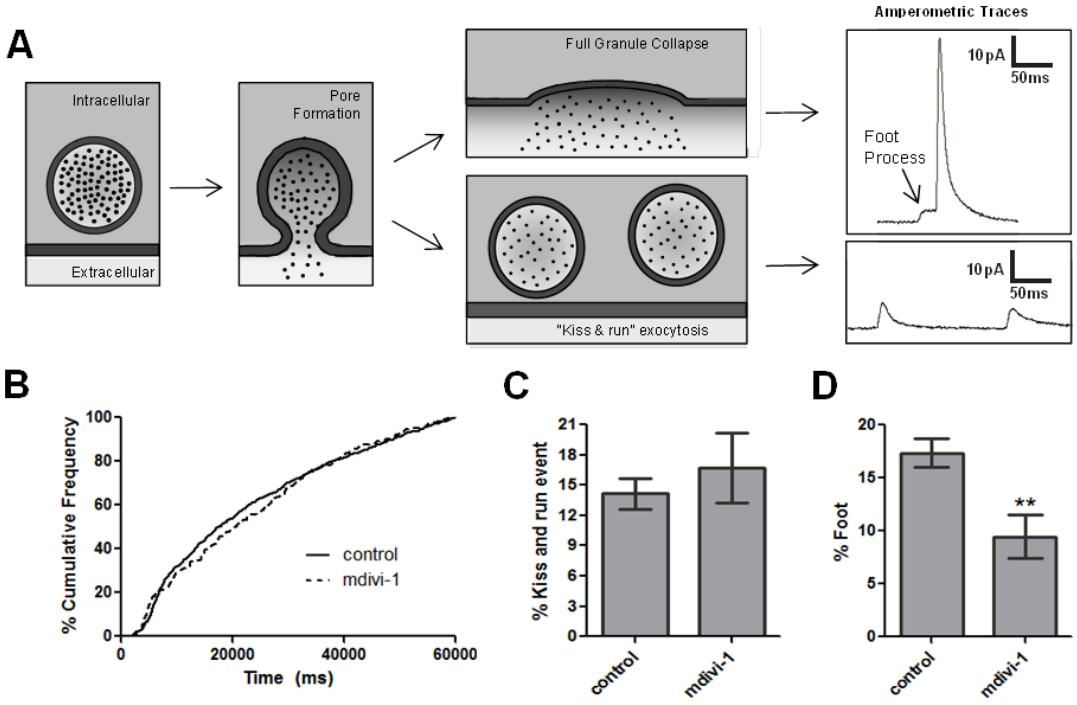

Figure 3.7 Role of Drp1 in stability of the platelet fusion pore.

(A) During rabbit platelet granule exocytosis, a fusion pore forms as indicated by the foot process, shown as the initial inflection in the top amperometric tracing. This pore can then dilate rapidly, resulting in full granule collapse and complete release of granule contents as indicated by the spike (*upper amperometric tracing*). Alternatively, the fusion pore may reseal in a kiss-and-run event. This phenomenon typically results in a shallow inflection in the current tracing representing the release of a small amount of serotonin (*lower amperometric tracing*). (B) Cumulative frequency analysis in the presence and absence of 10 μM mdivi-1 demonstrated no difference in the rate of platelet dense granule release. Amperometric spikes were evaluated to determine (C) the percentage of kiss-and-run events and (D) the percent of spikes preceded by a foot process in the presence and absence of mdivi-1. These results demonstrate that mdivi-1 interferes with the expansion of the fusion pore to full fusion through a foot process, as indicated by the significant difference between the %foot values for mdivi-1-treated and control platelets ($p<0.01$). Data represent the average $\pm$ S.E.M. of 107 control tracings and 39 tracings from platelets exposed to mdivi-1.

In this work, the spikes with an integrated area between 30 fC (approximately 100 times the RMS noise of each tracings) and 100 fC (approximately 30% of the average Q value) are classified as kiss and run events. Release events through fusion pores followed by either reclosure of the fusion pore or full release following foot process formation were monitored. The total %kiss-and-run events did not differ significantly between the two conditions (Fig. 3.7C). However, there was a significant difference between the fusion events completed by full fusion through a foot process in control platelets versus platelets exposed to mdivi-1 (Fig. 3.7D) (% foot is 17.35$\pm$1.37 for control and 9.46$\pm$2.01 for mdivi-1 conditions, $p<0.01$). In contrast to the effects of mdivi-1, compound E had no effect on platelet pore formation (Fig. 3.6F). These results indicate that inhibition of Drp1 impairs fusion pore stability.

3.3.4 Drp1 Antagonism Inhibits Thrombus Formation

Inhibition of Drp1 following infusion of mdivi-1 has previously been demonstrated to block reperfusion injury in cardiac, renal and retinal ischemia models.[38-40] The protective effect has been attributed to prevention of mitochondrial fragmentation since Drp1 is known to function in mitochondrial fission.[32, 41] However, antiplatelet compounds can also confer protection against reperfusion injury, and platelet function was not evaluated in previous studies.

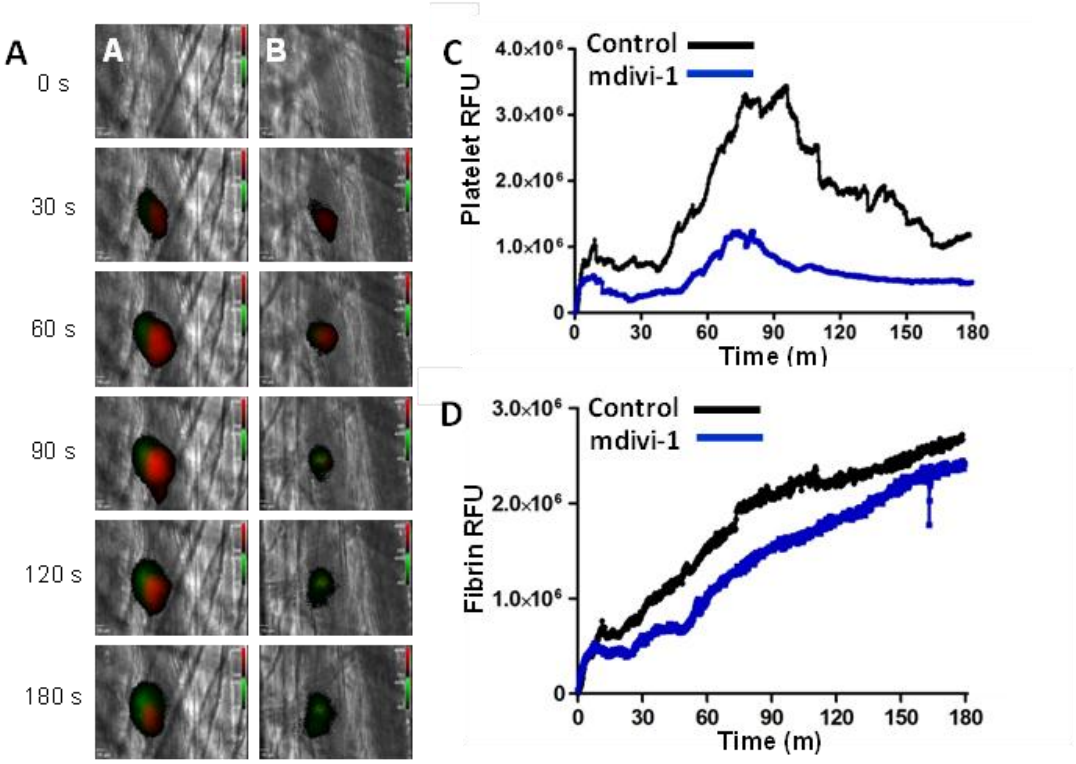

Figure 3.8 Effect of mdivi-1 on platelet accumulation and fibrin generation during thrombu formation following laser injury of cremaster arterioles.

Mouse platelet-specific anti-CD42b antibody conjugated to Dylight 649 (0.1 µg/g body weight) and fibrin-specific mouse anti-human fibrin II β-chain monoclonal antibody conjugated to Alexa 488 (0.5 µg/g body weight) were infused into the mouse. Mdivi-1 (50 mg/kg) was subsequently infused intravenously 5 minutes prior to the initial laser injury. Representative binarized images of the appearance of fluorescence signals associated with platelets (*red*) and fibrin (*green*) over 180 seconds following laser-induced vessel wall injury in a wild type mouse are shown in panels (A) vehicle alone and (B) 50 mg/kg mdivi-1. (C) Median integrated platelet fluorescence intensity and (D) median integrated fibrin fluorescence intensity at the injury site are plotted versus time. Data are from 28 thrombi in 3 mice for control condition and 24 thrombi in 3 mice for mdivi-1 condition.

Since inhibition of Drp1 inhibits platelet exocytosis, we determined whether pharmacological inhibition of Drp1 on thrombus formation could control thrombus formation following vascular injury. Platelet accumulation (Fig. 3.8A, *red*) and fibrin formation (Fig. 3.8A, *green*) were monitored following laser-induced injury of cremaster arterioles prior to (Fig. 6A; supplementary video S1) and following infusion of mdivi-1 (Fig. 3.8B; supplementary video S2). A 59% reduction in platelet accumulation ($p < 0.001$, as determined by AUC) was observed following infusion of mdivi-1 (Fig. 3.8C). In contrast, there was no significant effect of mdivi-1 on fibrin generation following laser-induced vascular injury (Fig. 3.8D), consistent with other interventions specifically targeting platelet function in this model.[42]

3.4 Discussion

These experiments evaluate the role of Drp1 in platelet function using small molecules. The indication that Drp1 functions in granule exocytosis was originally derived from a chemical genetic screen of >300,000 compounds to identify inhibitors of platelet granule secretion. This unbiased forward screen identified a compound, ML160, which also demonstrated activity in an assay designed to identify inhibitors of the product of yeast *Dnm1*, the yeast ortholog of Drp1. Following the identification of ML160 as an inhibitor of platelet exocytosis, we used the two well-characterized dynamin family inhibitors, dynasore and MiTMAB, which also blocked platelet granule secretion (Fig. 3.3). This result implicates dynamin family proteins in platelet granule release. To evaluate the

role of Drp1 in granule release, we used the mdivi-1, which is selective for Drp1 and has proven to be a useful compound in its study.[35, 39, 40, 43, 44] Mdivi-1 inhibits exocytosis in the same concentration range that it inhibits the recombinant Drp1 GTPase activity. The fact that the inhibitory activity of various mdivi-1 analogs in the exocytosis assay mirror their activity against the recombinant Drp1 GTPase (Fig. 3.4) further supports the premise that Drp1 is the relevant target of mdivi-1 in the exocytosis assay.

Studies demonstrating a role for Drp1 in granule secretion[34, 36, 37] prompted us to evaluate the effect of mdivi-1 on serotonin release from individual granules using single-cell amperometry. Experiments were conducted with a low concentration of mdivi-1 (10 μM) so as not to impair total quantal release of serotonin [Q(fC)] and to enable direct comparison of tracings with untreated controls. Lower antagonist concentrations also decrease the likelihood of off-target effects. These studies demonstrated that mdivi-1 has a significant effect on spike width and the percent of foot processes associated with spikes (Figs. 3.5 and 3.7). Figure 3.5 shows representative traces from both control and mdivi-1-exposed platelets. Unlike the control platelets, mdivi-1-treated platelets show an extended release behavior for each fused granule. This result implies that mdivi-1 impairs the rate of expansion of the fusion pore, and thus, slows the time course for serotonin release from individual granules. Moreover, foot process formation was inefficient when platelets were exposed to mdivi-1, demonstrating that inhibition of Drp1 causes fusion pore instability. There are several potential mechanisms by which

Drp1 may control fusion pore dynamics. Drp1 colocalizes with mitochondria and δ-granule in platelets (Fig.3.2) and could participate in granule secretion via effects on mitochondria. In mast cells, either incubation with mdivi-1 or treatment with Drp1 siRNA blocks mitochondrial translocation required for activation-induced TNF-α and β-hexaminidase release.[34] Mitochondria play a prominent role in insulin secretion by generating required ATP and metabolites that stimulate secretory processes.[45] Silencing Drp1 impairs insulin secretion in the hypothalamus.[37] Mitochondria also contribute to synaptic vesicle release[46] and Drp1 has been shown to function in this capacity.[36] Mdivi-1 impairs mitochondrial permeability transition pore (MPTP) formation and reduces ischemia mediated death in cardiomyocytes.[38] However, under the conditions of our assay, we found no effect of mdivi-1 on mitochondrial membrane potential(data not shown). Similarly, mdivi-1 had no effect on platelet apoptosis as measured by annexin V binding (data not shown). In contrast, antimycin A, an inhibitor of mitochondrial respiration, impaired mitochondrial membrane potential without blocking granule secretion.Thus, impairment of mitochondrial membrane potential is not a likely explanation for the effects of mdivi-1 on granule secretion. An alternative possibility is that Drp1 acts to control fusion pore formation at the site of stalk formation. Unlike classical dynamins, Drp1 lacks a pleckstrin homology domain or SH3 domain and is not known to act at sites of membrane fusion. Nonetheless, Drp1 interacts with membranes and could potentially influence pore

expansion directly. Further studies will be required to determine the mechanism by which Drp1 controls platelet fusion pore dynamics.

Inhibition of Drp1 blocked platelet accumulation during thrombus formation following vascular injury. In contrast, fibrin generation was unaffected (Fig. 3.8). This observation is consistent with the fact that fibrin generation following laser-induced injury of the cremaster arteriole is independent of platelet accumulation.[42] Infusion of mdivi-1 has previously been shown to decrease infarct size in murine ventricles in an *in vivo* model of cardiac ischemia-reperfusion injury.[38] Systemic infusion of 50 mg/kg of mdivi-1 has also been used to reverse ischemic renal injury and tubular apoptosis induced by reperfusion following renal ischemia.[39] The effect was attributed to suppression of ischemia-induced mitochondrial fragmentation. Similarly, mdivi-1 was shown to inhibit early neurodegenerative events and increase retinal ganglion cell survival following acute retinal ischemia.[40] Our results using the same mdivi-1 concentration demonstrate that mdivi-1 is an antiplatelet agent in the setting of injury-induced thrombus formation. A limitation of our studies is that we cannot restrict the activity of mdivi-1 to platelets following systemic infusion. We cannot rule out an effect of mdivi-1 on endothelial cells in our assay. Nonetheless, since antiplatelet therapy can prevent tissue damage following reperfusion[47-49] and mdivi-1 interferes with platelet secretion, effects on platelet function must also be considered when assessing the role of Drp1 in reperfusion injury. The

combination of maintaining vascular patency and inhibiting apoptosis may be useful in the treatment of ischemic injury.

Chapter 4

Exploring the Role of Phospholipids in Platelet Aggregation and Secretion

4.1 Introduction

Since fusion between the granular membrane and the plasma membrane is a critical step of exocytosis, the characteristics and actions of lipid species is clearly of innate importance.[1-3] Phospholipids constitute the majority of the lipids in both the plasma and granular membranes. Sphingolipids, including phosphotidylcholine (PC) and sphingomyelin (SM), are the most abundant, and they are localized primarily in the outer leaflet of the plasma membrane in resting cells. Aminophospholipids, including phosphatidylserine (PS) and phosphatidylethanolamine (PE), are the second most abundant phospholipids in the plasma membrane, and they are generally localized to the inner leaflet of the plasma membrane via an ATP-dependent aminotranslocase enzyme in resting cells.[4-6] Activation of the cell deactivates aminotranslocase activity and activates Ca^{2+}-dependent lipid scramblase, which results in exposure of PS to the outer leaflet, creating a more negatively charged cell surface. It has been shown that both the asymmetric distribution at rest and scrambling of the phospholipids upon activation are critical for the chemical messenger secretion process; in fact, disruption of the phospholipid asymmetry and redistribution impairs exocytosis.[1, 8-11] For example, in the case of Scott's syndrome, where lipid scramblase activity is diminished, patients exhibit a hemostatic imbalance because PS cannot be exposed to the platelet surface properly.[12]

Platelets are dynamic secretory cells, essential for hemostasis and also involved in thrombosis and many other physiological processes.[13] In platelets, phospholipids play particularly important roles in aggregation and secretion.[4-6, 14, 15] Phospholipids in the platelet membrane serve as binding sites for coagulation factors and also have catalytic activity in thrombotic reactions. In resting platelets, the PC and SM in the outer leaflet of the plasma membrane minimize the binding of any coagulation factors. Upon vascular damage and platelet activation, PS is exposed to the platelet surface, which facilitates the binding of a variety of coagulation factors via ionic and stereoselective interactions.[5] Furthermore, phospholipids can amplify the blood coagulation process by several orders of magnitude. For example, PS accelerates the tenase and prothrombinase reactions by facilitating the binding of vitamin K-dependent coagulation factors and allowing conformational changes for maximum function of the coagulation proteins, leading to production of coagulation complexes.[5] In addition to their procoagulant activity, phospholipids can also perform anticoagulation activity through feedback inhibition of thrombin formation.[4, 5] Although PS is often assumed to be the most important phospholipid species due to its strong interaction with coagulation factors, recent studies reveal that other phospholipids in the plasma membrane are also involved in blood coagulation. Moreover, there is evidence that membrane PS level and activity is regulated by other phospholipids, especially PE and PC.[4]

However, the exact role of membrane phospholipids in platelet activation and aggregation is not well characterized.

In addition to aggregation behavior, asymmetric distribution of the phospholipids is also necessary for platelet secretion. Phospholipid content not only influences the fluidity and the curvature of the membrane but it also promotes shape change and spreading of the platelets during exocytosis. In fact, it has been shown that phospholipids can mediate both the mechanism and the kinetics of exocytotic events in PC 12 and chromaffin cells (model exocytotic systems).[8-10, 16] However, there is little known about phospholipid regulation of platelet secretion.

In this work, we examine the effect of membrane phospholipids on the major platelet functions of aggregation and exocytosis. To examine aggregation, platelets were incubated with different phospholipids in a microfluidic device and exposed to ADP, which is a strong platelet aggregation agonist that does not induce secretion. Microfluidic devices coated with endothelial cells were used in this work to mimic the vascular environment.

Platelets have three different types of granules, and herein, we performed both ensemble and single cell analysis to elucidate the secretion from all three types. The bulk assays that were performed to assess the changes in the secretion behavior of platelets include HPLC detection of serotonin, a PF4 ELISA assay, and a β-hexoseaminadase assay to monitor platelet δ-granule, α-granule, and lysosome secretion, respectively. Moreover, single cell CFMA measurements

enabled evaluation of the phospholipid content effects on δ-granule quantal release and kinetics of the release. Results showed that, in fact, not only PS but all the other phospholipids considered influence both platelet aggregation and secretion. With the exception of PE, the phospholipids considered decreased platelet aggregation. Although PS incubation decreased the secretion of δ-, α-, and lysosomal granules, PE and SM enrichment increased secretion from platelet lysosomes. CFMA measurements showed that PC and PS regulate granule recruitment and influence the frequency of secretion events while PS enrichment improves the stability of the fusion event. Overall, this work demonstrates the involvement of membrane phospholipids in variety of platelet functions and highlights the importance of phospholipid-protein interactions in regulation of platelet behavior.

4.2 Materials and Methods

4.2.1 Platelet Isolation and Phospholipid Incubation

Murine blood was drawn via cardiac puncture using 1 mL syringes pre-filled with 200 µL ACD, and platelet-rich plasma was isolated using the procedure described previously. [17] Briefly, whole blood was centrifuged at 130xg for 10 min without brake, and the upper plasma layer was transferred to new tubes. Platelets were pelleted from the plasma by centrifugation at 500xg for 10 min and resuspended in fresh Tyrode's buffer.

100 μM PS, PC, PE, and SM solutions were prepared by drying appropriate volumes of phospholipids as received in chloroform in glass vials with a stream of nitrogen and sonicating in Tyrode's buffer for 2 hours, until all cloudiness had disappeared from the solutions. Phospholipid solutions were then filtered using 0.2 μm filters. Platelets were incubated with phospholipid or negative control solutions for 2h.

4.2.2 Relative Quantification of Phospholipid Enrichment

Relative enrichments of PS, PC, PE, and SM in platelets were assessed using ultra-performance liquid chromatography coupled to tandem mass spectrometry (UPLC-MS/MS). Following incubation with PS, PC, PE, SM, or Tyrode's buffer (control), platelets were washed twice by centrifugation at 1000xg and resuspended in 6:1 Tyrode's buffer: ACD. After the final wash, platelets were resuspended in 100 μL Tyrode's buffer. Plateles were mixed with 400 μL $CHCl_3$/200 μL MeOH/10 μL 19.1 μM PAF-d_4 (internal standard) and sonicated for 20 min. 100 μL 0.1% acetic acid in 0.1 M NaCl was then added and samples were sonicated for an additional 10 min. Samples were centrifuged for 5 min at 1500 RCF, and the upper aqueous layer was removed and discarded. The lower organic layer was dried under vacuum, and phospholipids were resuspended in 200 μL 0.1 % acetic acid in 40/60 A/B (A was 20 mM ammonium acetate in water, pH 5, and organic mobile phase; B was 9:1 ACN:acetone) by 1 hour

sonication. Samples were centrifuged at 1500 RCF for 5 min and transferred to fresh tubes prior to UPLC-MS/MS analysis.

UPLC-MS/MS analysis was performed using a Waters Acquity Triple Quadrupole Mass Spectrometer using a modified version of the chromatography suggested by and a Waters BEH C8 2.1 x 100 mm column.[18] Deuterated platelet-activating factor (PAF-d_4) was used as an internal standard. Chromatography used 0.6 mL/min initial: 40% A, 60% B held for 1 min; 2 min: 20% A, 80% B; 2.5 min: 16% A, 84% B held for 0.25 min; 3 min: 14% A, 86% B held for 0.25 min; 3.5 min: 12.3% A, 87.7% B held for 0.25 min; 4 min: 5% A; 95% B held for 1 min; 5.5 min: 40% A, 60% B held for 1.5 min. Electrospray ionization tandem mass spectrometry (ESI-MS/MS) was operated in positive ionization mode using the following parameters: capillary, 3.8 kV; extractor, 3.00 V; rf lens, 0.30 V; source temperature, 120 °C; desolvation temperature, 400 °C; cone gas flow, 20 L/hr; desolvation gas flow, 800 L/hr; collision gas flow, 0.2 mL/min; low-mass resolution (Q1), 12.00; high-mass resolution (Q1), 12.00; ion energy (Q1), 0.30; and varied collision energies listed in Table 4.1.

Spike recoveries were assessed by adding 5 µM PS, PC, PE, and SM to control platelet samples. Lipid extraction was performed as described above. PS, PC, PE, and SM were quantified in each of control, phospholipid-incubated, and recovery sample using a calibration curve prepared exactly as the platelet samples were prepared. To account for variation in pelleting behavior of platelets

induced by phospholipid incubation, phospholipid quantification results were normalized to average protein values of control- or phospholipid-incubated non-activated platelet pellets.

4.2.3 Device Fabrication for Aggregation Measurements

A microfluidic device, employed to monitor platelet aggregation behavior with varied phospholipid content, was fabricated as was previously described.[7] Briefly, microfluidic channels were fabricated in polydimethylsiloxane (PDMS) using standard photo-/soft lithography techniques. The cell culture channel dimensions were 450 μm (width) x 100 μm (height) x 2500 μm (length). After the PDMS layer with channels was fabricated, inlet and outlet holes were punched using a syringe needle, and the PDMS layer was washed to remove any remaining PDMS debris blocking channels. Then, the PDMS layer was bound to a clean glass substrate via oxygen plasma treatment to close the channel. After completion of a device, a 70 wt% ethanol solution was injected through the channel followed by a sterilized water rinse for sterilization purposes. This step was repeated three times, and after drying the channel, the device was exposed to UV light in a bio-hood for 5 minutes and then kept in the bio-hood until use.

4.2.4 Endothelial Cell Culture and Coating of the Microfluidic Device

Human endothelial cell line, Hy926, was purchased from American Type Culture Collection (ATCC, Manassas, VA). Dulbecco's Modified Eagle Medium (DMEM) with high glucose (formula: 4mM L-glutamine, 4.5g/L L-glucose, and 1.5g/L sodium pyruvate (Gibco®, Carlsbad, CA)), supplemented with 10% fetal bovine serum and 1% penicillin and streptomycin (Sigma Aldrich, Milwaukee, WI) was used as the culture media and cells were cultured in a T-flask in an incubator with 5% CO_2 at 37ºC. Cells were fed every other day and split once a week. Endothelial cells were used only in passages three through twelve.

A day or two before the experiments, a microfluidic device was first incubated for 30 minutes with a 250 µg/mL human fibronectin solution in an incubator. Meanwhile, trypsinized endothelial cells from a T-flask were washed and re-suspended into the same culture media at a cell density of ~10^7 cells/mL. The cell suspension was injected through the device inlet into the cell culture channel and kept in an incubator for 3 hours. The fresh cell culture media was then injected through the channel to remove any non-adherent endothelial cells remaining in the channel, and the device was maintained in an incubator, feeding the cells every 12 hours. A monolayer of endothelial cells was achieved within 48 hours (80% of the devices), and devices that did not resulted in a complete, uniform monolayer of endothelial cells within 48 hours were discarded (20% of the devices).

4.2.5 Adhesion of Platelets Incubated with Phospholipids

Devices with a uniform monolayer of endothelial cells were selected for experiments, and the channel was washed with fresh Tyrode's buffer before exposure of endothelial cells to a stream of platelets. To facilitate visual distinction of platelets from endothelial cells, platelets were labeled with CMFDA[19] (Invitrogen) dye prior to phospholipid incubation. After phospholipid incubation, platelets were activated with 5 µM ADP and introduced into the inlet. Flow control was accomplished using a syringe pump, and platelet suspensions were introduced onto the device through Teflon tubing. The endothelial cell-coated chamber was exposed to a stream of platelets for 20 minutes at a constant flow rate of 30 µL/hr. This flow rate was chosen to minimize the shear stress generated by moving fluid and avoid mechanical platelet activation. After endothelial cell exposure to platelets, the cell culture channel was washed with fresh Tyrode's buffer and fluorescence images were obtained on an inverted microscope (Nikon, Melville, NY) equipped with a CCD camera (QuantEM, Photometrics, Tucson, AZ) using Metamorph Ver. 7.7.5 imaging software. Platelets adhered to endothelial cells were counted, and for each experimental condition, five images (450µm x 500µm each) were averaged; in each case, five biological replicates were measured.

4.2.6 Bulk Platelet Secretion Measurements

Platelet δ-granule secretion was measured after incubation of the PRP with phospholipids using HPLC as was previously described in Chapter 1. For α-granule secretion, a PF4 ELISA assay was purchased from R&D systems and used as directed. Lysosomal secretion was measured via a β-hexoseaminadase assay.[20] Briefly, following incubation of platelets with phospholipid solutions, platelets were exposed to 10 U/mL thrombin solution or Tyrode's buffer (as control). Platelets were spun at 500xg to pellet. Supernatant portions were used for the analysis of the secreted species (serotonin by HPLC, PF4 with ELISA assay, and secreted hexoaminidase with β-hexoseaminadase assay). Moreover, to determine the total amount of the analyte of interest found in each granule, an aliquot of the PRP samples for each condition was lysed prior to activation and analyzed. Thus, for each assay, the total analyte amount stored in platelets, secreted via thrombin activation, and released in unstimulated conditions were determined. A BCA protein assay was used for normalization of the results to prevent any differences in the data due to the differences in the platelet count.

4.2.7 Total Protein Quantitation

Total protein in pelleted platelets was quantified with a Pierce Bicinchoninic acid (BCA) assay from Thermo Scientific, used as directed. Protein was extracted from platelet pellets with mammalian protein extraction reagent from Thermo Scientific, used as directed.

4.2.8 CFMA Measurements

Chapter 1 describes the fabrication of microelectrodes and the experimental setup for the CFMA experiments in detail.[21] After incubation, a drop of the PRP was added to the experimental chamber filled with Tyrode's buffer supplemented with the phospholipid of interest. An individual platelet was activated by 10 U/mL of thrombin solution. Current versus time data were collected for 90 s. Since the completion of CFMA measurements with all the phospholipid conditions on the same day was not possible, each phospholipid condition was compared with its own control measured from the same platelet sample on the same day. Data were analyzed as was previously described. The numbers of individual platelets analyzed per phospholipid condition were: (control =20, PC= 21); (control= 47, PE= 27); (control=20, PS=18); and (control=58, SM=45).

4.3 Results

4.3.1 Relative Quantitation of Phospholipids

Quantification of lipid species is quite challenging. Herein, relative phospholipid enrichment of platelet membranes was assessed using a UPLC-MS/MS method. Mobile phase composition and column selection were based on a previously published work reported by Rainville and Plumb,[18] and chromatography was modified from the same report to a 7 min separation by adjusting the chromatographic conditions to the conditions for elution for each compound. An absolute quantification method was not possible because the phospholipid standards contained mixtures of fatty acid tails with a common headgroup. Instead, fragmentation transitions for the primary component of each phospholipid were monitored, and lipids extracted from phospholipid-incubated platelets were compared to those extracted from control platelets. Phospholipid concentration values were then normalized to extracted protein values from platelet pellets incubated with phospholipids and washed under the same conditions as the platelets from which the phospholipids were extracted. The transitions that were used for the assessment of the enrichment for each phospholipid are given in Table 4.1. All phospholipid transitions were monitored in all platelet samples, and enrichment was only observed in the phospholipid in which the platelets had been incubated. Thus, 2h incubation was enough time for platelets to take up the phospholipid that they were incubated in without up/down

regulating the other endogenous phospholipids. This allowed us to directly compare the effect of enrichment of each particular phospholipid on the platelet secretion and aggregation behavior. The percent increase in phospholipid content was 58.14 ± 36.01, 59.89 ± 10.93, 325.6 ± 47.24, 193.3 ± 50.97 for PS, PC, PE and SM conditions, respectively. Surprisingly, the % enrichment for PE and SM conditions were drastically higher than the PC and PS conditions. For PE, this is perhaps due to the very small quantities of the PE species monitored in the control samples.

4.3.2 Phospholipids and Platelet Aggregation

While all other experiments used thrombin activation, the microfluidic adhesion experiment used ADP activation to specifically investigate adhesion of platelets because ADP is known to induce platelet adhesion but not secretion.[22] Although the adhesion of ADP-activated platelets from each condition was relatively consistent, the number of platelets adhered to endothelial cells varied from day to day, and thus, comparisons of platelet adhesion to endothelial cells under each phospholipid condition were done with respect to the number of control platelets adhered to endothelial cells.

The ratios measured for each condition were tested to see if they were statistically different from 1 because a ratio of 1 indicates the same number of adhered platelet in the control and phospholipid-enriched platelets. As seen in the Figure 5.2, platelets incubated with PC, PS, and SM showed reduced adherence to endothelial cells compared to the control condition, with ratios of 0.311±0.036, 0.625±0.075, and 0.516±0.125 for PC, PS, and SM, respectively. In contrast, platelets incubated with PE adhered to the endothelial layer in significantly higher numbers, with a ratio of 1.553±0.022 (p values are 0.0001, 0.037, 0.0004, 0.0023 for PC, PE, PS, and SM, respectively).

4.3.3 Assessment of α-granule, δ-granule, and Lysosomal Release at Altered Phospholipid Levels with Bulk Secretion Assays

Since a method that enables measurement of α-granule and lysosome release with sub-ms time resolution at single platelet level is not available, bulk secretion assays were performed under conditions with phospholipid enrichment. The bulk δ-granule secretion will be compared with single cell data (vida infra). In all cases, the amount of secreted molecules from each type of granule was normalized according to platelet protein content.

Table 4.1 Summary of the UPLC-MS/MS analysis of each phospholipid

Phospholipid Incubation Condition	Control	PS	PC	PE	SM
Transition used for relative quantitation	n/a	812.5→627.4	782.9→86.1	718.3→577.3	703.8→184.1
Instrumental Precision (RSD)	n/a	9.312	15.94	15.93	7.635
Biological Precision (RSD)	n/a	17.46	17.58	13.31	23.59
Recovery (% ± SD) at 5 µM	n/a	83.06 ± 6.474	107.3 ±6.374	85.39 ± 13.26	64.75 ± 5.559
Total protein in pelleted platelets (µg/mL ± SD)	53.55 ± 5.00	44.26 ± 4.98	40.65 ± 4.99	37.48 ± 5.34	44.89 ± 5.60
Percent increase in platelets upon incubation (range in 4 replicates)	n/a	12.57 – 100.5	51.56 –75.99	288.5 – 392.9	145.7 – 245.9
Average percent increase (Percent ± SD)	n/a	58.14 ± 36.01	59.89 ± 10.93	325.6 ± 47.24	193.3 ± 50.97

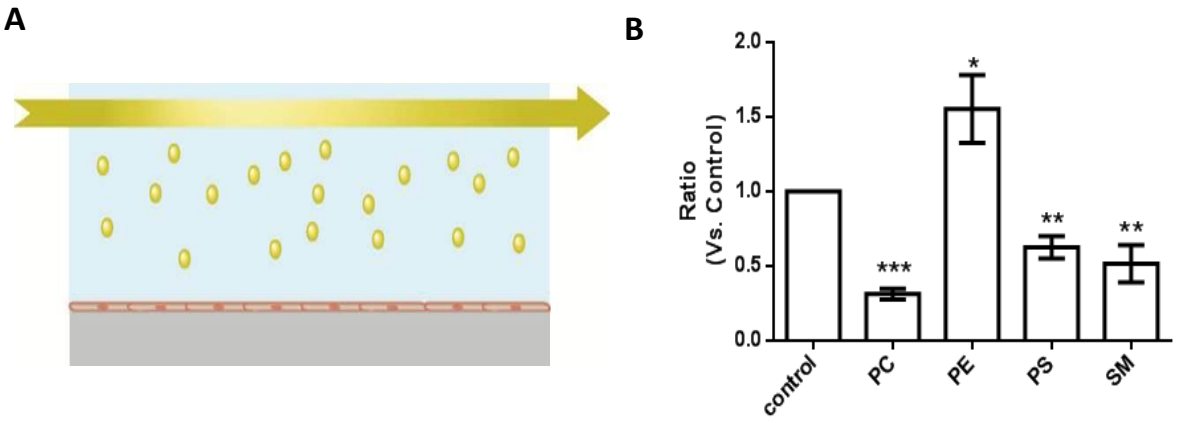

Figure 4.1 Platelet aggregation measurements.

(A) Design of the microfluidic device used for the measurements. (B) Ratio of the platelet numbers adhered at each condition to control. (p values are 0.0001, 0.037, 0.0004, 0.0023 for PC, PE, PS, and SM respectively *denotes $p<0.05$, ** denotes $p< 0.01$, *** denotes $p<0.001$).[7]

Bulk assay results show that an increase in the PS content impaired both α- and δ- granule secretion. While platelets not treated with any phospholipid secreted 0.0281±0.0017 μg serotonin/μg protein, PS incubation led to a decrease in the average amount of serotonin secreted to 0.0093±0.0019 μg serotonin/μg protein (Figure 4.2D; $p=0.002$). A more drastic effect was observed in α-granule secretion; upon PS enrichment, PF4 secretion was almost completely attenuated, showing similar PF4 values with the unactivated platelets (Figure 4.2B). PS also impaired lysosomal secretion. However, unlike α-and δ- granular release, lysosomal secretion increased with enriched PE and SM levels compared to control ($p=0.0003$ for PE, $p<0.0001$ for SM). This shows that PE and SM facilitate lysosomal release and may indicate that PE and SM interact with proteins that promote lysosomal secretion, including cytoskeletal proteins or membrane proteins that help anchor the lysosomal membrane with the plasma membrane. In previous work, an increased lysosomal activity upon SM accumulation was reported through SM binding to the LAMP 1 on lysosomes in stress-resistant cells.[23]

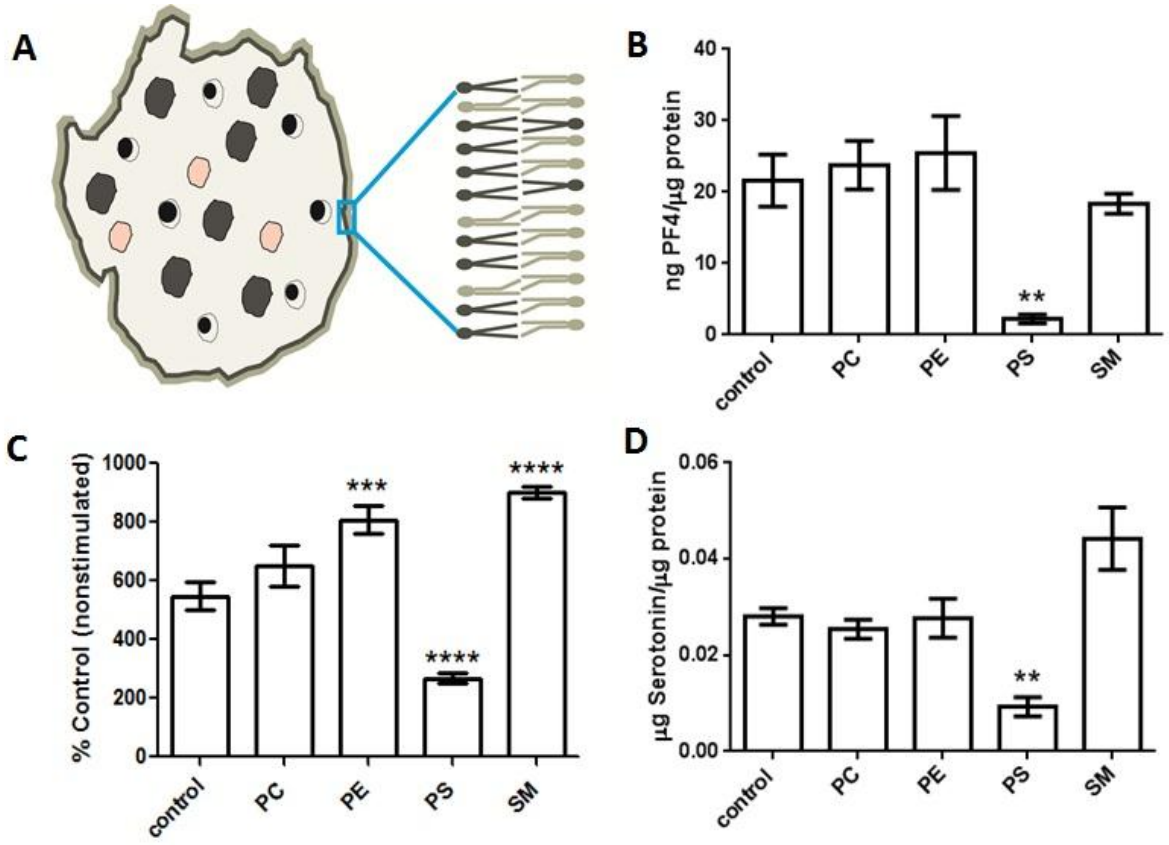

Figure 4.2 Assessment of phospholipid effect on platelet granule secretion.
(A) A representative figure illustrating three different platelet granule types; δ-granule, bull eye shape; lysosome, pink shape; and α-granule, uniformly filled irregular shapes. Phospholipids are asymmetrically distributed. (B) PF4 release from α-granules after different phospholipid enrichment. (C) Lysosomal release increased with PE and SM enrichment and decreased with PS uptake. (D) δ-granule secretion was also suppressed at high PS concentrations. *p<0.05, **p<0.01, ***p<0.001, ****p<0.0001 compared to control.

4.3.4 Effect of Phospholipids on Platelet δ-Granule Secretion

The time resolution of the CFMA technique enables a more detailed characterization of the δ-granule secretion and reveals the biophysical mechanistic underpinnings of the bulk measurements [21]

PC did not affect the quantity of the serotonin released from platelet granules or the kinetics of the release events(Figure 4.3A). However, the number of δ-granules released per secretion event was significantly lower for PC-enriched platelets (N= 7.20±0.63 for control; N= 5.36±0.55 for PC condition p= 0.0337). Moreover the cumulative frequency of the release analysis showed that in early stages of secretion, the control and PC-treated platelets release granules with similar frequency, but that PC-enriched platelets slow granule release frequency before control platelets. This implies that the PC may influence the granular recruitment which will be discussed later in detail.

Although incubation of the platelets with PE and SM resulted in great enrichment of these phospholipids, neither of these platelet pools showed a significant change in the platelet δ-granule secretion (Figure 4.4 and 4.5). It should be noted that PE incubation gave rise to the highest number of events with a foot feature; however this effect was not significant compared to control condition (p=0.075).

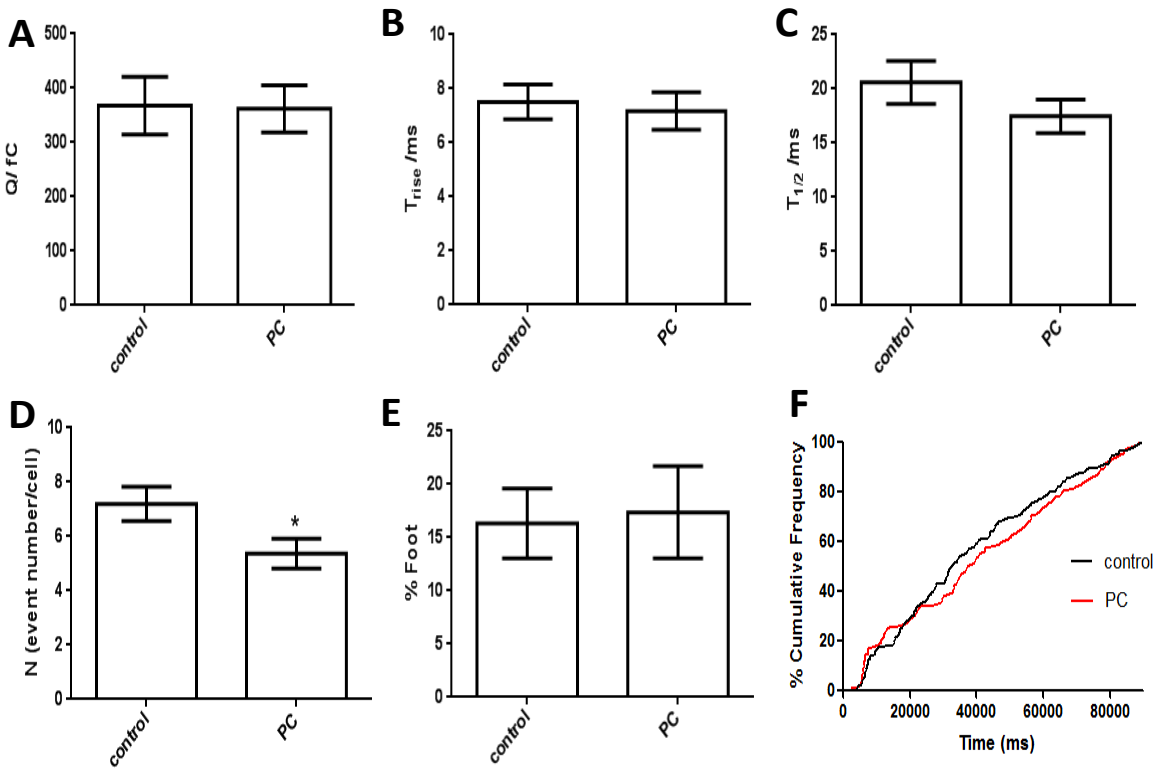

Figure 4.3 Effect of PC on δ-granule quantal release and release kinetics.
(A) PC did not influence the amount of serotonin released from single granules. Kinetics of the release (B) and (C) were also unchanged. (D) A lower number of granules exocytosed from single platelets with comparable fusion pore stability (E). (F) Cumulative frequency analysis shows initially fast but later slowed granule trafficking in PC-enriched platelets.*p=0.05.

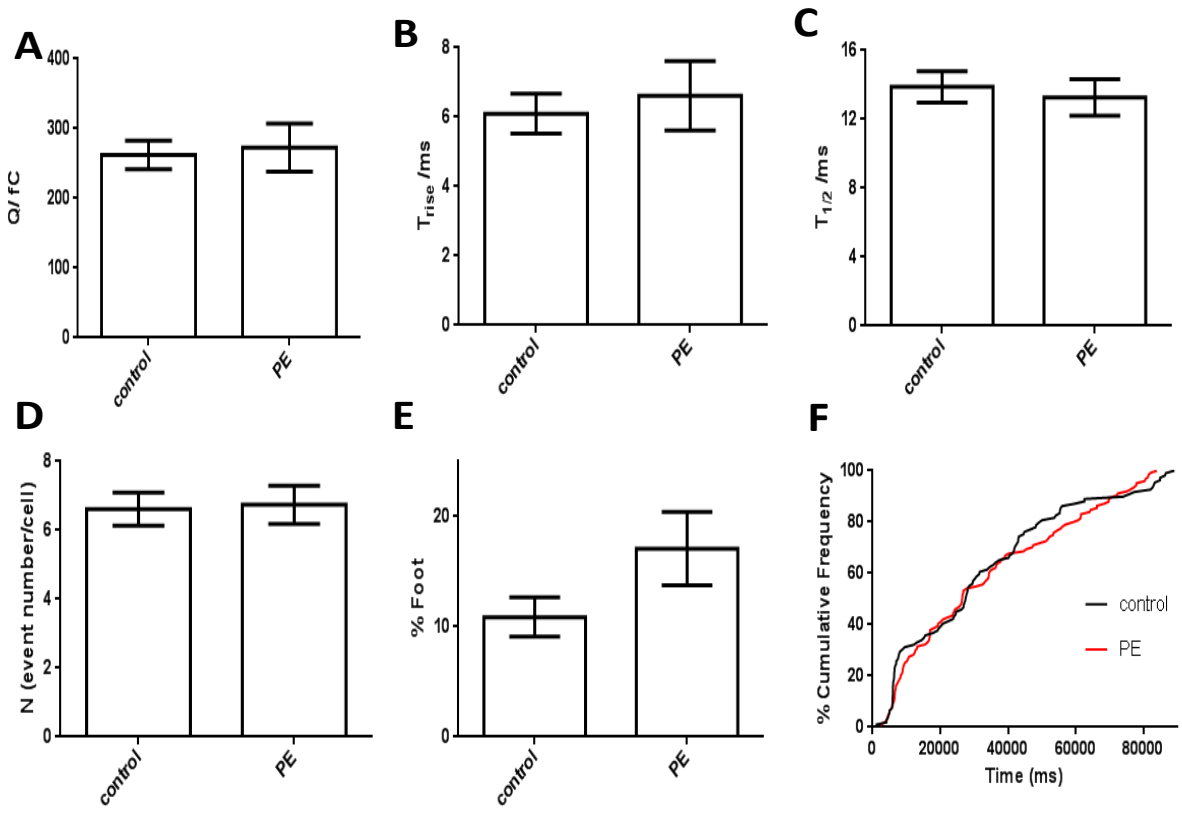

Figure 4.4 Effect of PE on δ-granule quantal release and release kinetics.
(A) PE did not influence the amount of serotonin released from single granule. Kinetics of the release (B) and (C) were also unchanged. (D) Similar number of granules were exocytosed from individual platelets with comparable fusion pore stability (E). Cumulative frequencies of the release are the same for each condition (F).

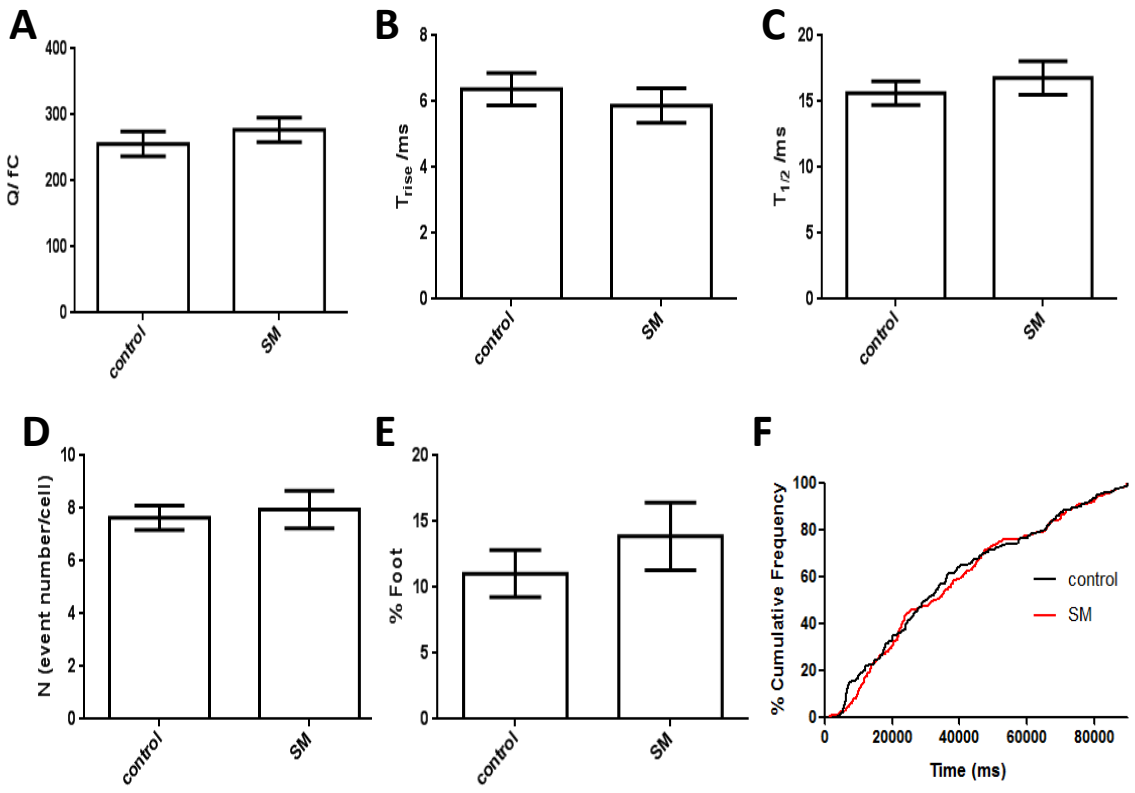

Figure 4.5 Effect of SM on δ-granule quantal release and release kinetics.
(A) SM did not change the amount of serotonin released from single granule, (B) and (C) kinetics of the release; (D) number of granules exocytosed from single platelet; (E) fusion pore stability or (F) cumulative frequency of the release. $p>0.05$

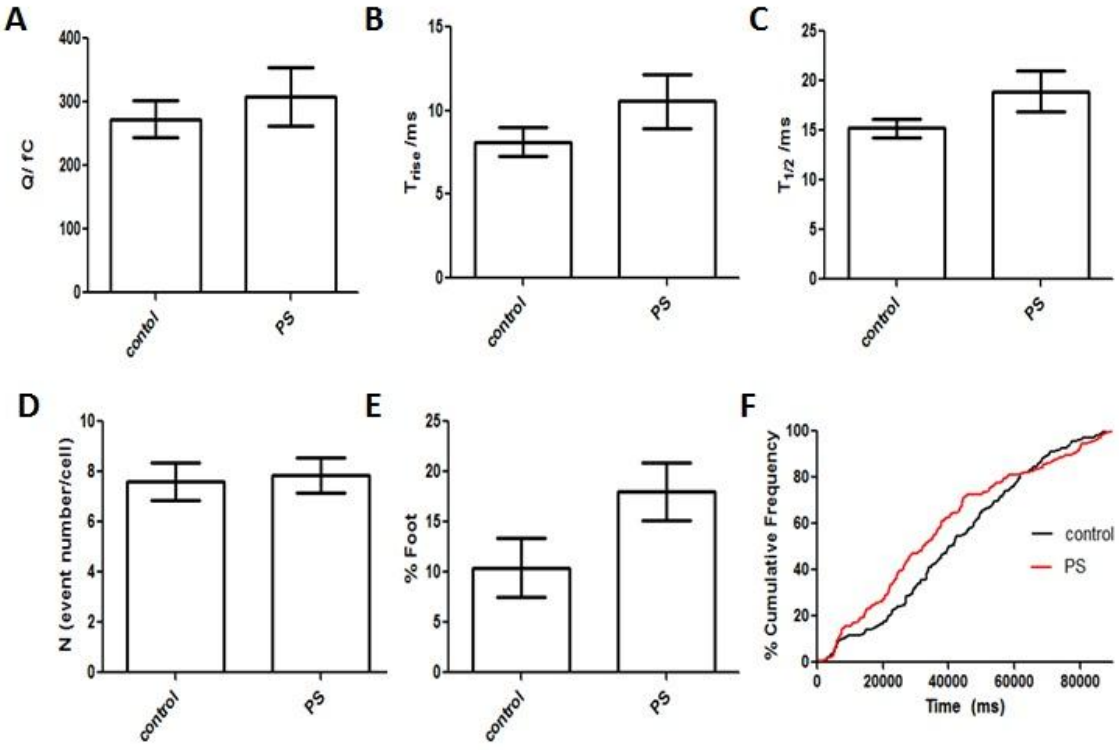

Figure 4.6 Effect of PS on δ-granule quantal release and release kinetics.
(A) PS did not influence the amount of serotonin released from single granules. Similar T_{rise} (B) but higher $T_{1/2}$ (C) values obtained. (D) Number of granules exocytosed from single platelets did not change.(E) PS increased fusion pore stability. (F) Cumulative frequency analysis shows initially fast but later slowed granule trafficking in PS-enriched platelets.*p=0.05.

PS was the phospholipid that altered the platelet δ-granule secretion the most. Upon PS enrichment, the platelet's quantal secretion did not change (Q= 262.70±36.06; 317.50±29.10 fC for control and PS conditions, respectively; p=0.246). Since the average number of granules secreted from individual platelets did not change between the conditions, it can be concluded that the total amount of serotonin secretion does not change with PS enrichment. This contradicts with bulk serotonin secretion measurement in which PS lowered the amount of serotonin extruded. Since single cell measurements are performed by measuring the action of one cell at a time in a relatively isolated space, it is unlikely that the activated secretion of one platelet will have a downstream effect of activation on another one. In bulk measurement, however, this interaction is unavoidable; initially activated platelets will secrete chemical messengers that will activate the platelets that were not initially activated. The discrepancy between the single cell and ensemble measurement is likely the impairment of the downstream effect. However, without single cell measurements it is not possible to observe the actual response to the stimulation, nor the heterogeneity in the response changing from platelet to platelet.

Although a similar amount of serotonin is extruded from platelet granules in both control and PS-enriched conditions, the secretion kinetics slow at higher membrane PS concentrations ($T_{1/2}$ values are 12.39±3.01 and 21.67±2.38 ms for control and PS conditions, respectively; p=0.0048). Although the number of granules secreted from individual platelets (N numbers) did not change, similar to

PC-treated platelets, the platelets enriched with PS also showed two different phases in terms of frequency of exocytosis (Figure 4.6F). In the early phase, the granules that were docked before activation were released with a comparable frequency to the control condition. However, the frequency of the granular secretion decreases, showing slower granule trafficking and docking compared to the control condition. Finally, fusion pore analysis showed that PS enrichment increased the stability of the fusion pore, with foot events occurring in 23.6±4.6% of the total secretion events, compared to 12.4±3.0% foot events observed for control.

4.4 Discussion

Phospholipids are the major components of the plasma and granule membrane, and in addition to their structural importance as a cellular barrier that separates the intracellular and extracellular environment, they are also dynamically involved in and regulate many cellular processes. In platelets, the phospholipid components are especially critical because it is likely that phospholipids are involved in platelet aggregation and secretion. However, there is not much known about how the different lipids regulate platelet behavior. In this work, the most common membrane phospholipids (PC, PS, PE and SM) were used to study the effect of phospholipid enrichment on both platelet aggregation (using a microfluidic device to mimic the vascular environment) and granular secretion

(using CFMA and bulk secretion assays to evaluate the importance of phospholipids in platelet α- and δ- granule and lysosomal release).

Platelets were incubated with each of the phospholipids for 2h, long enough to enrich the platelets with the phospholipid of interest but short enough to minimize the up or down regulation of the synthesis of other phospholipids. MS analysis confirmed that only the phospholipid content that the platelets were incubated in changed, without any significant change in the composition of other phospholipids. This allowed an unambiguous evaluation of the effect of each phospholipid in platelet function.

Use of microfluidic devices coated with endothelial cells simulated blood vessels for evaluation of platelet aggregation. To separate platelet aggregation from secretion we used ADP, a strong agonist for platelet aggregation but not secretion.[22] 5 μM ADP provided a moderate platelet activation and the ability to count the number of stained, adherent platelets for each condition. Although PS is mostly known for its procoagulant function, PS enrichment in fact diminished the platelet aggregation compared to control platelets. Besides providing a negatively charged surface to facilitate the binding of the coagulant factors, flipping of PS from inner leaflet of the plasma membrane to the outer leaflet provides reorganization of the coagulation proteins in the plasma membrane. Upon PS incubation, it is likely that the PS concentration on the outer leaflet of the platelet membrane increased and impaired the translocation of the PS from

inner leaflet to outer leaflet, thus diminishing the reorganization of the coagulation proteins that would facilitate platelet adhesion to endothelial cells. This observation is in agreement with the previous findings in which the higher plasma level of PS-decreased platelet coagulation and thrombus formation.[4, 14] On the other hand, this is the first report, to the best of our knowledge, that the anticoagulant effect of PC and SM has been shown. In resting platelets, PC and SM reside mostly on the platelet surface and prevent platelet activation by providing a mostly neutrally charged membrane. The enrichment of these two phospholipids may prevent platelet aggregation in the same manner. Unlike these three phospholipids, PE boosted platelet aggregation by causing 50% more platelet aggregation than control platelets. Previous work published by Zieseniss et al showed that oxidized PE is one of the major components of low density lipoproteins that cause very strong thrombotic function.[24] A similar effect explains our observations and reveals that PE synthesis and oxidation may be a good target for thrombosis prevention.

In addition to their role in platelet aggregation, phospholipids are major components of exocytosis. During exocytosis, phospholipids not only serve as a matrix and accommodate essential proteins for membrane fusion but, by controlling the fluidity and curvature of the membrane, they influence the energy required for each step of exocytosis, especially the formation and stability of the fusion pore.[16, 25-28] We first performed bulk secretion measurements on the all types of platelet granules. Both α- and δ- granule secretion diminished greatly

upon PS enrichment. None of PE, SM or PC enrichment changed the bulk exocytosis characteristics of these two granule populations. Surprisingly, lysosomal release was enhanced upon both PE and SM enrichment. It is known that phospholipids interact with the exocytotic machinery; moreover, it is shown that there are specific sub-units of proteins involved in recruitment and secretion of specific types of platelet granules. A similar scenario may be true for lysosomal release where specific interactions of PE and SM are required. Although SM regulation of lysosomal function has been reported in other cell types[23] there is not any precedent work on platelets; thus, future work will explore these data further.

Amperometric recordings of δ-granule secretion enabled detailed evaluation of the secretion at altered phospholipid levels. Neither PE nor SM caused any change in the quantal release or the secretion kinetics. However, PS enrichment resulted in longer secretion events with a prolonged spike width (higher $T_{1/2}$) (Figure 4.6C). Although PC treatment did not influence the amount of serotonin released per granule or the kinetics of release, significantly lower numbers of granules were released from the platelets enriched with PC ($p=0.033$). Moreover, cumulative frequency analysis of the release showed that upon activation, both control and PC-treated platelets release their granules around the same pace but that PC-treated cells lag later in the secretion event. In early moments of the exocytosis, the granules that are released immediately constitute the already docked granules. Release of the other granules requires recruitment of the

granules to the site of fusion and docking. Both low N numbers and slower release frequency indicate the possible effect of PC on granule recruitment and docking. A possible effect of PC on vesicle requirement in PC12 cells has been reported previously.[8] Moreover, recent work has demonstrated that PC enriched in axons of neurons shows a proximal to distal gradient which is regulated by actin dynamics. This type of inter-regulation may be possible between platelet PC and cytoskeleton where the disruption in PC localization interferes with actin function and recruitment to the membrane. [29] Although this would reveal a unique regulatory pathway for platelet granular release, further work needs to be done to test this hypothesis. A more apparent two phase frequency of release was also observed with PS-enriched platelets, although the N numbers were not different. This implies a regulatory effect of PS on granular recruitment but not docking.

Although PE and SM support negative membrane curvature, PS packs better on positively curved membranes. PC forms almost a flat layer, with minimal influence on membrane curvature. The role of phospholipid curvature in exocytosis becomes more prominent during fusion pore formation. [16, 25-28] Fusion pores are highly curved membrane structures that require phospholipids with positive curvature to pack in the outer leaflet and the phospholipids with negative curvature to pack on the inner leaflet for stabilization. To achieve a stable fusion pore, the phospholipid with appropriate curvature should be on the appropriate side of the membrane. As expected, the % of fusion events with a foot (stable fusion pore) did not change with PC enrichment. Although both PE and SM

incubations slightly increased the % of foot events, the changes were not significant (p=0.075 for PE and 0.353 for SM). While it is known that the lipids with negative curvature stabilize the fusion pore better, PS (with positive curvature) provided more stable fusion pores compared to untreated platelets. This can be attributed to the exposed PS on the surface of the membrane upon activation which stabilizes the positive curvature of the fusion pore. Previous work reported the time of PS transport from inner leaflet to outer leaflet of the membrane as 3 min.[4] During 90 s of amperometric recordings, it is likely that more than half of the PS was exposed to the plasma outer surface. Moreover, PS-enriched PC12 cells also displayed more stable fusion pore events which was attributed to the interaction of PS with synaptotagmin that gave rise to highly bended membrane with negative curvature. [16, 25-28, 30] Platelets have synaptotagmin-like protein 1 and its interaction with PS is not known.[31]

Herein, we have demonstrated how different phospholipids can act on different aspects of platelet function. We demonstrated that although PE does not affect platelet α- and δ-granule secretion, it over activates the thrombotic function of platelets. Moreover, this work highlights the possible interaction of phospholipids with important proteins involved in the secretion process. Elucidating the function of lipid-protein interactions will improve our current understanding of platelet secretion since it is obvious that the platelet secretion is regulated synergistically by both protein and lipid species.

Chapter 5

Cholesterol Effects on Granule Pools in Chromaffin Cells Revealed by Carbon-Fiber Microelectrode Amperometry

Adapted from:

Koseoglu S, Love SA, Haynes CL. Cholesterol effects on vesicle pools in chromaffin cells revealed by carbon-fiber microelectrode amperometry. *Anal Bioanal Chem*. 2011;400:2963-2971

5.1 Introduction

Upon stimulation, many cells release chemical messenger molecules through the tightly regulated process of exocytosis. Understanding the underpinnings and driving forces of this highly conserved process is critical from both a fundamental and applied perspective. Since exocytosis involves coalescence of the cellular and granular membranes to form a fusion pore that then dilates to release granular content, components of the membrane are likely critical in how, and if, this process proceeds. The cellular plasma membrane has two important components that may influence the fidelity of exocytosis: proteins and lipids. Soluble N-ethylmaleimide-sensitive factor attachment protein receptor (SNARE) membrane proteins have been studied extensively and are known for their role in membrane mixing.[1-4] Knowledge about the effect of membrane lipids on exocytosis, however, is limited.[5, 6] Cholesterol is one of the major lipids found in the membrane, with numerous structural and functional capacities. Cholesterol lends structure to the membrane, facilitating the formation of cholesterol-rich microdomains that are sometimes called lipid rafts.[4, 7] It has been shown that these lipid rafts are important regulators of SNARE function. [3, 4, 8] For example, syntaxin (a SNARE protein) embedded in cholesterol-rich rafts has been shown to be the preferential site for exocytosis. In addition, depletion of membrane cholesterol disrupts these domains and decreases the number of exocytotic events in PC12 cells, an immortal chromaffin cell line often used to model exocytotic processes.[3] Although the direct effects of lipid modulation on

exocytosis have not been explored, the localization of other SNARE proteins, including SNAP25 and SNAP23, in these cholesterol-rich domains has been reported.[4] Furthermore, cholesterol may influence the energetics of fusion pore formation, stability of the fusion pore, and the overall energy dissipation based on the fluidity and the curvature of the membrane[7, 9-12]

Clearly, a better understanding of the role of cholesterol in exocytosis is necessary. Choice of a model cell is particularly critical when studying fundamental aspects of exocytosis. Chromaffin cells are neuroendocrine cells found in the adrenal gland, and they store and release catecholamines. Besides their importance in the physiological fight-or-flight response, they have been widely used as model cells for neuron secretion based on common progenitor cells.[9, 13, 14] Careful study of these granules using total internal reflection fluorescence microscopy with fluorescent timer proteins, capacitance, and amperometry measurements has demonstrated that chromaffin cell granules are spatially distributed according to their age and that they have varied capacity for exocytosis.[15, 16] Newly assembled granules (about 140 granules in mouse chromaffin cells) constitute the readily releasable pool (RRP); this pool is already primed and docked at the plasma membrane and releases instantaneously upon chromaffin cell activation. The slowly releasable pool (SRP) is an intermediate pool that is in dynamic equilibrium with the RRP, showing a delayed release response compared with the readily releasable pool. The oldest granules (an average of 4,000 in mouse chromaffin cells) make up the reserve pool (RP),

granules localized in the interior of the cell, requiring transport to the plasma membrane before exocytosis.[15-17]

Both spectroscopic and electrochemical analyses reveal that these pools can be selectively activated with different secretagogues.[18-20] Nicotine and K^+ stimulations preferentially activate the younger granules (mainly the RRP) whereas Ba^{2+} selectively activates the older (mainly RP) granules. Although it has recently been demonstrated that membrane cholesterol content influences the release behavior of the RRP granules in chromaffin cells, [9, 10] there is no information about how or whether the release of older granules changes with the cellular cholesterol content. Moreover, the effect of membrane cholesterol on subsequent release events has not been explored. In this work, we systematically vary the membrane cholesterol content in primary culture chromaffin cells to study the effect of membrane cholesterol on release of different granule pools and the recovery of release in chromaffin cell granules. Our results show that, although cellular cholesterol level influenced the stability of fusion pore, it did not change the quantity or the kinetics of the younger granule release, due to the low occurrence of the events with a sustained fusion pore compared with the full fusion events. Moreover, cellular cholesterol content caused quantal and kinetic changes in the subsequent release events when cells were stimulated a second time. Finally, preferential release of the oldest granules upon Ba^{2+} stimulation showed different behavior than that of the younger granule pools, suggesting that these granule pools are biochemically and/or

morphologically distinct or that they are released from different sites of the plasma membrane.

5.2 Materials and Methods

5.2.1 Cell isolation and culture

For amperometry experiments, primary culture murine adrenal medullary chromaffin cells were isolated from wild-type brown mice (C57BL/6J, Jackson Laboratories) according to an approved University of Minnesota Institutional Animal Care and Use Committee protocol (#0807A40164). For cholesterol assay experiments, mice from the University of Minnesota tissue-sharing program were used for cell isolation due to the large number of cells required. A previously published procedure was used for cell isolation from mice.[21] Briefly, mice were euthanized, and the adrenal glands were excised from above/ adjacent to the kidneys and kept in ice-cold Dulbecco's modified eagle medium (DMEM) with Ham's nutrient 12 mix (DMEM/F12 1:1, Invitrogen, Carlsbad, CA) media until they were dissected on a PDMS board in chilled Locke's buffer (154 mM sodium chloride, 3.6 mM potassium chloride, 5.6 mM sodium bicarbonate, 5.6 mM glucose, and 10 mM HEPES in water sterile filtered and pH adjusted to 7.2; Sigma-Aldrich, St. Louis, MO) to remove cortical tissue. Removal of the medullary tissue was accomplished by digestion in neutral protease (Worthington Enzyme, Lakewood, NJ) with an activity of 25 U/mL followed by repeated washing and triteration in DMEM/ F12 media. Cell suspension was cultured in 35-mm Petri dishes (for carbon-fiber microelectrode amperometry (CFMA)

experiments) or multi-well plates (for cholesterol assays), incubated at 37 °C in a 5% CO_2 atmosphere and used within 48 h of cell harvest.

5.2.2 Manipulation and Measurement of Cellular Cholesterol Methyl-β-Cyclodextrin

(MBCD) is a well-known cholesterol carrier, and it can act as either a cholesterol acceptor or donor depending on the cholesterol/MBCD ratio.[22] In this work, both MBCD and cholesterol-saturated MBCD solutions were freshly prepared by dissolving MBCD/ cholesterol-saturated MBCD in DMEM/F12 and sonicating for 30 min, followed by pH adjustment to 7.3 and filtration. Cellular cholesterol was depleted upon incubation of the cells in 10 mM MBCD in DMEM/F12 media for 30 min.

Replenishment of the depleted cholesterol was achieved by an additional 30 min incubation of cells in 5 mM cholesterol-saturated MBCD in DMEM/F12 after depletion as described above. Cholesterol quantification was done using the Amplex red cholesterol assay kit (Invitrogen, Carlsbad, CA), and the amount of cholesterol was reported as nanograms cholesterol/microgram protein, where protein content was determined using a standard protein assay kit (Thermo Fisher Scientific, Waltham, MA). Briefly, followed by incubation, cells were washed with PBS buffer and lysed with M-PER protein extraction reagent. Then 0.1 mL of cell suspension was mixed with Pierce 660 Protein assay solution, and the absorbance at 660 nm was measured after 5 min of incubation. For quantitation of protein, a calibration curve was built by measuring the absorbance

of standard bovine serum albumin solutions with concentrations from 125 to1,500 µg/ml. For cholesterol analysis, 50 µl of cell suspension was added to a mixture of Amplex red reagent (300 µM), horseradish peroxidase (2 U/mL), and cholesterol oxidase (2 U/mL) in reaction buffer. After incubation for 1 h at 37 ºC, fluorescence measurements were done by microplate reader. The calibration curve for cholesterol analysis was also generated by using prepared cholesterol solutions with known concentrations of 2 to 20 µM. To obtain measurable cholesterol levels, for the cholesterol assay experiments, cells were obtained from 10–12 mice.

5.2.3 Microelectrode preparation and amperometry experiments

Carbon-fiber microelectrodes were fabricated according to a previously published procedure.[14] A carbon fiber (Thornel T650, Amoco Corp., Greenville, SC) was aspirated into a glass capillary, and the glass layer was tapered around the fiber using a resistively heated micropipette puller (PE-21, Narishige, Tokyo, Japan). The carbon fiber was trimmed with a scalpel to get an exposed length of less than 20 µm. Insulation was achieved by dipping the electrodes into preheated mixture of EPON resin 828 (Miller-Stephenson, Morton Grove, IL) with 15 % wt. 1,3-phenylenediamine hardener (Sigma-Aldrich, St. Louis, MO). Electrodes were allowed to cure at room temperature for 24 h followed by further curing at 100 °C for 12 h and at 150 °C for 12 h. Prior to amperometry experiments, electrodes were polished to a 45° angle using a diamond-embedded beveling wheel (Sutter Instrument Company, Novato, CA) and stored in isopropyl alcohol purified with

activated carbon until use. For electrical conductance, electrodes were backfilled with 4.0 M potassium acetate and 150.0 mM potassium chloride solution. Amperometry experiments were performed with an Axopatch 200B potentiostat (Molecular Devices, Inc., Sunnyvale, CA) using low-pass Bessel filtering (5 kHz), a sampling rate 20 kHz, and gain amplification of 20 mV/pA, all controlled by locally written LabVIEW software and National Instruments data acquisition boards. Cells were visually monitored during experiments with an inverted microscope equipped with phase contrast optics (Nikon Instruments, Melville, NY). To keep the cells at constant physiological temperature (37 °C), Petri dishes were kept in a temperature-controlled chamber (Warner Instruments, Hamden, CT). A two-electrode configuration was used, and the catecholamines, epinephrine, and norepinephrine were oxidized at +700 mV vs a Ag/AgCl reference electrode (BASi, West Lafayette, IN). To introduce chemical stimulation to the cell of interest, fire-polished glass capillaries were used with an average tapered diameter of 10 μm. Delivery of the secretagouge was provided by applying nitrogen pressure to the stimulant-filled capillary using a PicoSpritzer III (Parker Hannafin, Cleveland, OH).

Burleigh PCS500 piezoelectric micromanipulators (EXFO, Mississauga, Canada) were used to position both electrode and stimulating pipette on or near individual cells. The carbon-fiber microelectrode was positioned in contact with the cell of interest while the stimulating pipette was placed approximately 50 μm away from the cell in the same z plane. Potassium stimulation experiments were done in

buffer containing 150 mM NaCl, 12.5 mM Tris, 4.2 mM KCl, 5.6 mM glucose, 1.5 mM $CaCl_2$, and 1.4 mM $MgCl_2$. Potassium stimulation solution was prepared from 60 mM KCl, 94.2 mM NaCl, 12.5 mM Tris, 5.6 mM glucose, 1.5 mM $CaCl_2$, and 1.4 mM $MgCl_2$. Neither the buffer nor the stimulating solution contained Ca^{2+} for barium experiments. The buffer for barium stimulation experiments contained 150 mM NaCl, 5 mM KCl, 10 mM HEPES, 1.2 mM $MgCl_2$, and 5 mM glucose. The stimulation solution of 5 mM Ba^{2+} was prepared by adjusting the concentration of NaCl to obtain a buffer and stimulating solution with matching osmolarity. All the solutions were sterile filtered and pH-adjusted to 7.4. For the control condition, cells were washed twice with buffer solution and placed into the temperature-controlled chamber for electrochemistry experiments. For the condition which will be referred to as MBCD in the remainder of this paper, cells were exposed to 10 mM MBCD containing DMEM/F12 media for 30 min and then washed with buffer solution, and amperometry experiments were performed. The reload condition includes both the depletion of membrane cholesterol as it was described in the MBCD condition and a replenishment step with 30 min incubation of cells in 5 mM cholesterol-saturated MBCD in DMEM/F12. All the amperometry measurements were done within 2 h after the cells were removed from DMEM/F12 media. For K^+ single stimulation and Ba^{2+} stimulation experiments, cells were triggered 3 s after electrochemical recordings began. For double stimulation experiments, cells were triggered at 3 and 33 s after electrochemical recordings began.

For single stimulation data analysis, Q, T_{rise}, Tdecay, $T_{1/2}$, and foot% were used to determine how changes in membrane cholesterol influence the course of exocytosis (see Chapter 2 for details). The aim of the double stimulation experiments was to see whether membrane cholesterol content would influence the granule recycling and recovery of the cell after the first release event. For this reason, in addition to comparing each parameter to the control, ratios of these parameters (i.e., Q_1/Q_2, $(T_{rise})_1/(T_{rise})_2$, etc.) were also considered to get a better understanding of cell recovery between the first and second stimulation. In addition, cumulative frequency analysis enabled visualization of granule release over time for each condition.

5.3 Results and Discussion

5.3.1 Cholesterol Analysis

Cellular cholesterol content after each treatment was determined using well-known cholesterol and protein assays. The results are reported as cholesterol percentage compared with control. Methyl-β-cyclodextrin treatment reduced the cholesterol level to 55.1±3.5% of control. Although the reload condition gave an average cholesterol concentration of 134.1±27.2% of the control, there is a wide % range from 102–188% obtained from various replicates (data not shown). Although MBCD is sufficiently selective for cholesterol, there may be some phospholipid extraction that occurs due to the nonspecific interactions of MBCD with membrane phospholipids, resulting in enhanced cholesterol loading under the reload condition.[10, 22, 23] Despite this possible nonspecific interaction of MBCD

and phospholipids, the results from MBCD enabled cholesterol manipulation are in good agreement with a previous study examining cholesterol effects using metabolic depletion of membrane cholesterol. [23] In this work, the reload condition is treated simply as a high cholesterol level condition. Several previous studies have examined the localization of various structures, including receptors and caveolae, within the membrane of various cell types by using MBCD-enabled cholesterol manipulation, including reloading with MBCD-cholesterol complexes. Given the dynamic nature of the plasma membrane, these studies have seen disruptions that indicate the membrane is not necessarily fully restored to its original condition after MBCD–cholesterol reloading.[24-27]

5.3.2 K^+-stimulated Release vs. Ba^{2+}-stimulated Release

Different granule pools of the chromaffin cells can be targeted depending on the secretagouge used. As shown in previous studies, high K^+ triggers mainly the release of RRP granules whereas Ba^{2+} recruits the release of older granules.[13] Figure 5.1 shows sample amperometric traces from K^+ double stimulation (Fig. 5.1A) and Ba^{2+} stimulation (Fig. 5.1B) experiments. When cells were exposed to high K^+ concentration, the granules belonging to the RRP show an immediate response and release their granular content with a burst behavior. However, release of granules upon Ba^{2+} stimulation show a delayed response since these older granules need to be trafficked to the plasma membrane, supporting previous findings that RRP granules and RP granules have different levels of

competency for release of their contents.[15, 16] In addition, Ba^{2+} stimulation results in a sustained release over a longer period of time. From a collection of K^+-stimulated traces (n=27 cells) and Ba^{2+}- stimulated traces (n=18 cells), an average of 54±7 granules/ cell release their vesicular content following K^+ stimulation compared with 352±32 granules/cell when cells were triggered by the Ba^{2+} secretagogue ($p<0.0001$). Keeping in mind that the carbon-fiber microelectrode samples from only ~10% of the cell surface area, it is clear that the K^+- stimulation incites release of more than just the RRP, likely drawing at least a portion of the SRP as well.

5.3.3 Effect of Membrane Cholesterol on Release of Young Granular Pools

The RRP/SRP granules reside near the cellular membrane, and some are primed to immediately release their content upon depolarization of the membrane with K^+ (60 mM). Amperometry results, collected from 18, 17, and 20 cells for control, MBCD and reload conditions, respectively (Figure 5.2), show that the quantal release of catecholamine from these granules with varied membrane cholesterol content did not change (Q=671.8±96.5 fC, 720.8±99.1 fC, 493.4±70.4 fC for MBCD, control and reload, respectively, $p>0.05$).

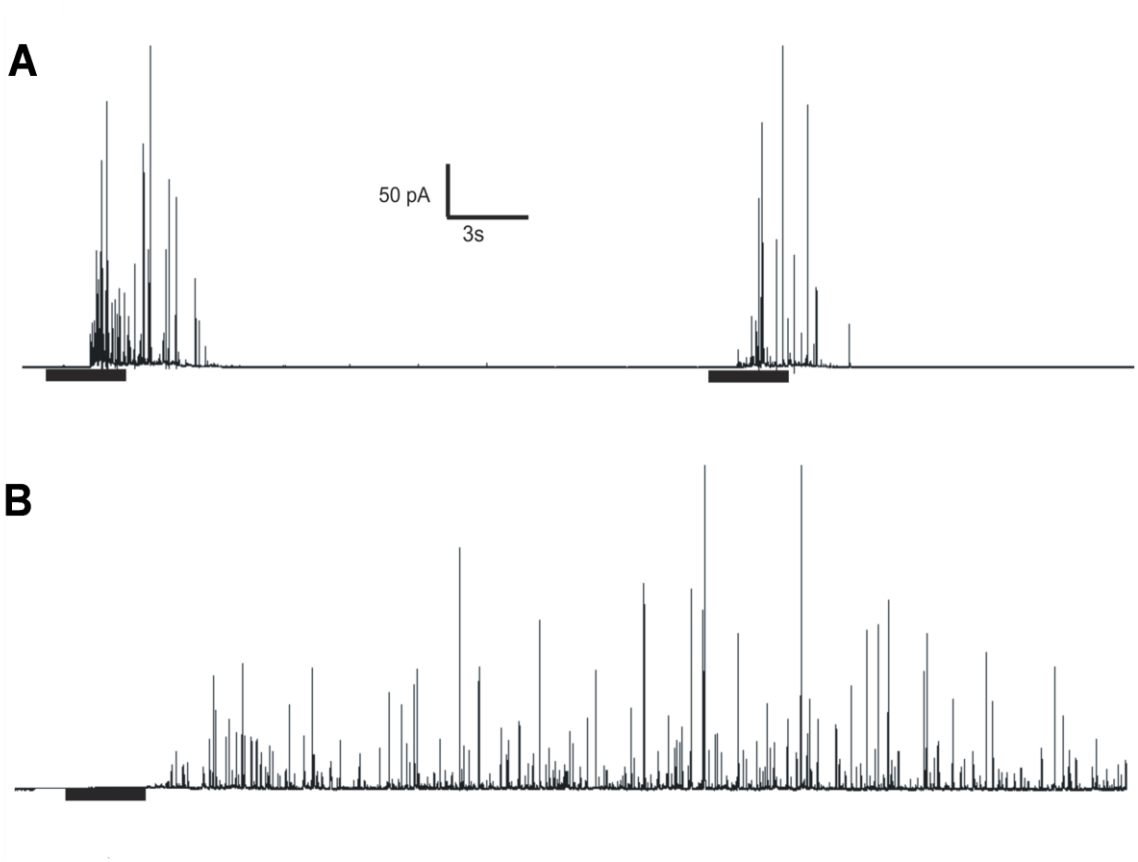

Figure 5.1 Representative amperometric traces of release from different chromaffin cell granular pools: (A) preferential release of RRP vesicles twice upon repeated stimulation with 60 mM K^+ and (B) release of RP granules with Ba^{2+} stimulation. The bar underneath the amperometric traces indicates the time and the duration of the stimulation.

This result indicates that changing the membrane cholesterol levels does not have any influence on the storage of chemical messenger molecules within RRP/SRP granules. Moreover, there was not a significant change in the kinetics of release events observed with altered membrane cholesterol levels (Figure 5.2C, $p>0.05$). This implies that membrane cholesterol does not affect the efficacy of the dilation of the fusion pore to the fully fused state or expansion of the granular matrix to release catecholamine content from RRP/SRP granules. This is somewhat surprising since the SNARE proteins, known to play an important role in cell–vesicle fusion, are influenced by membrane cholesterol levels.[2-4] Perhaps, in the already docked RRP vesicles, the SNARE protein function has already been performed, making membrane cholesterol levels less influential than in granules that must be trafficked and docked at the membrane upon stimulation. Another possible interpretation is based on the fact that the chromaffin cell's plasma membrane is known to have higher cholesterol content than the intracellular membrane and that intracellular cholesterol content is regulated based on the overall cholesterol level in the plasma membrane.[10, 22]

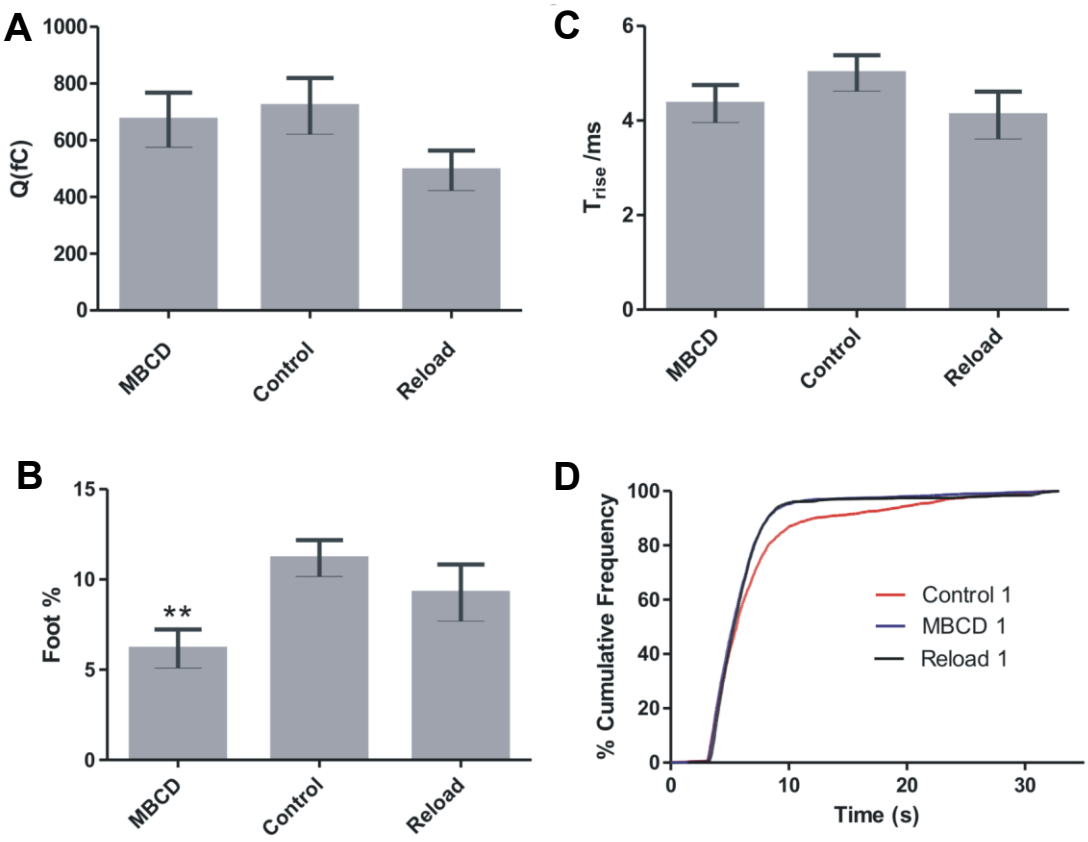

Figure 5 2 Analysis of the amperometric results from K^+-stimulated release at altered cellular cholesterol levels indicating: (A) there is not a significant change in quantal catecholamine storage/release, (B) low cholesterol levels destabilize the intermediate fusion pore state and fewer foot events occur when cells are treated with MBCD, and (C) the time required for full fusion to occur does not change, and d both high and low cholesterol levels facilitate the overall release process. (**represents $p<0.001$)

The half time for transport of cholesterol from the endoplasmic reticulum to the plasma membrane upon cholesterol depletion is between 10 min and 1 h.[10, 22, 28] Hence, it is possible that, even under conditions of membrane cholesterol depletion by MBCD, the cholesterol rich domains still form via membrane rearrangement and cholesterol supply from different parts of the cell to meet the critical cholesterol concentration requirements for SNARE function. Given the dynamic nature of the plasma membrane, to differentiate between these two possible hypotheses, one would need either dynamic real-time single cell imaging of the lipid rafts or knockout mice for specific SNARE components involved in the docking and priming steps. While informative, these experiments are beyond the scope of the current work reported here. Among K^+-stimulated cells, there was, however, a significant decrease in foot events observed when membrane cholesterol concentration was depleted, and this effect was remedied upon replenishment of the membrane cholesterol (Foot%=6.1±1.1, 11.2±1.0, 9.3± 1.6 for MBCD, control, and reload, respectively). Although it is difficult to predict the exact effect of cholesterol on fusion pore properties, the stalk model for membrane fusion suggests that cholesterol supports the negative curvature of the fusion pore intermediate and stabilizes it. Thus, lower fusion pore occurrence at lower cholesterol level agrees with the stalk model of the fusion pore and shows that more cholesterol is needed to support the negative curvature of the fusion pore and/or the rigidity of the cell/granule membrane fusion site. Interestingly, cumulative frequency results show that both high and low

cholesterol levels facilitate the trafficking and release of RRP/SRP granules; the reasons for this will be addressed later (Figure 5.2D).

5.3.4 Effect of Membrane Cholesterol on Subsequent Release Event

Chromaffin cells can recycle their granular content through the process of endocytosis within 30 s after exocytosis.[21, 29] To explore the role of membrane cholesterol in granule recycling and subsequent release events, chromaffin cells were stimulated twice, at 3 and 33 s, with a 3-s bolus of 60 mM K^+ (n=27, 30, and 33 cells for control, MBCD, and reload conditions, respectively). Then, the ratio of the spike parameters from each stimulation were evaluated for significant differences from unity, indicating incomplete recovery after the initial stimulation. Results (Fig. 5.3) of this analysis show that chromaffin cells with normal cellular cholesterol levels (control) release less catecholamine in the second stimulation compared with the first stimulation, $(Q_1/ Q_2)_{control}$=1.491±0.136. This difference between the first and second stimulation becomes less prominent in the case with depleted membrane cholesterol $(Q_1/Q_2)_{MBCD}$=1.114± 0.126, which shows more complete quantal recovery of the cholesterol-depleted cells between subsequent release events ($p<0.05$). The high cholesterol condition shows indistinguishable behavior from the control condition, with $(Q_1/Q_2)_{Reload}$=1.338±0.088, further supporting better quantal recovery at low cholesterol levels. Although, regardless of cholesterol level, the parameter indicating total time of the release event ($(T_{1/2})_1/(T_{1/2})_2$; Figure 5.3B) did not change significantly from unity, while the time required for dilation of the fusion

pore did change between the first and second release events in the case of low cholesterol, with $(T_{rise})_1/ (T_{rise})_2$=1.402±0.1568 ($p<0.05$ compared with unity). Hence, there is more rapid transition from fusion pore to full dilation when cells are stimulated a second time in the case of depleted cellular cholesterol levels. The Foot% ratios were significantly larger than unity ($p<0.05$) for all the conditions ($(Foot\%)_1/(Foot\%)_2$=1.277±0.108, 1.292±0.113, 1.317±0.151 for MBCD, control, and reload conditions, respectively), suggesting that there is a change in the stability of the fusion pore from stimulation to stimulation. However, these ratios were not distinguishable from one another, arguing that cholesterol does not play a role in this change. This may be explained by the reconstruction of the cell membrane and granules during the exocytosis/endocytosis cycle, yielding fewer or smaller cholesterol-enriched microdomains for the second stimulation, and thus, less robust fusion pores.

5.3.5 Effect of Membrane Cholesterol on Reserve Pool Granules

The chromaffin cell reserve pool constitutes the older population of granules, and these vesicles do not get activated upon K^+ stimulation but release their vesicular content when stimulated by Ba^{+2}.[18-20] Although the mechanism of Ba^{2+} activation is still under debate, it is thought that Ba^{2+} can activate chromaffin cell secretion through T-type Ca^{2+} channels, which was shown to have similar permeability for both Ca^{2+} and Ba^{2+}.[13]

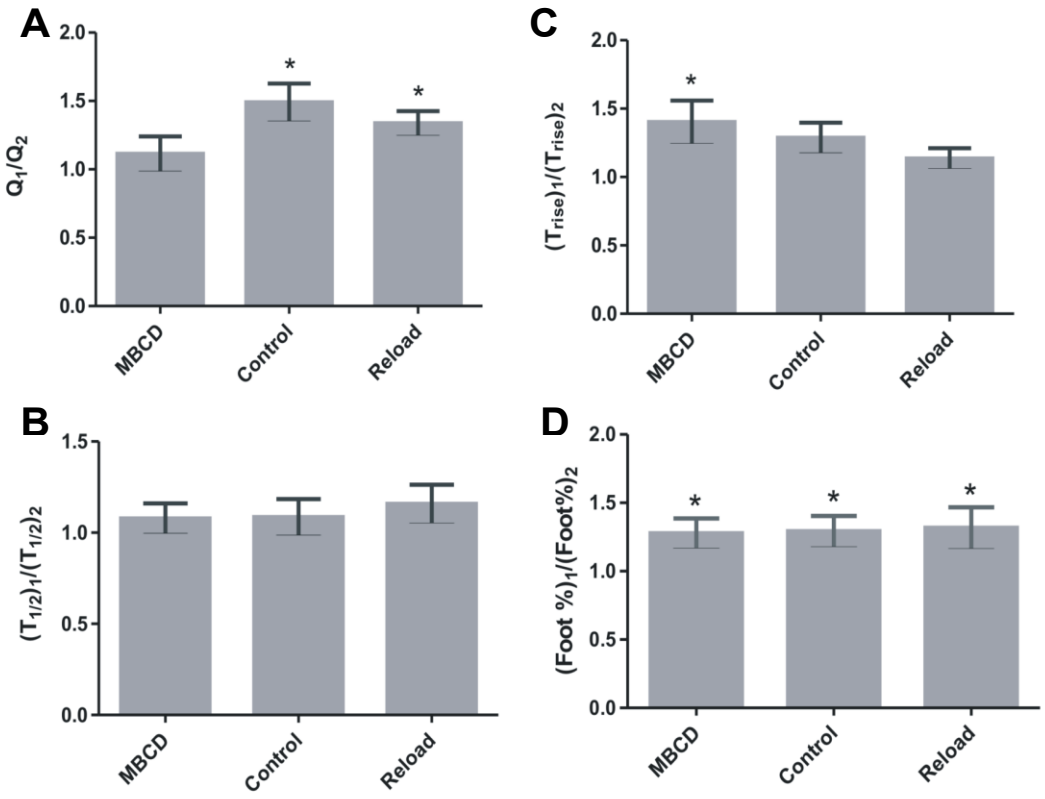

Figure 5.3 Ratiometric analysis of the double K^+ stimulation experiments.(A) In control and reload conditions, cells released less catecholamine in the second stimulation compared with the first one (significant difference from unity). Full quantal recovery was observed for cells treated with MBCD. (B) Total duration of the release event did not change between stimulations. (C) $(T_{rise})_1/(T_{rise})_2$ is significantly ($p<0.05$) different than unity for MBCD, indicating that transition from the fusion pore to full dilation process changes between the first and second release. (D) $(Foot\%)_1/ (Foot\%)_2$ showed significant changes in foot occurrence between the first and second release for all conditions

To avoid Ca^{2+} interference, Ca^{2+}-free solutions were used during Ba^{2+} stimulation experiments. Reserve pool granules were activated to release their granular content via delivery of a 3-s bolus of 5 mM Ba^{2+} to cells with altered membrane cholesterol levels (n=18, 21, and 20 cells for control, MBCD, and reload conditions, respectively).

Figure 5.4 shows representative amperometric traces of catecholamine release from control (Figures. 5.4A or 5.1B), MBCD (Figure 5.4B), and reload (Figure 5.4C) conditions. Clearly, there is a drastic reduction in the number of granules successfully releasing their content when the membrane cholesterol level is manipulated in either direction (no. of granules detected=352±32, 188±21, and 183±24 per cell for control, MBCD, and reload conditions, respectively). Assuming that this change is not a result of MBCD exposure itself, this result reveals that appropriate cholesterol levels are crucial for the efficient recruitment of the older granules to release. Moreover, although cholesterol does not influence the quantity of catecholamine released from the RP granules (based on Q analysis), depleted cholesterol levels slow down the kinetics of exocytosis (Figure 5.5).

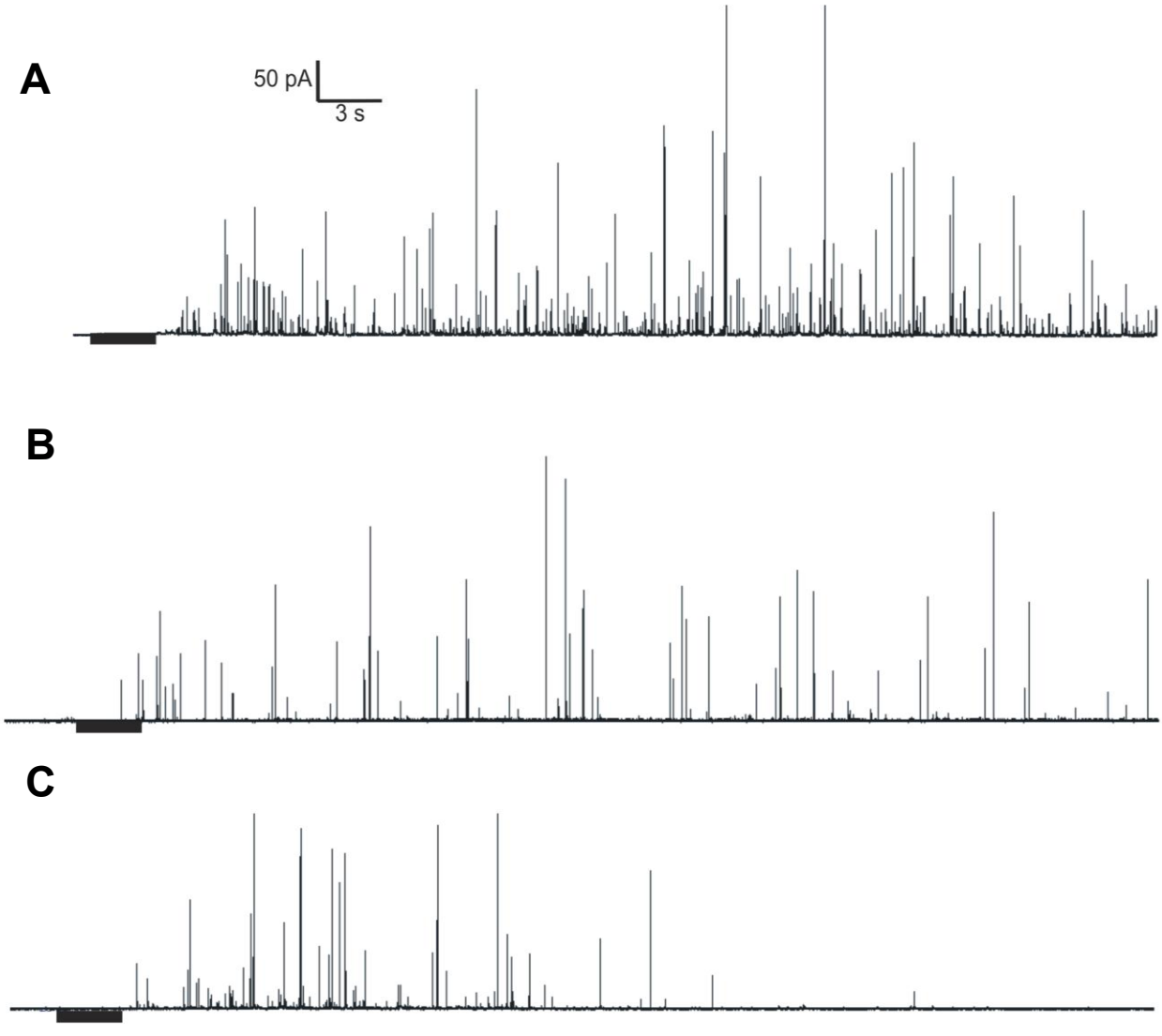

Figure 5.4 Representative amperometric traces of preferential release of RP granule release upon Ba^{2+} stimulation (A) control, (B) MBCD-treated, and (C) reloaded chromaffin cells

Unlike RRP granules, RP granules form a more stable fusion pore, with a higher occurrence of foot events at low membrane cholesterol levels (Foot%=15.2±1.59, 10.0±0.83, and 11.6±1.08 for MBCD, control, and reload conditions, respectively). Together, these data imply either that RP vesicles release their content from different sites on the membrane than RRP/SRP granules or that the structure of the fusion pore is different for RP granules, such that cholesterol destabilizes this intermediate state. Unfortunately, with current techniques, determination of the fusion pore structure with RP granules is not possible. Figures 5.4C and 5.5D demonstrate that, although higher cholesterol levels decrease the number of granules recruited for release, most of the granules release their content earlier than control and cholesterol-depleted cells, revealing that high cholesterol levels facilitate the trafficking and release of this granule pool; this relationship is the subject of future work.

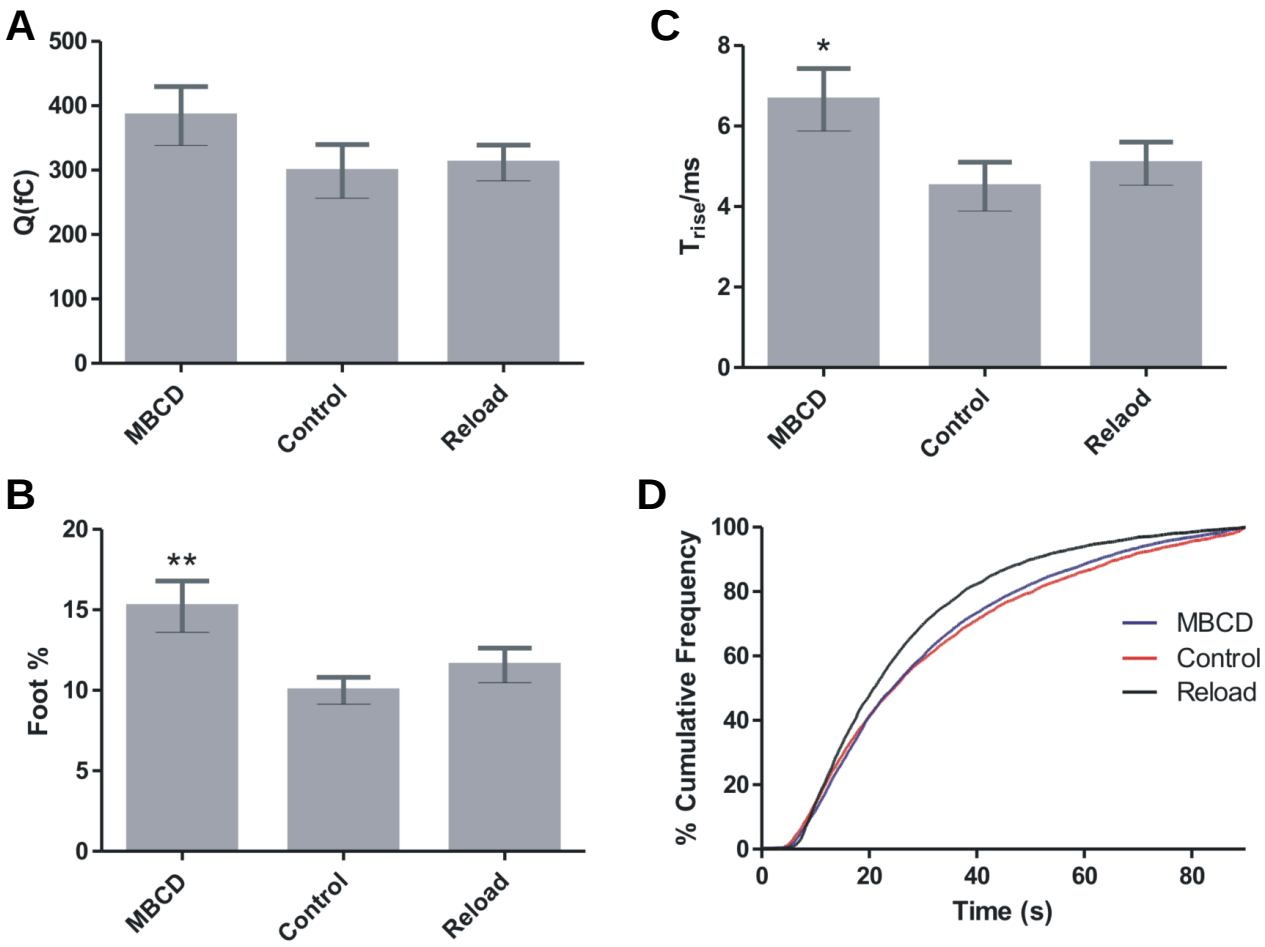

Figure 5. 5 Analysis of the amperometric data from Ba^{2+}-stimulated granule release: (A) shows no significant change in the quantal storage/release of RP granule content at altered cholesterol levels, (B) Foot% analysis shows that RP granules form more stable fusion pore intermediates at depleted cholesterol levels, and (C) higher rise time indicates slower transition from fusion pore to full dilation in RP granules of MBCD-treated cells, and d % cumulative frequency analysis of the all events shows more efficient trafficking at high cholesterol levels. (*denotes $p<0.005$ and **denotes $p<0.001$)

5.4 Comparison of Chromaffin Cells and Platelets

This work demonstrated that kinetics of chromaffin cell exocytosis is largely unchanged with altered cholesterol levels, unlike the recently measured behavior of exocytosing platelets.[30] This difference is likely due to the fact that, unlike platelets, chromaffin cells have a nucleus and a significant synthesis capacity that enables them to tightly regulate various cell functions. Accordingly, when plasma membrane cholesterol is depleted, chromaffin cells rescue the secretion kinetics and quantity of the release whereas the largely static, anuclear platelet cannot accomplish this task. Moreover, chromaffin cells store their granular content in a proteinaceous matrix, and expansion of the matrix following initial membrane fusion is considered one of the main driving forces of full fusion and release.[10, 18, 29, 31, 32] However, platelet secretory granules do not contain this type of matrix, and accordingly, full fusion events are more dependent on the membrane properties.[30] However, cholesterol alteration did result in similar fusion pore effects in platelets and chromaffin cell RRP granules, indicating similar fusion pore structures in these two distinct cell types.

References

Chapter 1

1. Michelson AD, Editor. *Platelets*. Academic Press; 2002.

2. White JG. Platelet membrane interactions. *Platelets*. 1999;10:368-381

3. King SM, McNamee RA, Houng AK, Patel R, Brands M, Reed GL. Platelet dense-granule secretion plays a critical role in thrombosis and subsequent vascular remodeling in atherosclerotic mice. *Circulation*. 2009;120:785-791

4. Flaumenhaft R. Molecular basis of platelet granule secretion. *Arterioscler Thromb Vasc Biol*. 2003;23:1152-1160

5. Reed GL, Fitzgerald ML, Polgár J. Molecular mechanisms of platelet exocytosis: Insights into the "Secrete" Life of thrombocytes. *Blood*. 2000;96:3334-3342

6. Ge S, Wittenberg NJ, Haynes CL. Quantitative and real-time detection of secretion of chemical messengers from individual platelets. *Biochem*. 2008;47:7020-7024

7. Ge S, White JG, Haynes CL. Quantal release of serotonin from platelets. *Anal Chem*. 2009;81:2935-2943

8. Ge S, Woo E, Haynes CL. Quantal regulation and exocytosis of platelet dense-body granules. *Biophys J*. 2011;101:2351-2359

9. King SM, Reed GL. Development of platelet secretory granules. *Semin Cell Dev Biol*. 2002;13:293-302

10. Kamykowski J, Carlton P, Sehgal S, Storrie B. Quantitative immunofluorescence mapping reveals little functional coclustering of proteins within platelet α-granules. *Blood*. 2011;118:1370-1373

11. Italiano JE, Richardson JL, Patel-Hett S, Battinelli E, Zaslavsky A, Short S, Ryeom S, Folkman J, Klement GL. Angiogenesis is regulated by a novel mechanism: Pro- and antiangiogenic proteins are organized into separate platelet alpha granules and differentially released. *Blood*. 2008;111:1227-1233

12. Blair P, Flaumenhaft R. Platelet alpha-granules: Basic biology and clinical correlates. *Blood Rev*. 2009;23:177-189

13. Handagama P, Rappolee DA, Werb Z, Levin J, Bainton DF. Platelet alpha-granule fibrinogen, albumin, and immunoglobulin g are not synthesized by rat and mouse megakaryocytes. *J Clin Invest*. 1990;86:1364-1368

14. McNicol A, Israels SJ. Platelet dense granules: Structure, function and implications for haemostasis. *Thromb Res*. 1999;95:1-18

15. Ambrosio AL, Boyle JA, Di Pietro SM. Mechanism of platelet dense granule biogenesis: Study of cargo transport and function of rab32 and rab38 in a model system. *Blood*. 2012;120:4072-4081

16. Thon JN, Italiano JE. Platelets: Production, morphology and ultrastructure. *Handb Exp Pharmacol*. 2012:3-22

17. Reed GL. Platelet secretory mechanisms. *Semin Thromb Hemost*. 2004;30:441-450

18. Omiatek DM, Dong Y, Heien ML, Ewing AG. Only a fraction of quantal content is released during exocytosis as revealed by electrochemical cytometry of secretory vesicles. *ACS Chem Neurosci*. 2010;1:234-245

19. Kim D, Koseoglu S, Manning BM, Meyer AF, Haynes CL. Electroanalytical eavesdropping on single cell communication. *Anal Chem*. 2011;83:7242-7249

20. White JG. Platelet secretion during clot retraction. *Platelets*. 2000;11:331-343

21. Gundelfinger ED, Kessels MM, Qualmann B. Temporal and spatial coordination of exocytosis and endocytosis. *Nat Rev Mol Cell Biol*. 2003;4:127-139

22. Chernomordik LV, Kozlov MM. Mechanics of membrane fusion. *Nat Struct Mol Biol*. 2008;15:675-683

23. Ge S, White JG, Haynes CL. Critical role of membrane cholesterol in exocytosis revealed by single platelet study. *ACS Chem Biol*. 2010;5:819-828

24. Jackson MB, Chapman ER. Fusion pores and fusion machines in Ca^{2+}-triggered exocytosis. *Annu Rev Biophys Biomol Struct*. 2006;35:135-160

25. Jackson MB, Chapman ER. The fusion pores of Ca^{2+} -triggered exocytosis. *Nat Struct Mol Biol*. 2008;15:684-689

26. Graham GJ, Ren Q, Dilks JR, Blair P, Whiteheart SW, Flaumenhaft R. Endobrevin/vamp-8-dependent dense granule release mediates thrombus formation in vivo. *Blood*. 2009;114:1083-1090

27. Ren Q, Barber HK, Crawford GL, Karim ZA, Zhao C, Choi W, Wang CC, Hong W, Whiteheart SW. Endobrevin/VAMP-8 is the primary V-SNARE for the platelet release reaction. *Mol Biol Cell*. 2007;18:24-33

28. Peters CG, Michelson AD, Flaumenhaft R. Granule exocytosis is required for platelet spreading: Differential sorting of α-granules expressing VAMP-7. *Blood*. 2012;120:199-206

29. Polgár J, Chung SH, Reed GL. Vesicle-associated membrane protein 3 (VAMP-3) and VAMP-8 are present in human platelets and are required for granule secretion. *Blood*. 2002;100:1081-1083

30. Schraw TD, Rutledge TW, Crawford GL, Bernstein AM, Kalen AL, Pessin JE, Whiteheart SW. Granule stores from cellubrevin/VAMP-3 null mouse platelets exhibit normal stimulus-induced release. *Blood*. 2003;102:1716-1722

31. Parlati F, Weber T, McNew JA, Westermann B, Söllner TH, Rothman JE. Rapid and efficient fusion of phospholipid vesicles by the alpha-helical core of a snare complex in the absence of an n-terminal regulatory domain. *Proc Natl Acad Sci U S A*. 1999;96:12565-12570

32. Chen D, Lemons PP, Schraw T, Whiteheart SW. Molecular mechanisms of platelet exocytosis: Role of snap-23 and syntaxin 2 and 4 in lysosome release. *Blood*. 2000;96:1782-1788

33. Flaumenhaft R, Croce K, Chen E, Furie B, Furie BC. Proteins of the exocytotic core complex mediate platelet alpha-granule secretion. Roles of vesicle-associated membrane protein, SNAP-23, and syntaxin 4. *J Biol Chem*. 1999;274:2492-2501

34. Flaumenhaft R, Rozenvayn N, Feng D, Dvorak AM. SNAP-23 and syntaxin-2 localize to the extracellular surface of the platelet plasma membrane. *Blood*. 2007;110:1492-1501

35. Feng D, Crane K, Rozenvayn N, Dvorak AM, Flaumenhaft R. Subcellular distribution of 3 functional platelet snare proteins: Human cellubrevin, SNAP-23, and syntaxin 2. *Blood*. 2002;99:4006-4014

36. Hui E, Johnson CP, Yao J, Dunning FM, Chapman ER. Synaptotagmin-mediated bending of the target membrane is a critical step in Ca^{2+}-regulated fusion. *Cell*. 2009;138:709-721

37. Hui E, Gaffaney JD, Wang Z, Johnson CP, Evans CS, Chapman ER. Mechanism and function of synaptotagmin-mediated membrane apposition. *Nat Struct Mol Biol*. 2011;18:813-821

38. Neumueller O, Hoffmeister M, Babica J, Prelle C, Gegenbauer K, Smolenski AP. Synaptotagmin-like protein 1 interacts with the gtpase-activating protein rap1gap2 and regulates dense granule secretion in platelets. *Blood*. 2009;114:1396-1404

39. Al Hawas R, Ren Q, Ye S, Karim ZA, Filipovich AH, Whiteheart SW. Munc18b/stxbp2 is required for platelet secretion. *Blood*. 2012;120:2493-2500

40. Zhang Z, Hui E, Chapman ER, Jackson MB. Phosphatidylserine regulation of Ca^{2+}-triggered exocytosis and fusion pores in PC12 cells. *Mol Biol Cell*. 2009;20:5086-5095

41. Uchiyama Y, Maxson M, Sawada T, Nakano A, Ewing A. Phospholipid mediated plasticity in exocytosis observed in PC12 cells. *Brain Res*. 2007;1151:46-54

42. Zwaal RF, Comfurius P, van Deenen LL. Membrane asymmetry and blood coagulation. *Nature*. 1977;268:358-360

43. Heemskerk JW, Bevers EM, Lindhout T. Platelet activation and blood coagulation. *Thromb Haemost*. 2002;88:186-193

44. Zwaal RF, Comfurius P, Bevers EM. Lipid-protein interactions in blood coagulation. *Biochim Biophys Acta*. 1998;1376:433-453

45. Grgurevich S, Krishnan R, White MM, Jennings LK. Role of in vitro cholesterol depletion in mediating human platelet aggregation. *J Thromb Haemost*. 2003;1:576-586

46. Churchward MA, Coorssen JR. Cholesterol, regulated exocytosis and the physiological fusion machine. *Biochem J*. 2009;423:1-14

47. Koseoglu S, Love SA, Haynes CL. Cholesterol effects on vesicle pools in chromaffin cells revealed by carbon-fiber microelectrode amperometry. *Anal Bioanal Chem*. 2011;400:2963-2971

48. Xia F, Xie L, Mihic A, Gao X, Chen Y, Gaisano HY, Tsushima RG. Inhibition of cholesterol biosynthesis impairs insulin secretion and voltage-gated calcium channel function in pancreatic beta-cells. *Endocrinology*. 2008;149:5136-5145

49. Linetti A, Fratangeli A, Taverna E, Valnegri P, Francolini M, Cappello V, Matteoli M, Passafaro M, Rosa P. Cholesterol reduction impairs exocytosis of synaptic vesicles. *J Cell Sci*. 2010;123:595-605

50. Broos K, Feys HB, De Meyer SF, Vanhoorelbeke K, Deckmyn H. Platelets at work in primary hemostasis. *Blood Rev*. 2011;25:155-167

51. Weiss HJ, Lages B, Hoffmann T, Turitto VT. Correction of the platelet adhesion defect in delta-storage pool deficiency at elevated hematocrit--possible role of adenosine diphosphate. *Blood*. 1996;87:4214-4222

52. Müller F, Mutch NJ, Schenk WA, Smith SA, Esterl L, Spronk HM, Schmidbauer S, Gahl WA, Morrissey JH, Renné T. Platelet polyphosphates are proinflammatory and procoagulant mediators in vivo. *Cell*. 2009;139:1143-1156

53. Wagner DD, Burger PC. Platelets in inflammation and thrombosis. *Arterioscler Thromb Vasc Biol*. 2003;23:2131-2137

54. Rickles FR, Falanga A. Molecular basis for the relationship between thrombosis and cancer. *Thromb Res*. 2001;102:V215-224

55. Lesurtel M, Graf R, Aleil B, Walther DJ, Tian Y, Jochum W, Gachet C, Bader M, Clavien PA. Platelet-derived serotonin mediates liver regeneration. *Science*. 2006;312:104-107

56. Gibbins JM, Mahaut-Smith MP, Editors. *Platelets and megakaryocytes: Volume 1. Functional assays. [in: Methods mol. Biol. (totowa, nj. U.S).; 2004, 272]*. Humana Press. Inc.; 2004.

57. Neufeld HA, Towner RD, Pace J. A rapid method for determining atp by the firefly luciferin-luciferase system. *Experientia*. 1975;31:391-392

58. Wendeler M, Sandhoff K. Hexosaminidase assays. *Glycoconj J*. 2009;26:945-952

59. Spiller DG, Wood CD, Rand DA, White MR. Measurement of single-cell dynamics. *Nature*. 2010;465:736-745

60. Bakstad D, Adamson A, Spiller DG, White MR. Quantitative measurement of single cell dynamics. *Curr Opin Biotechnol*. 2012;23:103-109

61. Fritzsch FS, Dusny C, Frick O, Schmid A. Single-cell analysis in biotechnology, systems biology, and biocatalysis. *Annu Rev Chem Biomol Eng*. 2012;3:129-155

62. Adams RN. Carbon paste electrodes. *Anal. Chem.* 1958;30:1576

63. Wightman RM, Jankowski JA, Kennedy RT, Kawagoe KT, Schroeder TJ, Leszczyszyn DJ, Near JA, Diliberto EJ, Viveros OH. Temporally resolved catecholamine spikes correspond to single vesicle release from individual chromaffin cells. *Proc Natl Acad Sci U S A*. 1991;88:10754-10758

64. Leszczyszyn D, Jankowski J, Viveros O, Diliberto E, Near J, Wightman R. Nicotinic receptor-mediated catecholamine secretion from individual chromaffin cells - chemical evidence for exocytosis. *J Biol Chem*. 1990;265:14736-14737

65. Sakmann B, Neher E, Editors. *Single-channel recording: Second edition*. Plenum; 1995.

66. Bard AJ, Faulkner LR. *Electrochemical methods: Fundamentals and applications*. Wiley; 1980.

67. Robinson D, Venton B, Heien M, Wightman R. Detecting subsecond dopamine release with fast-scan cyclic voltammetry in vivo. *Clin Chem*. 2003:1763-1773

68. Venton B, Wightman R. Psychoanalytical electrochemistry: Dopamine and behavior. *Anal Chem*. 2003:414A-421A

69. Michael D, Travis ER, Wightman RM. Color images for fast-scan CV measurements in biological systems. *Anal Chem*. 1998;70:7

70. Jackson B, Dietz S, Wightman R. Fast-scan cyclic voltammetry of 5-hydroxytryptamine. *Anal Chem*. 1995:1115-1120

71. Pihel K, Schroeder T, Wightman R. Rapid and selective cyclic voltammetric measurements of epinephrine and norepinephrine as a method to measure secretion from single bovine adrenal-medullary cells. *Anal. Chem.* 1994:4532-4537

72. Heien M, Johnson M, Wightman R. Resolving neurotransmitters detected by fast-scan cyclic voltammetry. *Anal Chem*. 2004:5697-5704

73. Zhang B, Heien M, Santillo M, Mellander L, Ewing A. Temporal resolution in electrochemical imaging on single PC12 cells using amperometry and voltammetry at microelectrode arrays. *Anal Chem*. 2011:571-577

74. Mosharov E, Sulzer D. Analysis of exocytotic events recorded by amperometry. *Nature Methods*. 2005:651-658

75. Chen T, Luo G, Ewing A. Amperometric monitoring of stimulated catecholamine release from rat pheochromocytoma (PC12) cells at the zeptomole level. *Anal Chem*. 1994:3031-3035

76. Jankowski J, Schroeder T, Ciolkowski E, Wightman R. Temporal characteristics of quantal secretion of catecholamines from adrenal-medullary cells. *J Biol Chem*. 1993:14694-14700

77. Schroeder T, Jankowski J, Kawagoe K, Wightman R, Lefrou C, Amatore C. Analysis of diffusional broadening of vesicular packets of catecholamines released from biological cells during exocytosis. *Anal Chem*. 1992:3077-3083

78. Amatore C, Bouret Y, Travis E, Wightman R. Adrenaline release by chromaffin cells: Constrained swelling of the vesicle matrix leads to full fusion. *Angewandte Chemie-Int Ed*. 2000:1952-1954

79. Heien M, Phillips P, Stuber G, Seipel A, Wightman R. Overoxidation of carbon-fiber microelectrodes enhances dopamine adsorption and increases sensitivity. *Analyst*. 2003:1413-1419

80. Amatore C, Arbault S, Bouret Y, Guille M, Lemaitre F, Verchier Y. Invariance of exocytotic events detected by amperometry as a function of the carbon fiber microelectrode diameter. *Anal Chem*. 2009:3087-3093

81. Cahill P, Walker Q, Finnegan J, Mickelson G, Travis E, Wightman R. Microelectrodes for the measurement of catecholamines in biological systems. *Anal Chem*. 1996:3180-3186

82. Keithley R, Heien M, Wightman R. Multivariate concentration determination using principal component regression with residual analysis. *Trac-Trends in Anal Chem*. 2009:1127-1136

83. Travis E, Wightman R. Spatio-temporal resolution of exocytosis from individual cells. *Annu Rew Biophy Biomol Struct*. 1998:77-103

84. Segura F, Brioso M, Gomez J, Machado J, Borges R. Automatic analysis for amperometrical recordings of exocytosis. *J Neurosci Met*. 2000:151-156

85. Amatore C, Arbault S, Bonifas I, Guille M. Quantitative investigations of amperometric spike feet suggest different controlling factors of the fusion pore in exocytosis at chromaffin cells. *Biophys Chem*. 2009:124-131

86. Sombers L, Hanchar H, Colliver T, Wittenberg N, Cans A, Arbault S, Amatore C, Ewing A. The effects of vesicular volume on secretion through the fusion pore in exocytotic release from PC12 cells. *J Neurosci*. 2004:303-309

87. Kennedy R, Huang L, Atkinson M, Dush P. Amperometric monitoring of chemical secretions from individual pancreatic beta-cells. *Anal Chem*. 1993:1882-1887

88. Paras C, Kennedy R. Electrochemical detection of exocytosis at single-rat melanotrophs. *Anal Chem*. 1995:3633-3637

89. Hochstetler S, Puopolo M, Gustincich S, Raviola E, Wightman R. Real-time amperometric measurements of zeptomole quantities of dopamine released from neurons. *Anal Chem*. 2000:489-496

90. Bruns D, Jahn R. Real-time measurement of transmitter release from single synaptic vesicles. *Nature*. 1995:62-65

91. Zhou Z, Misler S. Amperometric detection of stimulus-induced quantal release of catecholamines from cultured superior cervical ganglion neurons. *Proc Natl Acad Sci U S A*. 1995;92:6938-6942

92. Pothos EN, Davila V, Sulzer D. Presynaptic recording of quanta from midbrain dopamine neurons and modulation of the quantal size. *J Neurosci*. 1998;18:4106-4118

93. Marquis BJ, Haynes CL. The effects of co-culture of fibroblasts on mast cell exocytotic release characteristics as evaluated by carbon-fiber microelectrode amperometry. *Biophys Chem*. 2008;137:63-69

94. Ge S, Wittenberg N, Haynes C. Quantitative and real-time detection of secretion of chemical messengers from individual platelets. *Biochem*. 2008;47:7020-7024

95. O'Connell P, Wang X, Leon-Ponte M, Griffiths C, Pingle S, Ahern G. A novel form of immune signaling revealed by transmission of the inflammatory mediator serotonin between dendritic cells and t cells. *Blood*. 2006:1010-1017

96. Westerink RH, Ewing AG. The PC12 cell as model for neurosecretion. *Acta Physiol (Oxf)*. 2008;192:273-285

97. Dong Y, Heien ML, Maxson MM, Ewing AG. Amperometric measurements of catecholamine release from single vesicles in mn9d cells. *J Neurochem*. 2008;107:1589-1595

98. Burgoyne RD. Control of exocytosis in adrenal chromaffin cells. *Biochim et Biophy Acta (BBA) - Reviews on Biomembranes*. 1991;1071:174-202

99. Rayport S, Sulzer D, Shi WX, Sawasdikosol S, Monaco J, Batson D, Rajendran G. Identified postnatal mesolimbic dopamine neurons in culture: Morphology and electrophysiology. *J Neurosci*. 1992;12:4264-4280

100. Bruns D. Detection of transmitter release with carbon fiber electrodes. *Methods*. 2004;33:312-321

101. Tatham PER, Duchen MR, Millar J. Monitoring exocytosis from single mast cells by fast voltammetry. *Pflügers Archiv European Journal of Physiol*. 1991;419:409-414-414

102. Detoledo G, Fernandezchacon R, Fernandez J. Release of secretory products during transient vesicle fusion. *Nature*. 1993:554-558

103. Pihel K, Hsieh S, Jorgenson J, Wightman R. Electrochemical detection of histamine and 5-hydroxytryptamine at isolated mast cells. *Anal Chem*. 1995;67:4514-4521

104. Kozminski K, Gutman D, Davila V, Sulzer D, Ewing A. Voltammetric and pharmacological characterization of dopamine release from single exocytotic events at rat pheochromocytoma (pc12) cells. *Anal Chem*. 1998;70:3123-3130

105. Amatore C, Arbault S, Bonifas I, Bouret Y, Erard M, Ewing A, Sombers L. Correlation between vesicle quantal size and fusion pore release in chromaffin cell exocytosis. *Biophys J*. 2005:4411-4420

106. Monck J, Oberhauser A, de-Toledo G, Fernandez J. Is swelling of the secretory granule matrix the force that dilates the exocytotic fusion pore. *Biophys J*. 1991:39-47

107. Troyer K, Wightman R. Temporal separation of vesicle release from vesicle fusion during exocytosis. *J Biol Chem*. 2002:29101-29107

108. Borges R, Diaz-Vera J, Dominguez N, Arnau M, Machado J. Chromogranins as regulators of exocytosis. *J Neurochem*. 2010:335-343

109. Voets T, Moser T, Lund P, Chow R, Geppert M, Sudhof T, Neher E. Intracellular calcium dependence of large dense-core vesicle exocytosis in the absence of synaptotagmin i. *Proc Natl Acad Sci U S A*. 2001:11680-11685

110. Segovia M, Ales E, Montes M, Bonifas I, Jemal I, Lindau M, Maximov A, Sudhof T, de Toledo G. Push-and-pull regulation of the fusion pore by synaptotagmin-7. *Proc Natl Acad Sci U S A*. 2010:19032-19037

111. Ngatchou A, Kisler K, Fang Q, Walter A, Zhao Y, Bruns D, Sorensen J, Lindau M. Role of the synaptobrevin c terminus in fusion pore formation. *Proc Natl Acad Sci U S A*. 2010:18463-18468

112. Fang Q, Berberian K, Gong L, Hafez I, Sorensen J, Lindau M. The role of the c terminus of the snare protein snap-25 in fusion pore opening and a model for fusion pore mechanics. *Proc Natl Acad Sci U S A*. 2008:15388-15392

113. Amatore C, Arbault S, Bouret Y, Guille M, Lemaître F, Verchier Y. Regulation of exocytosis in chromaffin cells by trans-insertion of lysophosphatidylcholine and arachidonic acid into the outer leaflet of the cell membrane. *Chembiochem*. 2006;7:1998-2003

Chapter 2

1. Flaumenhaft R. Molecular basis of platelet granule secretion. *Arterioscler Thromb Vasc Biol*. 2003;23:1152-1160

2. Gader AG, Ghumlas AK, Hussain MF, Haidari AA, White JG. The ultrastructure of camel blood platelets: A comparative study with human, bovine, and equine cells. *Platelets*. 2008;19:51-58

3. Pelagalli A, Belisario MA, Tafuri S, Lombardi P, d'Angelo D, Avallone L, Staiano N. Adhesive properties of platelets from different animal species. *J Comp Pathol*. 2003;128:127-131

4. Choi W, Karim ZA, Whiteheart SW. Protein expression in platelets from six species that differ in their open canalicular system. *Platelets*. 2010;21:167-175

5. White JG. Platelet membrane interactions. *Platelets*. 1999;10:368-381

6. White JG. Platelet secretion during clot retraction. *Platelets*. 2000;11:331-343

7. Feng D, Crane K, Rozenvayn N, Dvorak AM, Flaumenhaft R. Subcellular distribution of 3 functional platelet snare proteins: Human cellubrevin, SNAP-23, and syntaxin 2. *Blood*. 2002;99:4006-4014

8. Ge S, Wittenberg NJ, Haynes CL. Quantitative and real-time detection of secretion of chemical messengers from individual platelets. *Biochem*. 2008;47:7020-7024

9. Ge S, White JG, Haynes CL. Quantal release of serotonin from platelets. *Anal Chem*. 2009;81:2935-2943

10. Ge S, White JG, Haynes CL. Critical role of membrane cholesterol in exocytosis revealed by single platelet study. *ACS Chem Biol*. 2010;5:819-828

11. Gunay-Aygun M, Huizing M, Gahl WA. Molecular defects that affect platelet dense granules. *Semin Thromb Hemost*. 2004;30:537-547

12. Weiss HJ, Lages B, Hoffmann T, Turitto VT. Correction of the platelet adhesion defect in delta-storage pool deficiency at elevated hematocrit--possible role of adenosine diphosphate. *Blood*. 1996;87:4214-4222

13. King SM, McNamee RA, Houng AK, Patel R, Brands M, Reed GL. Platelet dense-granule secretion plays a critical role in thrombosis and subsequent vascular remodeling in atherosclerotic mice. *Circulation*. 2009;120:785-791

14. McNicol A, Israels SJ. Platelet dense granules: Structure, function and implications for haemostasis. *Thromb Res*. 1999;95:1-18

15. Gibbins JM, Mahaut-Smith MP, Editors. *Platelets and megakaryocytes: Volume 1. Functional assays. [in: Methods mol. Biol. (totowa, nj. U.S).; 2004, 272]*. Humana Press. Inc.; 2004.

16. White JG. The secretory pathway of bovine platelets. *Blood*. 1987;69:878-885

17. Omiatek DM, Dong Y, Heien ML, Ewing AG. Only a fraction of quantal content is released during exocytosis as revealed by electrochemical cytometry of secretory vesicles. *ACS Chem Neurosci*. 2010;1:234-245

18. Kim D, Koseoglu S, Manning BM, Meyer AF, Haynes CL. Electroanalytical eavesdropping on single cell communication. *Anal Chem*. 2011;83:7242-7249

19. Amatore C, Bouret Y, Travis E, Wightman R. Adrenaline release by chromaffin cells: Constrained swelling of the vesicle matrix leads to full fusion. *Angewandte Chemie-Int Ed.*. 2000:1952-1954

20. Koseoglu S, Love SA, Haynes CL. Cholesterol effects on vesicle pools in chromaffin cells revealed by carbon-fiber microelectrode amperometry. *Anal Bioanal Chem*. 2011;400:2963-2971

21. Grouse LH, Rao GH, Weiss DJ, Perman V, White JG. Surface-activated bovine platelets do not spread, they unfold. *Am J Pathol*. 1990;136:399-408

22. Nylander S, Mattsson C, Lindahl TL. Characterisation of species differences in the platelet adp and thrombin response. *Thromb Res*. 2006;117:543-549

23. Michelson AD, Editor. *Platelets*. Academic Press; 2002.

24. Amatore C, Bouret Y, Travis ER, Wightman RM. Interplay between membrane dynamics, diffusion and swelling pressure governs individual vesicular exocytotic events during release of adrenaline by chromaffin cells. *Biochimie*. 2000;82:481-496

25. Zwaal RF, Comfurius P, Bevers EM. Lipid-protein interactions in blood coagulation. *Biochimi Biophys Acta*. 1998;1376:433-453

26. Uchiyama Y, Maxson M, Sawada T, Nakano A, Ewing A. Phospholipid mediated plasticity in exocytosis observed in PC12 cells. *Brain Res*. 2007;1151:46-54

Chapter 3

1. Flaumenhaft R. Molecular basis of platelet granule secretion. *Arterioscler Thromb Vasc Biol*. 2003;23:1152-1160
2. Blair P, Flaumenhaft R. Platelet alpha-granules: Basic biology and clinical correlates. *Blood Rev*. 2009;23:177-189
3. Ge S, Wittenberg NJ, Haynes CL. Quantitative and real-time detection of secretion of chemical messengers from individual platelets. *Biochemistry*. 2008;47:7020-7024
4. Ge S, Woo E, White JG, Haynes CL. Electrochemical measurement of endogeneous serotonin release from human blood platelets. *Anal Chem*. 2011;in press
5. Ge S, White JG, Haynes CL. Quantal release of serotonin from platelets. *Anal Chem*. 2009;81:2935-2943
6. Ge S, White JG, Haynes CL. Critical role of membrane cholesterol in exocytosis revealed by single platelet study. *ACS Chem Biol*. 2010;5:819-828
7. Ge S, Woo E, Haynes CL. Quantal regulation and exocytosis of platelet dense-body granules. *Biophys J*. 2011;101:2351-2359
8. Praefcke GJ, McMahon HT. The dynamin superfamily: Universal membrane tubulation and fission molecules? *Nat Rev Mol Cell Biol*. 2004;5:133-147
9. Fang Q, Berberian K, Gong L, Hafez I, Sorensen J, Lindau M. The role of the c terminus of the snare protein snap-25 in fusion pore opening and a model for fusion pore mechanics. *Proc Natl Acad Sci U S A*. 2008:15388-15392
10. Wightman RM, Jankowski JA, Kennedy RT, Kawagoe KT, Schroeder TJ, Leszczyszyn DJ, Near JA, Diliberto EJ, Viveros OH. Temporally resolved catecholamine spikes correspond to single vesicle release from individual chromaffin cells. *Proc Natl Acad Sci U S A*. 1991;88:10754-10758

11. Graham GJ, Ren Q, Dilks JR, Blair P, Whiteheart SW, Flaumenhaft R. Endobrevin/VAMP-8-dependent dense granule release mediates thrombus formation in vivo. *Blood*. 2009;114:1083-1090
12. Jasuja R, Passam FH, Kennedy DR, Kim SH, van Hessem L, Lin L, Bowley SR, Joshi SS, Dilks JR, Furie B, Furie BC, Flaumenhaft R. Protein disulfide isomerase inhibitors constitute a new class of antithrombotic agents. *J Clin Invest*. 2012;122:2104-2113
13. Italiano JE, Richardson JL, Patel-Hett S, Battinelli E, Zaslavsky A, Short S, Ryeom S, Folkman J, Klement GL. Angiogenesis is regulated by a novel mechanism: Pro- and antiangiogenic proteins are organized into separate platelet alpha granules and differentially released. *Blood*. 2008;111:1227-1233
14. Peters CG, Michelson AD, Flaumenhaft R. Granule exocytosis is required for platelet spreading: Differential sorting of α-granules expressing VAMP-7. *Blood*. 2012;120:199-206
15. Dowal L, Sim DS, Dilks JR, Blair P, Beaudry S, Denker BM, Koukos G, Kuliopulos A, Flaumenhaft R. Identification of an antithrombotic allosteric modulator that acts through helix 8 of par1. *Proc Natl Acad Sci U S A*. 2011;108:2951-2956
16. Verhoeven AJ, Verhaar R, Gouwerok EG, de Korte D. The mitochondrial membrane potential in human platelets: A sensitive parameter for platelet quality. *Transfusion*. 2005;45:82-89
17. Flaumenhaft R, Dilks JR, Rozenvayn N, Monahan-Earley RA, Feng D, Dvorak AM. The actin cytoskeleton differentially regulates platelet alpha-granule and dense-granule secretion. *Blood*. 2005;105:3879-3887
18. Reems JA, Wang W, Tsubata K, Abdurrahman N, Sundell B, Tijssen MR, van der Schoot E, Di Summa F, Patel-Hett S, Italiano J, Gilligan DM. Dynamin 3 participates in the growth and development of megakaryocytes. *Exp Hematol*. 2008;36:1714-1727

19. Wang W, Gilligan DM, Sun S, Wu X, Reems JA. Distinct functional effects for dynamin 3 during megakaryocytopoiesis. *Stem Cells Dev*. 2011;20:2139-2151
20. Verma DP, Hong Z. The ins and outs in membrane dynamics: Tubulation and vesiculation. *Trends Plant Sci*. 2005;10:159-165
21. Ramachandran R. Vesicle scission: Dynamin. *Semin Cell Dev Biol*. 2011;22:10-17
22. Graham ME, O'Callaghan DW, McMahon HT, Burgoyne RD. Dynamin-dependent and dynamin-independent processes contribute to the regulation of single vesicle release kinetics and quantal size. *Proc Natl Acad Sci U S A*. 2002;99:7124-7129
23. Tsuboi T, McMahon HT, Rutter GA. Mechanisms of dense core vesicle recapture following "Kiss and run" ("Cavicapture") exocytosis in insulin-secreting cells. *J Biol Chem*. 2004;279:47115-47124
24. Fulop T, Doreian B, Smith C. Dynamin i plays dual roles in the activity-dependent shift in exocytic mode in mouse adrenal chromaffin cells. *Arch Biochem Biophys*. 2008;477:146-154
25. González-Jamett AM, Báez-Matus X, Hevia MA, Guerra MJ, Olivares MJ, Martínez AD, Neely A, Cárdenas AM. The association of dynamin with synaptophysin regulates quantal size and duration of exocytotic events in chromaffin cells. *J Neurosci*. 2010;30:10683-10691
26. Anantharam A, Bittner MA, Aikman RL, Stuenkel EL, Schmid SL, Axelrod D, Holz RW. A new role for the dynamin gtpase in the regulation of fusion pore expansion. *Mol Biol Cell*. 2011;22:1907-1918
27. Macia E, Ehrlich M, Massol R, Boucrot E, Brunner C, Kirchhausen T. Dynasore, a cell-permeable inhibitor of dynamin. *Dev Cell*. 2006;10:839-850
28. Quan A, McGeachie AB, Keating DJ, van Dam EM, Rusak J, Chau N, Malladi CS, Chen C, McCluskey A, Cousin MA, Robinson PJ. Myristyl

trimethyl ammonium bromide and octadecyl trimethyl ammonium bromide are surface-active small molecule dynamin inhibitors that block endocytosis mediated by dynamin i or dynamin ii. *Mol Pharmacol*. 2007;72:1425-1439

29. Smirnova E, Shurland DL, Ryazantsev SN, van der Bliek AM. A human dynamin-related protein controls the distribution of mitochondria. *J Cell Biol*. 1998;143:351-358
30. Friedman JR, Lackner LL, West M, DiBenedetto JR, Nunnari J, Voeltz GK. Er tubules mark sites of mitochondrial division. *Science*. 2011;334:358-362
31. Montessuit S, Somasekharan SP, Terrones O, Lucken-Ardjomande S, Herzig S, Schwarzenbacher R, Manstein DJ, Bossy-Wetzel E, Basañez G, Meda P, Martinou JC. Membrane remodeling induced by the dynamin-related protein drp1 stimulates bax oligomerization. *Cell*. 2010;142:889-901
32. Santel A, Frank S. Shaping mitochondria: The complex posttranslational regulation of the mitochondrial fission protein drp1. *IUBMB Life*. 2008;60:448-455
33. Zhao J, Liu T, Jin S, Wang X, Qu M, Uhlén P, Tomilin N, Shupliakov O, Lendahl U, Nistér M. Human mief1 recruits drp1 to mitochondrial outer membranes and promotes mitochondrial fusion rather than fission. *EMBO J*. 2011;30:2762-2778
34. Zhang B, Alysandratos KD, Angelidou A, Asadi S, Sismanopoulos N, Delivanis DA, Weng Z, Miniati A, Vasiadi M, Katsarou-Katsari A, Miao B, Leeman SE, Kalogeromitros D, Theoharides TC. Human mast cell degranulation and preformed tnf secretion require mitochondrial translocation to exocytosis sites: Relevance to atopic dermatitis. *J Allergy Clin Immunol*. 2011;127:1522-1531.e1528

35. Cassidy-Stone A, Chipuk JE, Ingerman E, Song C, Yoo C, Kuwana T, Kurth MJ, Shaw JT, Hinshaw JE, Green DR, Nunnari J. Chemical inhibition of the mitochondrial division dynamin reveals its role in bax/bak-dependent mitochondrial outer membrane permeabilization. *Dev Cell*. 2008;14:193-204
36. Verstreken P, Ly CV, Venken KJ, Koh TW, Zhou Y, Bellen HJ. Synaptic mitochondria are critical for mobilization of reserve pool vesicles at drosophila neuromuscular junctions. *Neuron*. 2005;47:365-378
37. Carneiro L, Allard C, Guissard C, Fioramonti X, Tourrel-Cuzin C, Bailbé D, Barreau C, Offer G, Nédelec E, Salin B, Rigoulet M, Belenguer P, Pénicaud L, Leloup C. Importance of mitochondrial dynamin-related protein 1 in hypothalamic glucose sensitivity in rats. *Antioxid Redox Signal*. 2012;17:433-444
38. Ong SB, Subrayan S, Lim SY, Yellon DM, Davidson SM, Hausenloy DJ. Inhibiting mitochondrial fission protects the heart against ischemia/reperfusion injury. *Circulation*. 2010;121:2012-2022
39. Brooks C, Wei Q, Cho SG, Dong Z. Regulation of mitochondrial dynamics in acute kidney injury in cell culture and rodent models. *J Clin Invest*. 2009;119:1275-1285
40. Park SW, Kim KY, Lindsey JD, Dai Y, Heo H, Nguyen DH, Ellisman MH, Weinreb RN, Ju WK. A selective inhibitor of drp1, mdivi-1, increases retinal ganglion cell survival in acute ischemic mouse retina. *Invest Ophthalmol Vis Sci*. 2011;52:2837-2843
41. Chang CR, Blackstone C. Dynamic regulation of mitochondrial fission through modification of the dynamin-related protein drp1. *Ann N Y Acad Sci*. 2010;1201:34-39
42. Vandendries ER, Hamilton JR, Coughlin SR, Furie B, Furie BC. Par4 is required for platelet thrombus propagation but not fibrin generation in a mouse model of thrombosis. *Proc Natl Acad Sci U S A*. 2007;104:288-292

43. Cui M, Tang X, Christian WV, Yoon Y, Tieu K. Perturbations in mitochondrial dynamics induced by human mutant pink1 can be rescued by the mitochondrial division inhibitor mdivi-1. *J Biol Chem*. 2010;285:11740-11752
44. Lackner LL, Nunnari J. Small molecule inhibitors of mitochondrial division: Tools that translate basic biological research into medicine. *Chem Biol*. 2010;17:578-583
45. Wiederkehr A, Wollheim CB. Mitochondrial signals drive insulin secretion in the pancreatic β-cell. *Mol Cell Endocrinol*. 2012;353:128-137
46. Keating DJ. Mitochondrial dysfunction, oxidative stress, regulation of exocytosis and their relevance to neurodegenerative diseases. *J Neurochem*. 2008;104:298-305
47. Ye Y, Perez-Polo JR, Birnbaum Y. Protecting against ischemia-reperfusion injury: Antiplatelet drugs, statins, and their potential interactions. *Ann N Y Acad Sci*. 2010;1207:76-82
48. Hu H, Batteux F, Chéreau C, Kavian N, Marut W, Gobeaux C, Borderie D, Dinh-Xuan AT, Weill B, Nicco C. Clopidogrel protects from cell apoptosis and oxidative damage in a mouse model of renal ischaemia-reperfusion injury. *J Pathol*. 2011;225:265-275
49. Iwama D, Miyamoto K, Miyahara S, Tamura H, Tsujikawa A, Yamashiro K, Kiryu J, Yoshimura N. Neuroprotective effect of cilostazol against retinal ischemic damage via inhibition of leukocyte-endothelial cell interactions. *J Thromb Haemost*. 2007;5:818-825

Chapter 4

1. Chasserot-Golaz S, Coorssen JR, Meunier FA, Vitale N. Lipid dynamics in exocytosis. *Cell Mol Neurobiol*. 2010;30:1335-1342
2. Chernomordik LV, Kozlov MM. Mechanics of membrane fusion. *Nat Struct Mol Biol*. 2008;15:675-683
3. Chernomordik L, Kozlov MM, Zimmerberg J. Lipids in biological membrane fusion. *J Membr Biol*. 1995;146:1-14
4. Heemskerk JW, Bevers EM, Lindhout T. Platelet activation and blood coagulation. *Thromb Haemost*. 2002;88:186-193
5. Zwaal RF, Comfurius P, Bevers EM. Lipid-protein interactions in blood coagulation. *Biochim Biophys Acta*. 1998;1376:433-453
6. Zwaal RF, Comfurius P, van Deenen LL. Membrane asymmetry and blood coagulation. *Nature*. 1977;268:358-360
7. Kim D, Haynes CL. Neutrophil chemotaxis within a competing gradient of chemoattractants. *Anal Chem*. 2012;84:6070-6078
8. Uchiyama Y, Maxson M, Sawada T, Nakano A, Ewing A. Phospholipid mediated plasticity in exocytosis observed in PC12 cells. *Brain Res*. 2007;1151:46-54
9. Zhang Z, Hui E, Chapman ER, Jackson MB. Phosphatidylserine regulation of ca2+-triggered exocytosis and fusion pores in PC12 cells. *Mol Biol Cell*. 2009;20:5086-5095
10. Amatore C, Arbault S, Bouret Y, Guille M, Lemaître F, Verchier Y. Regulation of exocytosis in chromaffin cells by trans-insertion of lysophosphatidylcholine and arachidonic acid into the outer leaflet of the cell membrane. *Chembiochem*. 2006;7:1998-2003
11. Kato N, Nakanishi M, Hirashima N. Transbilayer asymmetry of phospholipids in the plasma membrane regulates exocytotic release in mast cells. *Biochemistry*. 2002;41:8068-8074

12. Bevers EM, Comfurius P, Dekkers DW, Zwaal RF. Lipid translocation across the plasma membrane of mammalian cells. *Biochim Biophys Acta*. 1999;1439:317-330
13. Flaumenhaft R. Molecular basis of platelet granule secretion. *Arterioscler Thromb Vasc Biol*. 2003;23:1152-1160
14. Silver MJ. Role of calcium ions and phospholipids in platelet aggregation and plug formation. *Am J Physiol*. 1965;209:1128-1136
15. Rozenvayn N, Flaumenhaft R. Phosphatidylinositol 4,5-bisphosphate mediates Ca^{2+}-induced platelet alpha-granule secretion: Evidence for type ii phosphatidylinositol 5-phosphate 4-kinase function. *J Biol Chem*. 2001;276:22410-22419
16. Zhang Z, Jackson MB. Membrane bending energy and fusion pore kinetics in ca(2+)-triggered exocytosis. *Biophys J*. 2010;98:2524-2534
17. Peters CG, Michelson AD, Flaumenhaft R. Granule exocytosis is required for platelet spreading: Differential sorting of α-granules expressing VAMP-7. *Blood*. 2012;120:199-206
18. Rainville P, Plumb R. Separating phospholipids with uplc/ms. 2007
19. Ku CJ, D'Amico Oblak T, Spence DM. Interactions between multiple cell types in parallel microfluidic channels: Monitoring platelet adhesion to an endothelium in the presence of an anti-adhesion drug. *Anal Chem*. 2008;80:7543-7548
20. Blank U, Rivera J. Assays for regulated exocytosis of mast cells. *Current protocols in cell biology*. John Wiley & Sons, Inc.; 2006.
21. Kim D, Koseoglu S, Manning BM, Meyer AF, Haynes CL. Electroanalytical eavesdropping on single cell communication. *Anal Chem*. 2011;83:7242-7249
22. Gibbins JM, Mahaut-Smith MP, Editors. *Platelets and megakaryocytes: Volume 1. Functional assays. [in: Methods mol. Biol. (totowa, nj. U.S).; 2004, 272]*. Humana Press. Inc.; 2004.

23. Clement AB, Gamerdinger M, Tamboli IY, Lütjohann D, Walter J, Greeve I, Gimpl G, Behl C. Adaptation of neuronal cells to chronic oxidative stress is associated with altered cholesterol and sphingolipid homeostasis and lysosomal function. *J Neurochem*. 2009;111:669-682
24. Zieseniss S, Zahler S, Muller I, Hermetter A, Engelmann B. Modified phosphatidylethanolamine as the active component of oxidized low density lipoprotein promoting platelet prothrombinase activity. *J Biol Chem*. 2001;276:19828-19835
25. Lai AL, Tamm LK, Ellena JF, Cafiso DS. Synaptotagmin 1 modulates lipid acyl chain order in lipid bilayers by demixing phosphatidylserine. *J Biol Chem*. 2011;286:25291-25300
26. McMahon HT, Kozlov MM, Martens S. Membrane curvature in synaptic vesicle fusion and beyond. *Cell*. 2010;140:601-605
27. Churchward MA, Rogasevskaia T, Brandman DM, Khosravani H, Nava P, Atkinson JK, Coorssen JR. Specific lipids supply critical negative spontaneous curvature--an essential component of native Ca^{2+}-triggered membrane fusion. *Biophys J*. 2008;94:3976-3986
28. Fuller N, Benatti CR, Rand RP. Curvature and bending constants for phosphatidylserine-containing membranes. *Biophys J*. 2003;85:1667-1674
29. Yang HJ, Sugiura Y, Ikegami K, Konishi Y, Setou M. Axonal gradient of arachidonic acid-containing phosphatidylcholine and its dependence on actin dynamics. *J Biol Chem*. 2012;287:5290-5300
30. Richard JP, Leikina E, Langen R, Henne WM, Popova M, Balla T, McMahon HT, Kozlov MM, Chernomordik LV. Intracellular curvature-generating proteins in cell-to-cell fusion. *Biochem J*. 2011;440:185-193
31. Neumueller O, Hoffmeister M, Babica J, Prelle C, Gegenbauer K, Smolenski AP. Synaptotagmin-like protein 1 interacts with the gtpase-activating protein rap1gap2 and regulates dense granule secretion in platelets. *Blood*. 2009;114:1396-1404

Chapter 5

1. Chamberlain LH, Burgoyne RD, Gould GW. Snare proteins are highly enriched in lipid rafts in pc12 cells: Implications for the spatial control of exocytosis. *Proc Natl Acad Sci U S A*. 2001;98:5619-5624
2. Jahn R, Scheller RH. Snares--engines for membrane fusion. *Nat Rev Mol Cell Biol*. 2006;7:631-643
3. Lang T, Bruns D, Wenzel D, Riedel D, Holroyd P, Thiele C, Jahn R. Snares are concentrated in cholesterol-dependent clusters that define docking and fusion sites for exocytosis. *EMBO J*. 2001;20:2202-2213
4. Salaün C, Gould GW, Chamberlain LH. Lipid raft association of snare proteins regulates exocytosis in pc12 cells. *J Biol Chem*. 2005;280:19449-19453
5. Amatore C, Arbault S, Bouton C, Coffi K, Drapier J, Ghandour H, Tong Y. Monitoring in real time with a microelectrode the release of reactive oxygen and nitrogen species by a single macrophage stimulated by its membrane mechanical depolarization. *Chembiochem*. 2006:653-661
6. Uchiyama Y, Maxson M, Sawada T, Nakano A, Ewing A. Phospholipid mediated plasticity in exocytosis observed in PC12 cells. *Brain Res*. 2007;1151:46-54
7. Churchward MA, Coorssen JR. Cholesterol, regulated exocytosis and the physiological fusion machine. *Biochem J*. 2009;423:1-14
8. Salaün C, James DJ, Chamberlain LH. Lipid rafts and the regulation of exocytosis. *Traffic*. 2004;5:255-264
9. Amatore C, Arbault S, Bonifas I, Bouret Y, Erard M, Guille M. Dynamics of full fusion during vesicular exocytotic events: Release of adrenaline by chromaffin cells. *ChemPhysChem*. 2003;4:147-154
10. Wang N, Kwan C, Gong X, de Chaves EP, Tse A, Tse FW. Influence of cholesterol on catecholamine release from the fusion pore of large dense core chromaffin granules. *J Neurosci*. 2010;30:3904-3911

11. Zhang Z, Hui E, Chapman ER, Jackson MB. Phosphatidylserine regulation of Ca^{2+}-triggered exocytosis and fusion pores in PC12 cells. *Mol Biol Cell*. 2009;20:5086-5095
12. Churchward MA, Rogasevskaia T, Höfgen J, Bau J, Coorssen JR. Cholesterol facilitates the native mechanism of ca2+-triggered membrane fusion. *J Cell Sci*. 2005;118:4833-4848
13. García AG, García-De-Diego AM, Gandía L, Borges R, García-Sancho J. Calcium signaling and exocytosis in adrenal chromaffin cells. *Physiol Rev*. 2006;86:1093-1131
14. Wightman RM, Jankowski JA, Kennedy RT, Kawagoe KT, Schroeder TJ, Leszczyszyn DJ, Near JA, Diliberto EJ, Viveros OH. Temporally resolved catecholamine spikes correspond to single vesicle release from individual chromaffin cells. *Proc Natl Acad Sci U S A*. 1991;88:10754-10758
15. Moser T, Neher E. Estimation of mean exocytic vesicle capacitance in mouse adrenal chromaffin cells. *Proc Natl Acad Sci U S A*. 1997;94:6735-6740
16. Voets T, Neher E, Moser T. Mechanisms underlying phasic and sustained secretion in chromaffin cells from mouse adrenal slices. *Neuron*. 1999;23:607-615
17. Dinkelacker V, Voets T, Neher E, Moser T. The readily releasable pool of vesicles in chromaffin cells is replenished in a temperature-dependent manner and transiently overfills at 37 degrees c. *J Neurosci*. 2000;20:8377-8383
18. Haynes CL, Siff LN, Wightman RM. Temperature-dependent differences between readily releasable and reserve pool vesicles in chromaffin cells. *Biochim Biophys Acta*. 2007;1773:728-735
19. Duncan RR, Greaves J, Wiegand UK, Matskevich I, Bodammer G, Apps DK, Shipston MJ, Chow RH. Functional and spatial segregation of

secretory vesicle pools according to vesicle age. *Nature*. 2003;422:176-180

20. Wiegand UK, Duncan RR, Greaves J, Chow RH, Shipston MJ, Apps DK. Red, yellow, green go!--a novel tool for microscopic segregation of secretory vesicle pools according to their age. *Biochem Soc Trans*. 2003;31:851-856
21. Love SA, Haynes CL. Assessment of functional changes in nanoparticle-exposed neuroendocrine cells with amperometry: Exploring the generalizability of nanoparticle-vesicle matrix interactions. *Anal Bioanal Chem*. 2010;398:677-688
22. Zidovetzki R, Levitan I. Use of cyclodextrins to manipulate plasma membrane cholesterol content: Evidence, misconceptions and control strategies. *Biochim Biophys Acta*. 2007;1768:1311-1324
23. Zhang J, Xue R, Ong W, Chen P. Roles of cholesterol in vesicle fusion and motion. *Biophys J*. 2009;97:1371-1380
24. Taverna E, Saba E, Rowe J, Francolini M, Clementi F, Rosa P. Role of lipid microdomains in p/q-type calcium channel (cav2.1) clustering and function in presynaptic membranes. *J Biol Chem*. 2004;279:5127-5134
25. Dreja K, Voldstedlund M, Vinten J, Tranum-Jensen J, Hellstrand P, Swärd K. Cholesterol depletion disrupts caveolae and differentially impairs agonist-induced arterial contraction. *Arterioscler Thromb Vasc Biol*. 2002;22:1267-1272
26. Klein U, Gimpl G, Fahrenholz F. Alteration of the myometrial plasma membrane cholesterol content with beta-cyclodextrin modulates the binding affinity of the oxytocin receptor. *Biochemistry*. 1995;34:13784-13793
27. Mahammad S, Dinic J, Adler J, Parmryd I. Limited cholesterol depletion causes aggregation of plasma membrane lipid rafts inducing t cell activation. *Biochim Biophys Acta*. 2010;1801:625-634

28. Liscum L, Dahl NK. Intracellular cholesterol transport. *J Lipid Res*. 1992;33:1239-1254
29. Borges R, Diaz-Vera J, Dominguez N, Arnau M, Machado J. Chromogranins as regulators of exocytosis. *J Neurochem*. 2010:335-343
30. Ge S, White JG, Haynes CL. Critical role of membrane cholesterol in exocytosis revealed by single platelet study. *ACS Chem Biol*. 2010;5:819-828
31. Amatore C, Bouret Y, Travis E, Wightman R. Adrenaline release by chromaffin cells: Constrained swelling of the vesicle matrix leads to full fusion. *Angewandte Chemie-Int Ed*. 2000:1952-1954
32. Amatore C, Bouret Y, Travis ER, Wightman RM. Interplay between membrane dynamics, diffusion and swelling pressure governs individual vesicular exocytotic events during release of adrenaline by chromaffin cells. *Biochimie*. 2000;82:481-496